



DISPLACED GEOSTATIONARY ORBITS USING SOLAR SAILING

by

Sander Hiddink

in partial fulfillment of the requirements for the degree of

Master of Science

in Aerospace Engineering

at the Delft University of Technology, to be defended publicly on Wednesday January 20^{th} at 14:00.

Thesis committee:

Prof. Dr. Ir. P. N. A. M. Visser, Chair
Ir. R. Noomen, Supervisor
Ir. B. T. C. Zandbergen, External member

An electronic version of this thesis is available at http://repository.tudelft.nl/.



ACKNOWLEDGEMENTS

Writing this thesis report is (almost) my last task as a student and makes me rethink about all the student years that lay behind me, it was a great time. Of course I lived in Delft to study, but the other great experiences and friends made it the awesome time it was. Throughout my years in Delft, I have made so many friends who had a great impact on my personal development and supported me when times were tougher. Unfortunately it is not possible to name everyone, but I would like to mention a small selection more specifically here.

First I would like to thank all my friends, too much to name but I will try to mention the most important groups. Let's start with my high school friends of the JordanFive who I still see regularly and hope to do so for a long, long time. I also want to thank my lovely housemates at 'Het Perron', for all the nice dinners, drinks and of course numerous games of FIFA. The students of the 9^{th} floor, who where always there for a nice a talk about either thesis work when I was desperately stuck or just about anything else when I needed some distraction from this thesis work, especially during the uncasual Fridays. A special thanks goes of course out to my lovely girlfriend, Sarah, who made graduating at the 9^{th} floor an even greater pleasure. And furthermore I would like to thank all the friends I made elsewhere at the faculty especially my boardmembers of the epic 66^{th} board of the VSV 'Leonardo da Vinci'.

I also would like to thank Ron Noomen, my supervisor during my graduation project. Thank you for all the weekly meetings where you provided me help, guidance and advice on my thesis work and let's not forget the nice conversation about all kinds of things during these meetings. Pieter Visser and Barry Zandbergen, my thanks goes to you for taking time out of your busy schedules to read and evaluate my thesis work.

And last, but definitely not least, I want to thank my family for their unlimited support, leading me to the person I am now. Especially my parents Tonny and Deli who have always been there for me, loved me, supported me and shared experiences with me both in Zeist and other places. And of course my little sister Mirjam, for all the great days, dinners and parties, especially 'Belgische Bieren Borrels' we had during my years in Delft.

SUMMARY

Solar sailing is a propulsion method using sunlight as energy source, meaning it does not make use of propellants as conventional methods do. The principle of solar sailing is simple: a large lightweight sail acts as a mirror reflecting impinging light. According to the wave-particle duality light can be interpreted as a stream of photons travelling at the speed of light. As these photons impinge upon a solar sail, they transfer their momentum on the sail and thus the spacecraft. This energy transferred is the propulsive force in solar sailing. The achievable force is in the order of mN [48] and thus not very large, but in the frictionless environment that space is it can have considerable effects. Since this force works continuously, the energy input can rise to vast levels over time.

One of the possible applications for using a solar sail on a space mission is a displaced geostationary orbit. A geostationary satellite remains at a fixed position with respect to Earth's surface due to its orbital characteristics. A natural geostationary orbit can only be achieved at a specific altitude, eccentricity and inclination, meaning all geostationary satellites orbit the Earth in exactly the same orbital plane. This limitation causes the geostationary band to get more crowded every year and this is why the concept of displaced geostationary satellites is interesting. For this concept, a satellite is put in an orbit that is altered in order to lay outside the standard geostationary band while the relevant orbital properties remain constant and its position thus stays fixed above the Earth' surface.

In this thesis a spacecraft equipped with a solar sail is used to achieve such a displaced orbit. Even though the thrust levels possible using a solar sail are limited, the fact that it allows for continuous thrust and does not rely on any propellant make it a promising candidate for this concept. This thesis investigates the feasibility of this idea. A differential evolutionary algorithm is used to search for orbital trajectories that fulfil the set requirements. Promising results were found considering increasing vertical displacement of the orbital plane above the equatorial plane. Using a sail performance of 1 mm/s² and a trajectory of three revolutions, a displaced orbit with an average offset of 3 km with respect to the desired position throughout the trajectory was found. These results were found considering the most favourable conditions valid around the winter solstice. During other periods of the year, the direction of the sunline has changed and the performance of the solutions found decreases to approximately 20 km average offset. With a desired displacement of 25 km, this is clearly unacceptable high.

It can therefore be concluded that achieving a displaced geostationary orbit is possible, although only for a limited time. The solutions found only hold for the conditions valid around December 21, the winter solstice. Throughout the year, the conditions change considerably and become less favourable. As a result no valid solution trajectories were found during March-September. The concept of a displaced geostationary satellite solely using solar sailing as a propulsion method thus unfortunately seems infeasible.

CONTENTS

Ac	knov	wledgements	iii
Su	ımma	ary	v
Ta	ble o	of Contents	ix
Li	st of A	Acronyms	хi
Li	st of S	Symbols	xiii
1	Intr	roduction	1
_		Subject	1
		1.1.1 Geostationary Solar Sailing Orbits	
		1.1.2 Relevance proposed research	2
		Problem Definition	2
		Research Question	
	1.4	Report Structure	3
2	Sola	nr Sailing	5
	2.1	Heritage	
		2.1.1 Mission studies and possible applications	
		2.1.2 Solar sail missions	
	2.2	Solar Radiation Pressure	
		2.2.1 Solar Radiation Pressure	
	2.2	2.2.2 Other Radiation	
	2.3	Solar Sail Spacecraft	
		2.3.2 Square Sail	
		2.3.3 Sail	
		2.3.4 Booms	
		2.3.5 Spacecraft	
	2.4	Performance	
	2.5	Geostationary Satellites	15
	2.6	Orbital Requirements	16
3	Orb	ital Dynamics	19
•		Reference Frames	
		3.1.1 Earth Centred Inertial	
		3.1.2 Earth Centred Fixed	20
		3.1.3 Transformation	20
		Coordinates Systems	
	3.3	Equations of Motion	
	3.4	Solar Sailing	
	3.5	Non-ideal Sail.	
		3.5.1 Reflectivity	
	2 6	3.5.2 Deformation	
		First-order calculation	
			20
4		nerical Methods	31
	4.1	Integration Methods	
		4.1.1 Single Step methods	31

VIII CONTENTS

	4.2	Ontimi	zation Methods
	4.2		
			Differential Evolutionary
		4.2.2	MOEA/D
5	Dwo	wam Cat	-Un 37
3		gram Set	e
	3.1		
			<u>ludat</u>
			C++
		5.1.3 F	Pagmo
		5.1.4	Other Software
	5.2	Progran	n Structure
		5.2.1	ingle Run
			Optimisation
	5.3		43
	3.3	_	nitial State
			bunline
			ail Orientation
			ail Acceleration
			<u> Cclipse</u>
			Perturbations
	5.4	Optimis	sation Algorithms
		5.4.1 I	Decision Vector
		5.4.2	learch Space
		5.4.3	Objective Function
6			and Validation 53
	6.1		
			ransformation between reference frames
		6.1.2 T	Transformation between coordinate system
		6.1.3 T	Tudat constants
	6.2	Settings	5
	6.3	Single B	l <mark>un</mark>
			tandard geostationary orbit
			Displaced geostationary orbit
			Elevated geostationary orbit
	6.4		for
		_	
	6.5		sation
			DE-Algorithms
		6.5.2	Decision Vector
7	Resi	ılts	67
			solstice conditions
			splacement
	1.2		0 Nodes, 1 mm/s ² characteristic acceleration
			0 Nodes, 10 mm/s ² characteristic acceleration
			0 Nodes, 0.1 m/s ² characteristic acceleration
	7.3		isplacement
			0 Nodes, 1 mm/s ² characteristic acceleration
			0 Nodes, 0.1 mm/s ² characteristic acceleration
		7.3.3	0 Nodes, 1 mm/s ² characteristic acceleration
	7.4	25 km d	isplacement
		7.4.1	0 Nodes, 1 mm/s ² characteristic acceleration
	7.5		
			0 Nodes, 1 mm/s ² characteristic acceleration
			0 Nodes, 10 mm/s ² characteristic acceleration
			0 Nodes, 10 mm/s ² characteristic acceleration, larger decision vector
			o modely to minimo official accordation, furgor according voctor

	•
Contents	13
CONTENTS	1/

		Other Conditions	84 84 85
{	3.1	Conclusions	
Bib	liog	graphy	95

LIST OF ACRONYMS

AU Astronomical Unit

CFRP Carbon Fiber Reinforced Plastic

DE Differential Evolution

DLR Deutsches Zentrum für Luft- und Raumfahrt

EoM Equations of Motion

ESA European Space Agency

GEO Geostationary Earth Orbit

IKAROS Interplanetary Kite-craft Accelerated by Radiation Of the Sun

ISS International Space Station

JAXA Japanese Aerospace Exploration Agency

JPL Jet Propulsion Laboratory

MOEA/D Multi-Objective Evolutionary Algorithm with Decomposition

NASA National Aeronautics and Space Administration

RK Runge-Kutta

SEP Solar Electric Propulsion

SRP Solar Radiation Pressure

Tudat TU Delft Astrodynamics Toolbox

LIST OF SYMBOLS

Symbol	Meaning	Unit
A	Area	m^2
а	Acceleration	m/s^2
a	Absorption coefficient	-
c	Speed of light	m/s
E	Energy	J
e	Eccentricity	-
F	Force	N
$\mathscr{F}_{blackbody}$	radiation flux	W/m^2
f	Force per mass	N/kg
G	Gravitational Constant	$m^3/(kg s^2)$
i	Inclination	rad
L_S	Luminosity	W
L_1	Lagrange point 1	-
m	Mass	kg
N	Number of nodes	-
n	Normal vector	-
P	Pressure	${ m N~m^{-1}}$
p	Momentum	N s
r	Distance	m
$ ilde{r}$	Reflection coefficient	-
T	Temperature	K
ν	Velocity	m/s
W	Flux	W/m
W_E	Flux at 1 AU from Sun	W/m
α	Pitch angle	rad
$oldsymbol{eta}$	Lightness number	-
heta	Angular radius	rad
heta	Cone angle	rad
ϵ	Emissivity coefficient	-
τ	Transmission coefficient	-
τ	Time of pericenter passage	S
Ω	Right ascension of the ascending node	rad
ω	Angular/radial velocity	rad/ s
ω	Argument of pericenter	rad
σ	Stefan-Boltzmann constant	$W/(m^2K^4)$
σ	Sail loading	kg/m ²
σ^*	Critical sail loading	kg/m^2
μ	Standard gravitational parameter	m^3/s^2
ϕ	Centre-line angle	rad

1

INTRODUCTION

Solar sailing is a propulsion method using sunlight as energy source, meaning it does not make use of propellants as conventional methods do. The principle of solar sailing is simple: a large, lightweight sail acts as a mirror reflecting impinging light. According to the wave-particle duality light can be interpreted as a stream of photons travelling at the speed of light. As these photons impinge upon a solar sail, they transfer their momentum on the sail and thus the spacecraft. This energy transferred is the propulsive force in solar sailing. The achievable force is in the order of mN [48] and thus not very large, but in the frictionless environment that space is it can have considerable effects. Since this force works continuously, the energy input can rise to vast levels over time.

Ever since James C. Maxwell suggested the existence of solar radiation pressure in 1873 and Pyotr Lebedev proved this phenomenon experimentally in 1900 [8], people have been thinking and writing about the possibilities of solar sailing. The first scientific analyses were performed in Russia, by Konstantin Tsiolkovsky and Fridrich Tsander. They wrote papers about huge mirrors of very thin sheets, using the pressure of light to attain "cosmic velocities". [31] This was followed by several initial studies but it was not until the early 1970's that the first serious, detailed study on an actual solar sailing mission was performed by NASA. [31] Unfortunately this mission was never actually flown, just as is the case for most following mission proposals. Eventually in 2010, the Japanese spacecraft IKAROS became the first spacecraft making use of a solar sail as propulsion method. [27] Solar sailing has unique characteristics, introducing new possibilities. Missions highly suitable for solar sailing include: polar observation, interplanetary missions and spacecraft at displaced equilibrium points. A displaced geostationary orbit is another application, the one where this research focuses on. Geostationary orbits are widely used by communication satellites and only exist in a specific, limited orbital band which threatens to become congested due to this increase of satellites. Therefore it is useful to see if their band of possible orbits can be extended using propulsion. The goal of this thesis is to find out to what extent it is possible to alter a geostationary orbit using solar sailing, while still maintaining the characteristics required for stable communication links.

This chapter gives the reader a feeling for the research at hand, it introduces the subject, the relevance of the study and makes the study more specific by introducing the research question and the corresponding problem definition.

1.1. SUBJECT

1.1.1. GEOSTATIONARY SOLAR SAILING ORBITS

As mentioned, solar sailing is a concept long known and investigated throughout the years. Many studies have been performed, multiple mission concepts have been proposed and two solar sail missions have actually been completed. A rather novel and therefore not well-investigated mission concept is the use of solar sailing to alter the orbit of a geostationary satellite enough so it travels outside the current belt of geostationary satellites. This concept could help the problem of ever increasing density of satellites orbiting the Earth, which could lead to overpopulation of the geostationary belt. This forms a growing threat of collisions, creation of space debris and communication-link related problems. As said, the concept of an elevated geo-

2 1. Introduction

stationary orbit could help reducing this threat, as the satellites will be placed in a different orbital plane.

R. Forward was the first to investigate the concept and concluded it should be possible to achieve such elevated orbits using a perforated high-performance sail. [16] However, calculations in this paper used a simplified case where a perfect circular orbit was assumed and the radial force component was neglected, making the conclusions premature as pointed out by H. Fischer [14] and C. van de Kolk [47]. Later these calculations were performed in a more detailed manner, concluding an elevated geostationary orbit is indeed possible for a high-performance sail. [5] This study proved similar results as obtained before by Forward, although certain assumptions were still made. Neglecting for example the oblateness of the Earth and assuming the sunlight directed in the equatorial plane in this research, still leaves enough room for improving models and definite results. Heiligers [21] studied an elevated geostationary orbit using the full non-linear equations of motion and taking into account all important perturbations, but here a concept using a hybrid propulsion method was considered. The main thrust is provided by solar electric propulsion (SEP), while the solar sail is only used to minimize the propellant usage.

1.1.2. RELEVANCE PROPOSED RESEARCH

Looking at literature, a geostationary satellite using a solar sail in order to change the orbit considerably is not a completely new subject. Already in the 1980's this concept was studied, although not in great detail. In later years, some research has been preformed for this specific case, but this was either simplified or combined with other forms of propulsion. A new study, using the complete, non-linear equations of motion and taking into account all relevant perturbations will provide more insight in the precise possibilities of this concept. Also further investigation of possible steering laws and their effect on the achievable orbit could reveal new considerations towards this field of research.

1.2. PROBLEM DEFINITION

A displaced geostationary orbit means that a trajectory is followed that has geostationary properties, while it is not a 'normal' geostationary orbit. The geostationary property mentioned here is maintaining a fixed position relative to the Earth surface. In order to achieve this a circular orbit which a specific rotational period is required, normally coupled with a specific semi-major axis. With an additional force, this trajectory can potentially be altered while maintaining the constant position. For example, a constant radial force in outward direction is experienced by a spacecraft as a decreased gravitational attraction. This means a spacecraft at a certain altitude will have a slightly higher orbital velocity compared to a natural orbit, a geostationary orbit would in this case therefore be achieved at a higher altitude. Using a solar sail such a force is not possible, but a continuous thrust in different directions is a possibility. In this way the same could be achieved (an orbital period of exactly a sidereal day) but in a displaced, different trajectory. In this case the focus is laid on finding an elevated orbit, where the spacecraft follows a trajectory similar to a geostationary orbit, but at an orbital plane slightly above the equatorial plane.

The search for such trajectories is performed using optimisation algorithms. Two types of parameters will be varied by this algorithm: the initial state of the satellite and the sail orientation throughout the orbit. These parameters will together form the decision vector and can be varied, while staying within certain constraints. All other variables, such as desired elevation and characteristic sail acceleration, are fixed for the optimisation and can be seen as the settings of the optimisation problem at hand. These parameters are thus not optimised, but their relevance will be investigated. Performed optimisations will be repeated using different settings in order to assess their importance and influence. This is most relevant for the characteristic acceleration, for the other settings a sensitivity analysis is performed.

1.3. RESEARCH QUESTION

After inspecting the status of the research topic in the previous section, it is now time to define the actual research question. For this project, the research question to be answered is:

Is it possible to achieve a displaced geostationary orbit using solely solar sailing as propulsion method?

The research goal is thus to find possible displaced geostationary orbits using only a solar sail as propulsion method. This is a broad question and not one to be answered in one go. Therefore it is necessary to

1.4. REPORT STRUCTURE 3

define a number of sub-questions which are crucial in answering the research question in a structured, scientific manner. These sub-questions will give more insight in the problem and will provide overview during the project and are shown below. During the report and thus in this report, an attempt will be made to answer these question satisfactory.

What are the orbital requirements of a geostationary satellite and what perturbations play a role?

In essence a geostationary orbit means the satellite stays at a fixed position relative to the Earth surface. It should be defined what the requirements are which commercial geostationary satellites are in practice subject to. Furthermore the relevant perturbations acting on the spacecraft, such as the oblateness of the Earth and radiation pressure from Earth and their influence on a spacecraft should be defined.

What are the exact properties of the sail considered?

Based on the literature study performed a realistic sail is defined, taking into account the mass, dimensions, lightness number and the attitude control possibilities. This sail should be used as a reference throughout the study, later these parameters can be changed in order to find the influence of these parameters on the found orbital solution. This does not imply that a complete sail will be designed, an approximation of the most relevant performance parameters of the sail are needed to perform calculations. Further design of the sail is reserved for possible future studies.

What is the best optimisation method to find and improve a solar sail geostationary orbit?

Several methods and approaches can be used to find an orbital solution for a perturbed non-Keplerian orbit, such as a displaced geostationary orbit. In order to find a periodic, stable orbit solution an optimizing scheme is used, it is important to investigate what is a suitable method to do this.

What is a realistic elevation using a realistic sail?

A large elevation of hundreds of kilometres would be a great result, but this seems not feasible looking at the limited thrust available using a solar sail. It should be investigated what elevation proves to be achievable using the selected sail.

What are the most important limitations for the achievable trajectory?

It is not expected that a perfectly stable geostationary orbit is realistic, but the goal of this thesis is to identify the best possible solution. Furthermore is should be made clear what limitations make the perfect orbit infeasible and what their effects are on the solution. Lastly the consequences this has on the possible use of the found trajectories will be addressed.

By answering the defined questions, the scientific research will ultimately lead to a satisfying answer to the research question. How this study is set out and what steps were taken in order to do this effectively will be shown in this report.

1.4. REPORT STRUCTURE

This chapter is to give the reader a feeling for the subject and has stated the research question and hopefully clarified the exact problem at hand. The remaining of this report will describe the study performed from theory to final results. Here follows a short overview of the subjects that will be handled, how these parts fit in the total research and the order they are presented in the report.

The main part of the report starts with an introduction on the concept of solar sailing. The chapter will start with a overview of the history, present state and future of solar sailing mission. After follows a discussion on the driving force of a solar sail, the so-called solar radiation pressure. The consequences for the spacecraft design will be followed by the performance of solar sail that will be considered in this study. The chapter is concluded with an introduction of geostationary orbits, their characteristics and orbital requirements defined for this research.

Chapter 3 introduces all the theory on orbital dynamics required for this research. This starts with a definition of the selected reference frames and coordinate systems, followed by the equation of motion without a sail, with a perfect sail, including a non-ideal sail and lastly the relevant perturbations. The chapter is fi-

1. Introduction

nalised by a simple calculation to get a feeling for the forces present and the elevation possible.

The next chapter introduces all numerical methods that were used in programming a simulator. This means both the integrator and optimisation methods are discussed, together with an explanation on their working and settings.

Chapter 5 presents the simulation tool that was programmed in order to perform the calculations and optimisations needed to answer the research question is presented. First the software used is introduced, followed by an overview of the program set-up, which is completed by a more detailed explanation of all the separate coding blocks that form the entire tool.

Before any relevant simulations and optimisations can be run, the working of the program has to be checked. Chapter 6 discusses the verification and validation methods applied in this study. Also the settings possible in the program are tested and their effect on the performance of the tool is tested. This leads to a reference case that is used as a start for the final runs that should provide actual results.

In Chapter 7 the final results obtained are presented. All relevant results are presented using trajectory plots, tables and of course a short discussion of every case. The chapter is finished by a discussion on the complete set of results obtained.

As might be expected the last chapter of the report contains its conclusions. This chapter looks back at the total work performed and ultimately tries to answer the research questions using the obtained results. This answer can be seen as a short reflection and discussion on all parameters affecting the results, as a simple, short and unambiguous answer is not possible. As is the case for all scientific research, certain considerations and assumptions relevant during the work leave room for improvement. This is certainly the case for this thesis as well. Therefore in the last section of this report, recommendations for further research are presented.

2

SOLAR SAILING

This chapter serves as an introduction to solar sailing and its possibilities. First the history of solar sailing is presented, starting with the first mentioning of possible usage of sunlight as a propulsion source. This is followed by the mission studies performed, actual missions flown in recent history and finally the planned missions for the near future. Section 2.2 describes the solar radiation (pressure) coming from the Sun; this sunlight, or solar radiation, is the source of energy which drives the solar sail. The next section describes the most important and relevant influences of a solar sail on the rest of the spacecraft design. This is followed by the performance of the sails considered in this report. Lastly a short introduction on geostationary satellites in general and specifically the requirements defined for them in this report, concludes this chapter.

2.1. HERITAGE

Ever since James C. Maxwell suggested the existence of solar radiation pressure in 1873 and Pyotr Lebedev proved this experimentally in 1900 [8], people have been thinking and writing about the possibilities of solar sailing. This started with science fiction authors writing stories about spaceships propelled by solar radiation pressure (SRP). The first scientific analyses were performed in Russia, by Konstantin Tsiolkovsky and Fridrich Tsander. They wrote papers about huge mirrors of very thin sheets, using the pressure of light to attain "cosmic velocities". [31] This was followed by several initial studies on solar radiation pressure and the possible use of it in space travel. Most studies focused on particular aspects of solar sailing, and did not result in complete mission proposals. In 1960 NASA launched its first communication satellite, Echo 1. Echo 1 was a large, reflective balloon used for passive communication with the Earth. Due to its large area-to-mass ratio, it provided the first experimental data of SRP in the Earth atmosphere.[4] However, it was not until the early 1970's that the first serious, detailed study on the actual use of solar sailing for propulsion was performed by NASA. [31] Unfortunately this mission, a Halley rendez-vous mission, was never actually flown, just as is the case for most mission proposals that followed. Eventually in 2010, the Japanese spacecraft IKAROS became the first actual spacecraft making use of a solar sail as propulsion method. [29] This success was followed by NASA in January 2011 when NanoSail-D deployed the first solar sail in low-Earth orbit. [34] The most recent solar sail mission was performed by The Planetary Society, in June 2015 they successfully carried out a first test flight. Furthermore several missions are planned for the near future. In the following sections these studies and actual flown missions will be discussed in more detail.

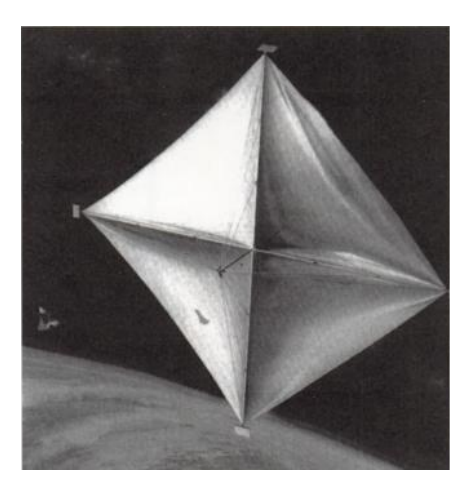
2.1.1. MISSION STUDIES AND POSSIBLE APPLICATIONS

Below, several mission concepts that have been suggested and studied in the past decades are described to give a short overview of possible applications of solar sailing. Firstly a mission study for a Halley rendezvous is described, followed by descriptions of several concepts for using solar sailing.

Halley rendezvous In 1973, the first serious mission study on solar sailing was started by NASA. This study began as a low-level study on solar sailing during which a trajectory enabling a rendezvous with the Halley comet was discovered, causing the study to be expanded considerably into a serious mission study. The mission proposed consisted of a spacecraft capable of meeting Halley in its perihelion after just four years of flight. For the sail both a square configuration and a heliogyro design were discussed,

6 2. Solar Sailing

see Figure 2.1. In order to achieve this spectacular flight performance, the sail would have huge dimensions: a square sail of 800×800 m or 12 7.5 km long blades for the heliogyro configuration. After analysis, the heliogyro design seemed more suitable, mainly based on deployment issues with the square sail. Unfortunately, in further studies NASA preferred solar-electric propulsion over solar sailing, since it seemed less risky. Financial constraints eventually stopped this mission being flown after all. [31]



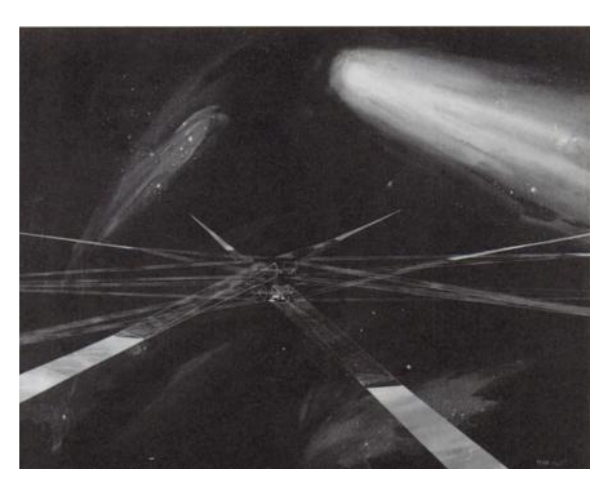


Figure 2.1: Sail designs for comet Halley rendezvous mission, square sail configuration (left) and heliogyro configuration.[31]

Solar polar mission The Sun is the center and the most prominent body in our solar system, being the largest body orbited by all others. Since it also is of unique nature and has a large influence on the conditions on Earth, the Sun is a particularly interesting body for observation. Studying the complete surface of the Sun can teach us much about the characteristics and origin of the Sun, Earth and the whole universe. A spacecraft in an inclined orbit is therefore highly desirable in observation of the complete surface of the Sun. Achieving such an orbit around the Sun results in massive ΔV demands due to its mass and distance to the Earth, a reason why it is almost unfeasible for conventional propulsion. Exposing a solar sail to SRP over a long time and in the vicinity of the Sun, can however provide such amounts of energy. Solar sails could thus enable inclined solar orbits needed to observe the complete surface of the Sun including its poles while maintaining a reasonable lift-off mass.

Mercury orbiter Missions to Mercury also demand high thrust levels, one of the reasons such missions have been rare until now. Mercury is the smallest and lightest planet in our Solar system and orbits closest to the Sun. This means that for a spacecraft orbiting Mercury a relatively high amount of acceleration from SRP is achievable. The high ΔV budget and high SRP combined thus make a Mercury orbiter mission suitable for the use of solar sailing.

Pluto mission Instead of a mission very close to the Sun, solar sailing could also be used for missions to the outer regions of our solar system. These missions are characterized by their high ΔV demand and long mission duration. These factors combined make them suitable for a solar sailing mission. A study of a solar sailing mission to Pluto and its comparison to a 'normal' spacecraft can be found in [15].

Sample return mission Sample return missions could provide very valuable information and new insight, however apart from a very small amount of dust collected by the Japanese spacecraft Hayabusa [26] only material from the Moon has ever been brought back to the Earth. Therefore a sample return mission is a major challenge and could be a possible target of a solar sail mission.

Geostorm The Geostorm mission is a mission concept for a spacecraft orbiting in the vicinity of the first Sun-Earth Lagrange point, L_1 . Around L_1 a Halo orbit is possible in which the spacecraft stays at a fixed distance between the Earth and the Sun. The Geostorm spacecraft would use a solar sail to achieve a Halo orbit around an artificial equilibrium point. This artificial equilibrium point lies twice as far from

2.1. Heritage 7

the Earth as the natural L_1 point. The spacecraft would be able to detect and predict solar storms in an early stage, thereby providing better possibilities in protecting electric circuits on Earth and satellites. [49]

Non-Keplerian periodic Earth orbits One of the most important characteristics of solar sailing is the continuous thrusting, affecting the acceleration of the spacecraft throughout the complete orbit. A satellite can therefore maintain an orbit elevated above the normal orbital plane, enabling orbits that are otherwise not possible and have never been achieved. A polar observation is a good example that could make use of such an orbit in order to improve its performance. The spacecraft could be brought into an orbit elevated high above the ecliptic, or even placed in a fixed position above the Earth. Both situations would provide continuous coverage of one of the Earth poles which is favorable for observation. A visualization of such a polar observation orbit is given in Figure 2.2. Another possibility is altering a geostationary orbit in order to change the track enough to lay outside the given belt of normal geostationary satellites. Apart from the ones mentioned, other forms of non-Keplerian orbits around either the Sun or the Earth could be made possible using solar sailing.

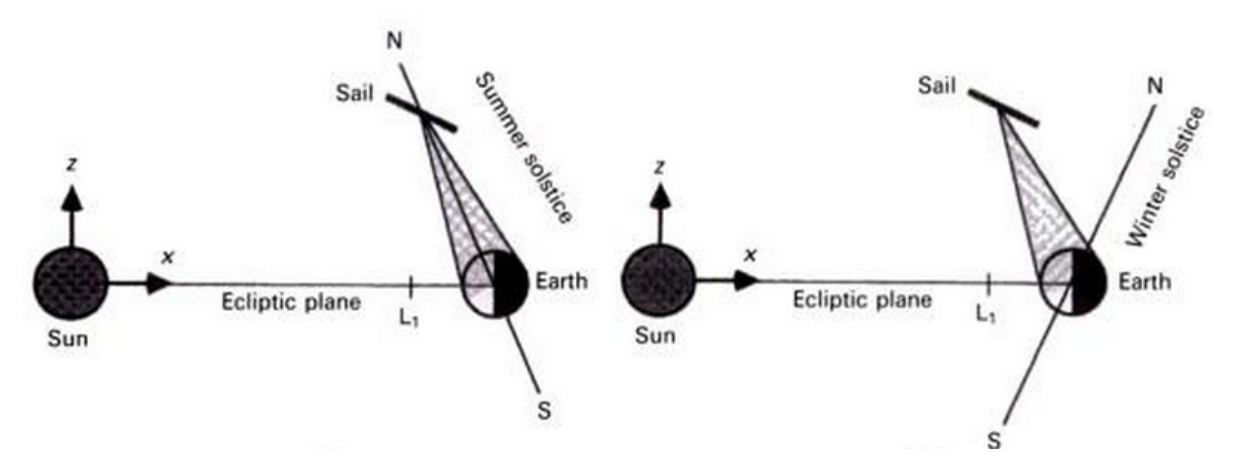


Figure 2.2: Polar observer mission orbit visualization.[31]

2.1.2. SOLAR SAIL MISSIONS

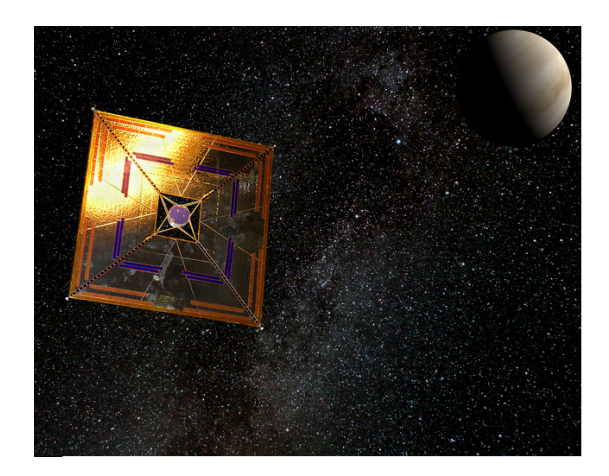
Although mission proposals using solar sailing have been around for decades, it lasted quite some time until the first solar sail spacecraft was eventually launched. Up to now three spacecraft have actually used solar sailing in their lifetime, IKAROS, NanoSail-D and most recently LightSail-A. Both missions achieved their mission goals and proved the potential of solar sailing. They provided valuable data and information for solar sailing and can be seen as the first steps in the implementation of solar sails in space missions. Multiple missions, such as NASA's Sunjammer project, are planned for the near future, a sign that solar sailing is becoming a more and more serious option for propulsion of spacecraft. A description of the IKAROS and NanoSail-D is given below, followed by a short introduction of missions planned in the near future.

IKAROS

On May 21 2010 IKAROS was launched, becoming the first spacecraft using a solar sail as a propulsion method. The Interplanetary Kite-craft Accelerated by Radiation of the Sun (IKAROS), is a mission of the Japanese Aerospace Exploration Agency (JAXA) to the planet Venus, using SRP as the main propulsion source during parts of the trajectory. The spacecraft is equipped with a square sail with a diagonal of 20 m, made of polyimide sheets with a thickness of only 7.5 μ m. The total spacecraft weights 310 kg and the body measures 1.6 by 0.8 m.[27] After launch and departure from Earth IKAROS performed its two stages of deployment successfully, making it the first interplanetary solar sail spacecraft.[29] Over the course of the following six months the sail provided a total change in ΔV of approximately 100 m/s. It carries multiple instruments on board, several of which monitored the deployment and acceleration of the sail, providing data needed to analyze the working of a solar sail in real time and in space environment. All in all IKAROS resulted in an impressive and highly important first step in the field of solar sailing, towards enabling solar sails for all kinds of future

8 2. Solar Sailing

missions. Figure 2.3 shows an artist impression and an actual picture of the spacecraft in orbit which was taken shortly after deployment.



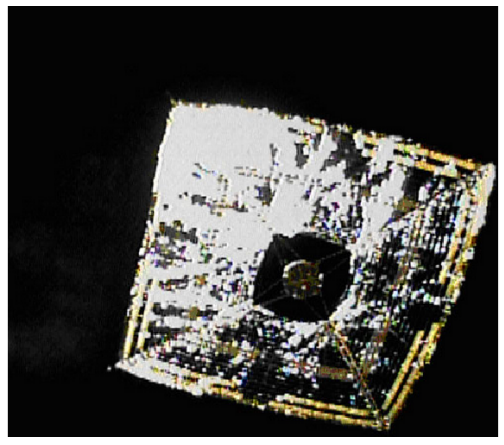


Figure 2.3: IKAROS spacecraft, an artist impression (left) and a picture of the spacecraft in orbit (right).[28]

NANOSAIL-D

Already in 2008 NASA launched its first spacecraft equipped with a solar sail, NanoSail-D. Unfortunately the launch with a Falcon 1 rocket ended in failure. [44] In the end of 2010 a replacement spacecraft, sometimes called NanoSail-D2, was successfully launched. Apart from some minor alterations this second spacecraft was the same as its predecessor. The NanoSail-D mission is a demonstrator mission in which NASA tested, and succeeded, the deployment of a solar sail in Earth orbit. Its sail has comparable properties to IKAROS in terms of thickness and material, although it is considerably smaller. The spacecraft had a launch mass of only 4 kg and uses a square sail of $10~\rm m^2$ area. [18] NanoSail-D was deployed at an altitude of approximately 650 km; at this altitude atmospheric drag is still a large factor, especially for a solar sail spacecraft with a high area-to-mass ratio. The spacecraft orbited Earth for 240 days before it burned up during reentry, well beyond the expected lifetime. [33]

LIGHTSAIL-A

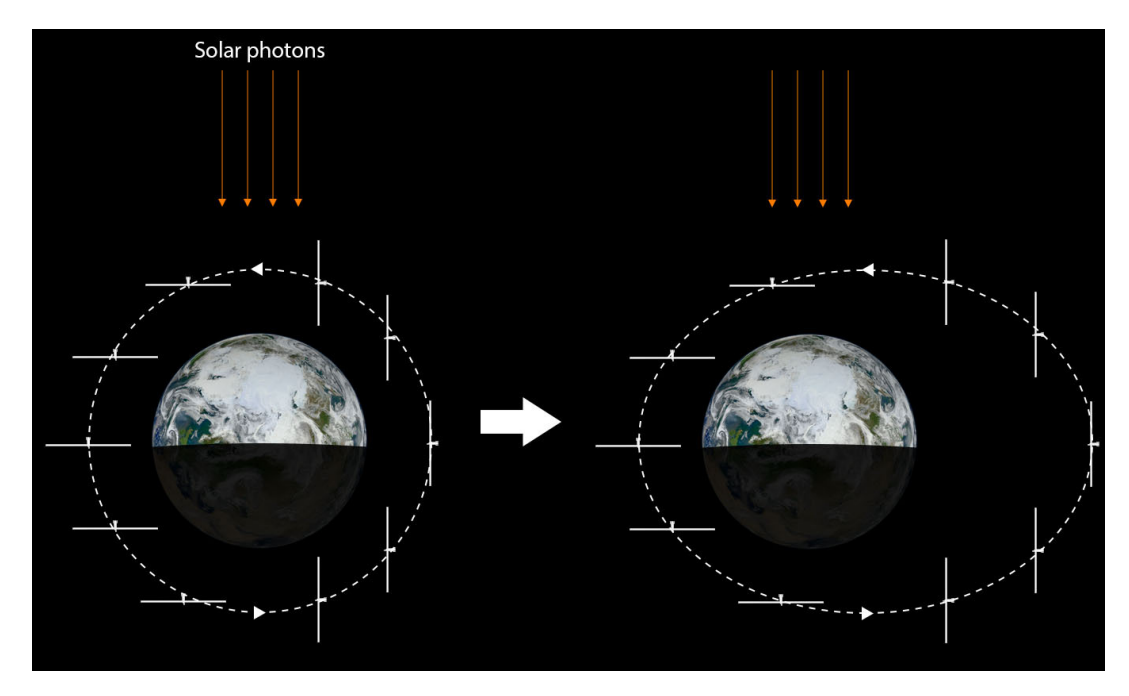
Last year The Planetary Society, a non-profit space advocacy group, performed a test flight using a demonstrator spacecraft. LightSail-A was launched into low-Earth orbit aboard an Atlas V rocket in May 2015, the spacecraft is similar to the eventual LightSail vehicle. It consist of a 30×10 cm three-unit cubesat connected to a solar sail. The sail consists of four components forming a square sail measuring $32~\text{m}^2$ in total, the sail is amde of Myral sheets with a thickness of $45\mu\text{m}$. [41] Even though difficulties occurred using the battery , the spacecraft eventually was able to deploy its sail. The Planetary Society declared the testflight a success after its

FUTURE MISSIONS

To date three solar sail spacecraft have successfully flown, but more mission are planned for the future. NASA's Sunjammer is a mission comparable to the Geostorm concept study mentioned before; it will find a stable position or Halo orbit around an altered Lagrange point. Sunjammer will contain a solar sail weighing 31 kg and measuring 1200 m^2 , making it the largest solar sail ever flown. The sail will experience a maximal thrust of 10 mN, which will help it to maintain an equilibrium position closer to the Sun. This position will allow it to measure potentially hazardous radiation from the Sun in an earlier stage than possible until now. [35]

The Planetary Society plan to launch the actual LightSail spacecraft in 2016. It will be launched to an altitude of 720 km, after which it will use its 32 m^2 sail to spiral away from the Earth. The sail will switch between two settings during its orbit, as can be seen in Figure 2.4. During the first half of each orbit, the sail is orientated directly towards the Sun and will achieve maximum acceleration, the other half of the time the sail is turned 90^o and therefore experience no acceleration. This will cause the apoapsis to increase by an expected 1 km per day.[25]

The Gossamer project is a collaboration between ESA and DLR, announced in 2009, its goal is purely technology demonstration as no scientific payload will be used. [19]The project consists of a three-stage roadmap



 $\textbf{Figure 2.4:} \ Planned \ orbital \ trajectory \ transformation \ of the \ Light Sail \ spacecraft.$

of missions with increasingly larger and better performing spacecraft. The first demonstrator mission have a 5×5 m sail, Gossamer-3 the last spacecraft should carry a 50×50 m sail which produces approximately 0.1 mm/s² acceleration allowing it to leave the gravitational pull of the Earth. Initially the first demonstrator mission was planned for 2013 and the launch of Gossamer-3 in 2015, however the project seems to have stalled as no updates are found from the last years. [9]

2.2. Solar Radiation Pressure

The most important body in our solar system, apart from the Earth, is undoubtedly the Sun. The Sun is the star around which all other bodies orbit and it contains more than 99.8% of the mass of the complete solar system. [7] Apart from its unique size and position it is also a completely different type of body. While other bodies are composed of solid or gaseous molecular material, the Sun is a giant plasma ball, heated by nuclear fusion in its core. Due to this fusion, extremely large amounts of energy are released, thereby heating up the material surrounding it and creating the plasma. This means the temperature profile of the Sun is also of a completely other order than that of planets. The surface temperature of planets is several 100 Kelvin and although their core temperature can rise to thousands of Kelvin [7] [10], this is cold compared to the Sun. In the core of the Sun temperatures rises to extreme temperatures around 15 MK, while at the surface the temperature is approximately 5,800 K. [7] Apart from its mass and thus large gravitational pull, this high temperature of the Sun is even more important regarding solar sailing, since the radiation coming from a body is mostly dependent on its temperature. Although not entirely true, for simplicity in this report the Sun is assumed to be a perfect sphere with a constant surface temperature, thus radiating equally in all directions and with constant intensity throughout time.

2.2.1. SOLAR RADIATION PRESSURE

With solar sailing one uses energy radiated from the Sun as source. The energy received, and thus force experienced, depends on the amount of energy radiated and the distance to that body. All bodies radiate energy; the amount radiated is related to its temperature by the Stefan-Boltzmann law: [50]

$$\mathcal{F}_{blackbody} = \sigma A T^4 \tag{2.1}$$

In this formula σ is the Stefan-Boltzmann constant, equal to $5.67 \cdot 10^{-8} \text{ Wm}^{-2} \text{K}^{-4}$. The temperature in this equation is called the blackbody or effective temperature. A black body is a theoretical body that is both a perfect absorber and emitter. The effective temperature of a body is the temperature a perfect black body

2. Solar Sailing

would have in order to radiate the same amount of energy that the actual body emits. This temperature is thus a theoretical value used to describe the radiation level of a body. For bodies without an internal heat source, the temperature is completely determined by the incident radiation and the effective temperature is equal to the equilibrium temperature. [7]

Using Equation 2.1 the radiation of a body can be calculated when its effective temperature is known. Assuming this energy is radiated uniformly over the whole sphere, the energy received by a sail at a certain distance can be found using:

$$\mathcal{F}_{received} = \mathcal{F}_{radiated} \cdot \frac{A_{sail}}{4\pi r^2} \tag{2.2}$$

With this formula the energy received by a unit surface at a certain distance from the Sun can be calculated. In this equation the relation between distance for the Sun and energy received is defined by the inverse square law, which assumes the Sun as an infinitely small point. The Sun actually has finite dimensions which causes a small deviation from this relation. This finite dimension also causes limb darkening, the Sun appears brightest in the center and darkens towards the outside, as can be seen in Figure 2.5. These two factors only play a role in the close vicinity of the Sun, at distances further than 10 solar radii or 0.047 AU, their effect becomes negligible.[31]

The solar constant W_E is the flux at a distance of 1 AU from the Sun and is known to be 1368 W/m². [31]

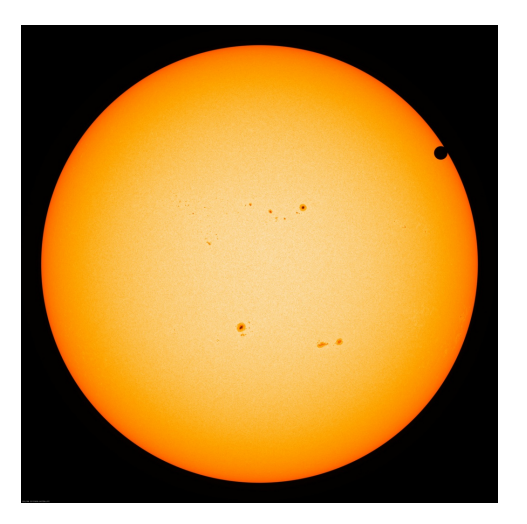


Figure 2.5: Limb darkening of the Sun. [36]

From this flux the total energy received by the sail can be found by simply multiplying with the area of the sail and the time considered. The energy received by a sail is thus calculated with:

$$E = W \cdot A \cdot \Delta t \tag{2.3}$$

Also the energy contained by a photon can be found, for this a quantum physics approach is needed. According to the relativistic mass-energy equivalence the energy of a particle is described as: [31]

$$E^2 = p^2 c^2 + (m_0 c^2)^2 (2.4)$$

Since a photon at rest has no mass, $m_0 = 0$ in the second right-hand term of Equation 2.4 and this term disappears, the energy of a photon simply becomes:

$$E_{photon} = pc (2.5)$$

In this formula *p* represents the momentum of a photon which depends on the frequency of the light, while *c* is the speed of light. The pressure exerted on the sail is the parameter defining the working of the solar sail. Pressure can be defined as the momentum transported per unit area, per unit time and thus mathematically written as:

$$P = \frac{\Delta p}{A\Delta t} \tag{2.6}$$

Now rewriting Equations 2.3 and 2.5 to expressions of respectively W and p, Equation 2.6 can be written as follows:

$$P = \frac{\Delta p}{A\Delta t} = \frac{E}{c} \cdot \frac{1}{A\Delta t} = \frac{W}{c}$$
 (2.7)

with:
$$W = \frac{L_S}{4\pi r^2}$$
 (2.8)

In these equations W is the energy flux received, which depends on the luminosity L_S of the Sun and the distance to it. The flux can also be expressed in terms of the solar flux $W_E = 1368 \text{ W/m}^2$, the energy flux measured at the Earth's distance to the Sun. Solar radiation pressure is the pressure exerted on a sail by incident photons, thus the energy comes from absorption of the photons. However, when the photons are reflected perfectly according to Newton's third law the force can be doubled. To get a feeling of the order of forces present an example calculation is done for a $10 \times 10 \text{ m}$ sail, located at 1 AU from the Sun. The sail is aligned perpendicular to the Sun-line and it is perfectly reflecting. According to Equation 2.9, the force on such a sail is then just below 1 mN, which is fairly small. It can therefore be concluded that any solar sail should be very well designed in order to be profitable. This pressure is only theoretical since ideal conditions are assumed; later in this report actual deviations from this ideal case and their effects will be discussed.

$$F = 2 \cdot \frac{W_E \cdot A}{c} = 2 \cdot \frac{1368 \cdot 100}{2.99792 \cdot 10^8} = 0.913 \text{ mN}$$
 (2.9)

2.2.2. OTHER RADIATION

In the previous section solar radiation and the energy it provides was introduced; in this section possible other radiation sources are discussed. The Sun not only emits electromagnetic radiation, it also is a source of highly energetic particles. This stream of charged particles is called solar wind and can also be seen as a possible propulsion force for solar sailing. However, it has been proven that this is not the case. Although these particles are highly energetic and hold much more energy per particle since they have a finite mass, there are too few particles to actually have a relevant effect on the solar sail pressure. According to literature the force is three orders of magnitude smaller compared to the force caused by photons and can thus be neglected. [48]

The Sun is by far the most radiative body in our solar system, but other bodies radiate as well. When a mission is performed in the vicinity of a planet the radiation coming from this planet could also be relevant due to the much smaller distance. The radiation coming from the Earth will be discussed in the remainder of this section. There are two kinds of radiation coming from the Earth: black-body and albedo.

The black-body radiation is emitted since Earth has a certain temperature and can be calculated using Equation 2.1. The equilibrium temperature of the Earth is measured to be 255 K, this is well below the average surface temperature of 288 K since the Earth is not a black body and has an emissivity smaller than unity. Because Earth has no noteworthy internal heat source this temperature can be used as black-body temperature. [7] The electromagnetic radiation emitted by the Earth is found to be $1.23 \cdot 10^{17}$ W. Using Equation 2.2 the radiation from Earth received by a spacecraft can be calculated. This is done for a number of altitudes, the results are shown in Table 2.1. It can be seen that in an orbit close to the Earth, the contribution of black-body radiation actually is definitely too large to be neglected. However, for a spacecraft in a GEO orbit the solar radiation is the dominant factor while the Earth radiation only measures 0.4 % of the SRP.

Like all bodies, Earth does not absorb all energy of the radiation received, part of it will be reflected as albedo radiation. The amount of radiation reflected is dependent on the properties of the bodies and is expressed using the bond albedo. This bond albedo, A_b , defines the fraction of the received radiation that is directly reflected; the Earth bond albedo is found to be 0.306. [7] Using this value and the ratio of the Earth radius and the altitude of the spacecraft the albedo radiation received can be calculated. The albedo radiation is calculated and compared to the solar radiation in the same manner as before for Earth's black-body radiation. The results are presented in Table 2.1 and are similar to the ones found before. The contribution of albedo radiation is even larger than that of Earth's black-body radiation: almost 30% at an altitude of 100 km, at GEO altitudes the perturbation is reduced to just 0.7%.

The results from Table 2.1 show that in low Earth orbits Earth radiation should definitely be taken into account. For distances around GEO orbits or even further away, the radiation from the Earth can be neglected in most cases. During eclipse, the black-body radiation of the Earth could play a role, since solar and albedo

2. Solar Sailing

radiation are not present there. For calculating the values from Table 2.1 the Earth is assumed as a point radiating. If low-Earth orbits are considered, this assumption is not valid and the results will deviate from the actual case. But since the actual values are of the same order of magnitude, these calculations are precise enough to gain insight into the size of the perturbations. For this feasibility study, not every small perturbation has to be taken into account. As both albedo and black-body radiation from the Earth are less than 1% of the direct SRP, their effect will not be considered relevant in this thesis. The numbers in Table 2.1 are calculated using the radiation power, this power does linearly translates to the force and acceleration received by a solar sail, as proven in Equations 3.8 and 3.9. The values presented will thus be equal when considering the acceleration.

Altitude	Black-body Earth	Relative	Albedo	Relative
	radiation power		radiation power	
[km]	$[{\rm W}{\rm m}^{-2}]$	[%]	$[{\rm W} {\rm m}^{-2}]$	[%]
100	232	17.0	405	29.7
500	206	15.1	360	26.3
1000	179	13.1	313	22.9
GEO	5.49	0.40	9.57	0.70

Table 2.1: Earth albedo and black-body radiation power relative to SRP.

2.3. SOLAR SAIL SPACECRAFT

The solar sail is clearly the most important instrument of the spacecraft on a solar sail mission. Its performance depends on many design choices, such as material, configuration and dimension. The most important design choices will be discussed in this section, the possibilities and their relevance are discussed shortly.

2.3.1. CONFIGURATION

Throughout literature, three configurations are presented as a possibility: the square sail, the heliogyro and a spinning disk sail. These three configurations are the most investigated and seem like the most appropriate choice for a solar sail mission. All three will be discussed shortly, looking at the design, properties and their (dis-)advantages.

Looking at the three conventional designs of solar sails, all three have characteristics which give them advantages over the other. There is no configuration that is clearly the best one, as this choice also depends on the chosen mission and resulting requirements. Looking at the actual performed solar sail missions and the ones planned in the near future, a square solar sail is chosen by both NASA, ESA and JAXA demonstrator missions. [18][32][27] Although it is not the most optimal design and deployment is not easy, apparently it is still considered the best choice, likely due to its simplicity. No further research into the configuration is possible due to time constraints, therefore the square sail design is selected as the best choice and will be used for calculations and design considerations in the remainder of this report. The size of the sail depends on the mission objective and further design of the spacecraft, meaning this can not be defined yet. Looking at relevant missions, a sail measuring approximately 50×50 m can is reasoned possible to achieve as both ESA and NASA plan to use a sail of these measurements in the near future. If such a sail does not provide sufficient acceleration, possibilities for a larger sail should be investigated.

2.3.2. SQUARE SAIL

The square sail configuration is the most straightforward configuration and is shown in Figure 2.6 at the left side. This design consists of a square sail supported by four booms, reaching from the centre part to the corners of the sail. For structural and deployment reasons the square sail consists of four triangle-shaped sails spanned between the four booms. The square sail is actually a specific case of a polygon solar sail. Of the regular polygons, the square sail has an optimal relation between sail area and the length of the needed booms according to an analysis performed in [31]. Although this conclusion is far from final, the design of all polygons seems fairly similar and thus only the square sail is considered.

Attitude control and stability of the sail can be provided by the addition of control vanes at the tip of the booms. According to [48] suitable control can be achieved with vanes that only rotate around the axis of the

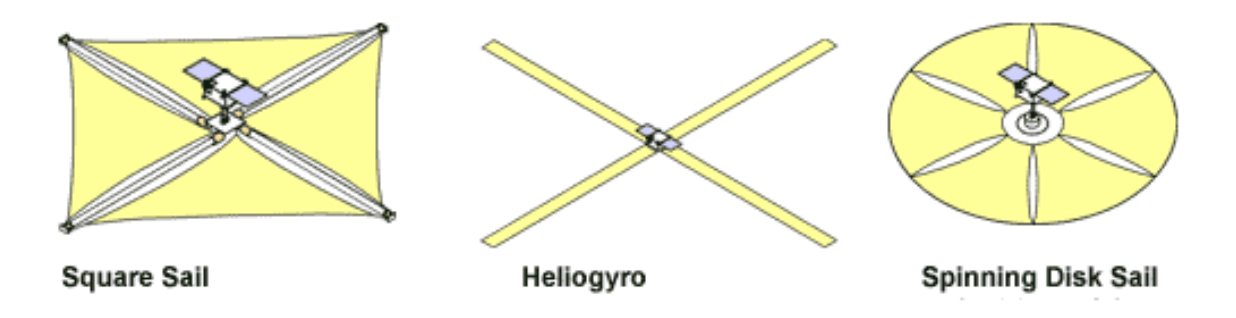


Figure 2.6: Visualization of the configurations; square, heliogyro and spinning disk sail.(NASA/JPL)

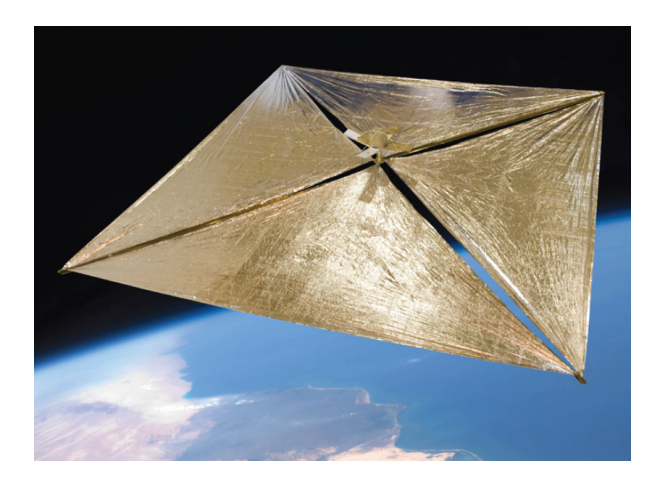


Figure 2.7: Square solar sail of the NanoSail-D spacecraft. [18]

boom they are connected to, therefore such vanes seem feasible to implement. Another way of providing control could be by creating an offset of the center of mass, however this is not equally effective at all attitudes with respect to the Sun. Combining both options could even lead to the optimal solution, but this decision is put off until the detailed design. The square sail is a fairly simple design and therefore also easily scaled. Another advantage is that its structural tension is used to keep the structure rigid and the sail flat. The main disadvantage of the square sail is the deployment; its shape and configuration induce difficulties in this process.

2.3.3. SAIL

A solar sail should be extremely lightweight and highly reflective, something that can not be achieved optimally using a single material. This means that the sail is to be made of a combination of three different materials; a reflective Sun side, an emissive anti-Sun side and a layer of base material in between. All three materials have an important role in the performance of the sail. The base material is the thickest layer and therefore has the largest influence on the mass and flexibility of the sail. Due to the extreme requirements, only a limited number of materials is suitable, all high quality and expensive polymers. The polymer not only has to be lightweight, but also resistant to high temperature (changes), suitable for production of very thin sheets and survive in space, a very hostile environment. According to multiple mission proposals Kapton is the best choice, a polymer from which sheets of only 5-7.5 μ m can be produced, while still providing enough strength. Both sides of the Kapton sheet should be vapor-coated with a suitable material in order to create a proper solar sail. One side will be covered with a highly reflective material, this side of the sail will act as a mirror. The reflectance of the material determines the fraction of the photons reflected and thus a higher reflectance increases the momentum transferred to the sail. Aluminium serves as a good choice for this coating: its reflectivity is 0.9 and a layer of only 20 nm can be applied to the Kapton. On the other side a coating of a highly emissive material will be applied, which will radiate unnecessary energy. This layer is needed to reduce the temperature of the sail, since about ten percent of the energy is absorbed inducing a large tem14 2. Solar Sailing

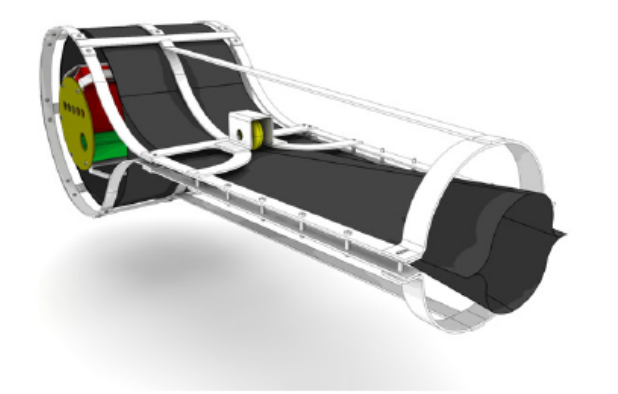




Figure 2.8: Visualization of mechanism of coiled boom (left) and CFRP boom in packed configuration. [40]

perature rise. For this side a coating of chromium is a proper choice: it has an emissivity of 0.7 and will be applied with a thickness of 20 nm as well.

In the future, high-performance sails with much better properties might become available. This would make considerably higher lightness numbers available and allow for more applications, production of even thinner Kapton sheets could provide another 2-3 times lower mass. Also a completely new base layer consisting of a carbon nano-tube sail might become a future option, this could make sails multiple times lighter, as these sheets weigh only $0.03 \, \text{g/m}^2$. [46] Lastly one could think of in-space production of solar sails without the polymer sheet, which would decrease the mass even further. However these sails would be extremely fragile and more temperature-sensitive, creating new difficulties. All of these concepts are still only ideas for the far future, no research is performed yet. These ideas are only mentioned here to show the potential of solar sailing; when such sails become reality a whole new range of missions becomes possible.

2.3.4. BOOMS

The main structural parts that hold the sail together are the four diagonal booms that govern the shape of the sail. These booms fulfil two functions: providing structural strength to keep the sail in shape and control the deployment phase. To provide this four coiled booms made of carbon fiber reinforced plastic (CFRP) are used. These booms consist of multiple layers of polymers and can thus be designed to satisfy the structural requirements; their specific mass is approximately 100 g/m. [12] A CFRP boom consists of two laminated sheets forming a tubular shape, which can be compressed to a flat shape and coiled together, see Figure 2.8. During deployment the booms will uncoil and return to their original form, thereby also unfolding the solar sail into its desired shape. Both the sail and booms are subjected to multiple forces and stresses, causing them to deform and affect the performance of the sail as discussed in Section 3.5.

2.3.5. SPACECRAFT

The solar sail is the most relevant subsystem of the spacecraft and dictates the total design of the spacecraft. It puts requirements on the payload in its allowed mass, size and orientation. The exact mass requirement can only be determined later in the mission design. Both the sail size and the desired orbit, and thus required lightness number, determine the allowed mass of the payload. The requirement of the size of the payload is determined mostly by the space available in the launcher after placement of the sail. The possibilities of the instruments will also be influenced by the placement, as the payload will be placed at the shadow side of the sail. The view of the instruments is therefore restricted, even when a hole in the center is present as was the case for IKAROS, see Figure 2.3. These limitations can be changing since the orientation of the sail is determined by orbital requirements. Deployment of the sail is a complex and risky phase of the mission, where many things could go wrong that would jeopardize the complete mission. The chosen deployment technique and process will give rise to restrictions and requirements on the complete spacecraft.

These requirements and restrictions will thus play a role in the final design of the spacecraft. However, since this research focuses on the orbital possibilities of solar sailing, these restrictions will not be researched thor-

2.4. Performance 15

oughly. Important restrictions limiting the choice of instruments or missions should be mentioned, but the exact implications of this is most likely left for other research.

2.4. Performance

For this thesis no detailed design of the actual sail is required, however the performance of a sail plays clearly a large role in the acceleration and thus the orbital perturbations. The exact detailed design of the spacecraft or even the sail is thus not needed, but some parameters need to be selected. As calculations later in this report will show, the sail performance is directly related to the lightness number of the sail. Although this thesis does not go into further detail of the exact design of the spacecraft and the solar sail, it is important to make some assumptions on the performance possible. Later in this research simulations will be performed and it is essential that a reasonable sail performance is assumed in order to say something about the actual feasibility of the found solutions.

Table 2.2 gives the performance parameters of a number of missions and mission studies. The sail loading is basically the mass-area ratio while the acceleration represents the maximal achievable acceleration in the vicinity of the Earth, which is calculated using Equation 2.9. The last column gives the elevation possible if all this force can be directed exclusively in upward direction, as will be discussed later in Section 3.7. Using the values presented in this table an assumption can be made for the performance of a possible solar sail. The table shows that very optimistic values have been used for the Halley mission study, that supposedly could be obtained using a massive heliogyro sail configuration. The high-performance sail mentioned in the last row is a suggested sail that could be produced in the far future, however this production is far from realisable. From these proposed values to the actual performance of IKAROS is a major step, however the design of IKAROS was not focussed specifically on the sail and its performance. Only a small sail was used mainly in order to prove the validity of the concept of solar sailing. The actual mission was a mission to Venus and although the spacecraft actually used the solar sail during part of its trajectory, it was not the main propulsion method for the complete transfer. But even this small sail obtained a cumulative acceleration adding up to approximately $\Delta V = 100 \text{ m/s}.[51]$

Looking at the Sunjammer the numbers are more promising, a sail loading of 22 g/m^2 is supposedly achievable with modern day technology and dimensions of $35 \times 35 \text{ m}$. For this thesis study a larger sail is assumed to be possible in the near future, a square sail with 50 m sides is clearly an optimistic presumption but seems reasonable enough to use here. This would double the sail area and improve the performance considerably. According to [31] and [30] solar sails in the near future should be able to achieve a solar sail loading of 9 g/m^2 . In the vicinity of the Earth this corresponds to a maximal acceleration of approximately 1 mm/s^2 . This value is taken as the reference value for the remainder of this research. However one should keep in mind that this number is rather high considering it is twice the value of the performances of planned future mission. However, the concept of elevated geostationary orbits is known to be more demanding for a solar sail than these missions and will only become commercial viable when a large step is made in the production and development of solar sails. Therefore this performance being larger than available seems reasonable. Literature suggest even better sails could become possible if enough is invested in the technique and sails made using nano technology may be able to achieve 6 mm/^2 , however this seems quite optimistic at the moment.

Although the sail loading is the actual property of the sail that is the relevant factor here, see 3.4, for Earth missions this parameter is linearly related to the characteristic sail acceleration. Therefore for the remainder of this report the performance of the sail will mainly be expressed using the characteristic sail acceleration rather than the physical parameter sail loading. The value of 1 mm/s² is thus chosen as the standard acceleration to work with. However it is only considered as a reference, flying using another performance should also be investigated. When the effect of changing the sail performance is known, more can be said about the importance of aiming indeed for such high numbers.

2.5. GEOSTATIONARY SATELLITES

Nowadays many satellites are launched every year, for several purposes. Besides specific scientific missions and flights to the International Space Station (ISS) commercial spaceflight has grown significantly over the last decades. The latter satellites are mainly communication satellites used for television, internet and navigation. A large share of these communication satellites are orbiting the Earth in a geostationary orbit, which

2. Solar Sailing

Satellite	Mass	Area	Sail loading	Acceleration
	[kg]	$[m^2]$	$[g/m^2]$	$[mm/s^2]$
IKAROS	310	200	$1.59 \cdot 10^3$	$5.7 \cdot 10^{-3}$
NanoSail-D	4	9	444	0.021
LightSail	4.5	32	141	0.065
Sunjammer	31	1200	26	0.35
Gossamer	81	2500	32.4	0.28
Near future	-	-	9	1
Halley mission study	-	-	5	1.8
High-performance sail	-	-	1.5	6

Table 2.2: Sail performance of missions, together with their achievable elevation.

means the spacecraft stays at a fixed position in space with respect to the Earth. The spacecraft thus maintains an equilibrium position with respect to the Earth surface. In order to achieve this, a number of requirements must be met. First of all the orbital period should be equal to a sidereal day, 23 hours, 56 minutes and 4 seconds, or 86 164 seconds. This sidereal day is defined as the period the Earth rotates once around its axis, measured with respect to the fixed stars. An orbit with a period equal to one sidereal day is called a geosynchronous orbit. When a spacecraft also is in a circular orbit, thus e = 0, the spacecraft will have a constant rotational velocity, equal to that of the Earth. Lastly, with the orbital plane in the equatorial plane, i = 0, the spacecraft will stay above a fixed position on Earth. When these three requirements are fulfilled, the orbit and the satellite are called geostationary.

As the period of a circular orbit solely depends on its radius, all geostationary spacecraft have the same altitude. For a spacecraft in a circular Kepler orbit, the gravitational attraction is counteracted by the centrifugal force and both thus have to be equal.

In this equation μ is the standard gravitational parameter, in case of the Earth with a value of $\mu=398,600.441$ m³/s² and ω is the rotational velocity, which can be found since the orbital period is one sidereal day. Using these values in the right-hand part of the equation, the radius of a geostationary orbit can be found to be 42,164 km, after subtracting the radius of the Earth the altitude is thus 35,786 km.

In theory a satellite at this altitude with the correct orbital velocity will stay exactly at a stable position compared to the Earth. Due to several perturbations, such as the Earth's non-spherical shape and attraction of the Sun and Moon, the spacecraft position of a geostationary satellite will however not be perfectly stable. Precession will change the longitudinal position of the spacecraft, while the orbit will also tend to become elliptical over time. Orbital stationkeeping manoeuvres are needed to maintain a fixed position. For this an annual ΔV budget of approximately 50 m/s is needed per geostationary satellite [43], the exact value depends on the characteristics and longitudinal position of the spacecraft.

The concept of a geostationary satellite was proposed by A. Clarke in 1945 [6], when he suggested using 3 geostationary satellites to provide a continuous and global radio coverage. The first spacecraft actually launched to a geostationary orbit was Syncom 3, launched in 1964. [42] Since then numerous satellites have been brought to a geostationary orbit. Since these satellites all orbit the Earth in the same orbital plane, only limited space is available. This space is currently divided into so-called slots which are assigned to certain companies of countries. This thesis will look for a way to create new possible slots using solar sailing. As solar sails offer almost continuous thrust, an orbital plane elevated above the equator might be achievable.

2.6. Orbital Requirements

As explained, several perturbation make it infeasible to keep a satellite at exactly the same position above the Earth. Therefore certain orbit requirements should be defined, which the orbit should fulfil in order to be suitable for geostationary communication. The geostationary belt is split up into different slots, which are assigned to be used for a certain satellite. The International Telecommunication Union decides on the

allocation of these slots needed for direct broadcast satellite services. The slots are defined by longitudinal boxes centred on a nominal longitude, with a tyrpical dimension of 0.1° . According to [43] it follows that geostationary satellites are kept within a station-keeping box that is related to these slots. If the satellite stays within this box, it is possible to achieve constant communication with the Earth, while using an antenna with a fixed orientation. Such a station-keeping box can be defined using a physical box around the desired spot, with dimensions typically around 75×75 km.

As the ground antenna is aiming in a certain direction it is in many cases more useful to define the allowed deviation in degrees. The maximum allowed longitude range is typically between 0.01 up to 0.5 degrees.[20] These requirements are often also expressed in Kepler orbital elements, with for example a maximum inclination and eccentricity of $i_{max} = 0.1^o$ and $e_{max} = 0.0005$. These values are related to the range of the longitude and latitude respectively and result in a station-keeping box of approximately 75×75 km as was mentioned before.

This thesis aims to find a orbital solution suitable for an elevated geostationary satellite. The orbital requirements defined for the resulting trajectories will be set an order of magnitude higher, at 7.5 km error in all directions. This more strict requirement is based on a number of reasons. First of all the program optimises trajectories of just three revolutions, meaning three days time. Requirements on the error during these three days should clearly be more strict than the general requirements as deviations tend to grow over time. Secondly, as shown in Section 3.7 the displacements that seem achievable will be some tens of kilometres at most. For a displacement of for example 30 km it make not sense to use a limitation of the orbital error similar to the displacement as the satellite will then still be able to interfere with the normal geostationary satellites. Lastly the requirement seems reasonable to achieve as the satellite has continuous thrust available as it is equipped with a solar sail. Normal geostationary have small thrusters on board to correct the orbital deviation a number of times per year. This means the deviation from the original position grows gradually over time and when it approaches the limits of the station-keeping box, an small propulsion shot is used to steer it back towards the centre of the box. Using continuous thrust it should be possible to keep the satellite much closer to the reference possible position. In this thesis the deviation from the desired position is assessed by looking at the offset seen when looking at the satellite from the Earth surface, a more thorough explanation and definition is provided in Section 5.4.3.

ORBITAL DYNAMICS

This chapter gives an overview of the orbital dynamics relevant for a solar sailing mission, starting with the basics of reference frames and coordinate systems. Orbital dynamics for spaceflight in general will be used as an introduction after. The influence of including a solar sail and solar radiation pressure on the trajectory will be the next part of the chapter. The orbital dynamics part is followed by a short discussion on the non-ideal circumstances that will always be present in real time and will perturb the perfect conditions assumed before. This is done using a quantitative analysis of the various sources of perturbing forces, their causes and their effects. Lastly a first-order calculation is performed in order to get an idea of the achievable displacements.

3.1. Reference Frames

Before any calculations can be performed, one should specify under which circumstances these calculations hold. For astrodynamical problems, this is done by defining a reference frame. A reference frame is defined by specifying both the origin and orientation of the fundamental axes of the system. These definitions allow to describe any point by a unique set of coordinates.

Physics and especially orbital dynamics is based on Newton's three laws describing the relations between time, space, acceleration and forces. These three laws only hold in an inertial reference frame, meaning it is at rest and not accelerating. Such an inertial reference frame can however never be defined properly. Therefore one can introduce a so-called 'locally inertial reference frame'. Such a frame can be defined for a number of objects falling freely in a uniform gravity field. The basic idea behind this is that free-fall is actually an inertial motion. Since true free fall is only possible in a uniform gravity field, the reference frame only holds in some limited region. [23] For this study, just as almost all problems, the distances considered are well within this region and an inertial reference frame can be assumed. Several kinds of reference frames exist, but only two are relevant and used in this thesis.

3.1.1. EARTH CENTRED INERTIAL

The reference frame used for most calculations is an Earth Centered Inertial (ECI) reference frame. An ECI-frame is a reference frame with its origin set at the center of the Earth whereas its axes are fixed relative to the stars. The direction of these axes can be defined in several ways, the most used ECI is the J2000 frame. In this frame the X-axis is defined as the mean equinox at 12:00 terrestrial time on January 1, 2000, while the rotation axis of the Earth is chosen as the Z-axis of this frame. The ECI used in this thesis is defined relative to the Earth at the start of the simulation. At t = 0 the X-axis points from the center of the Earth through the equator at zero longitude. The rotational axis of the Earth defines the Z-axis, and the Y-axis points through the equator at 90^{o} longitude thereby finishing this right-hand frame. This definition may seem trivial, but it is chosen for programming reasons. It should be noted that in some cases a more simple model is used and the equator is assumed to be in the ecliptic plane, this automatically changes the definition of the reference frame.

This ECI-frame is used to describe the position, velocity and acceleration of the spacecraft and is thus used during the integration. All forces and perturbations acting on the frame are therefore first converted to the

3. Orbital Dynamics

ECI-frame if needed.

3.1.2. EARTH CENTRED FIXED

The Earth Centered Fixed (ECF) reference frame, as the name suggest, has the center of the Earth as its origin. The direction of the axes is again defined at the start of the simulation, however for the ECF-frame they are fixed to the Earth surface. At the start of the simulation the axes of the ECF-frame are set exactly the same way as for the ECI-frame and both thus perfectly align. These axes are fixed to the Earth surface and thus the X-axis will stay set at zero longitude and will rotate along with the Earth. During one sidereal day, the frame completely rotates around its Z-axis, after which it is aligned with the ECI-frame again.

For some calculations the shape of the Earth and thus the position of the spacecraft relative to it are of importance. Here this is relevant for the calculation of the J_{22} perturbation, and the ECF-frame is thus used for these calculations. The same holds for the offset of the satellite to its desired stationary point as seen from Earth.

3.1.3. Transformation

Apart from choosing the best reference frame for a certain situation, also the relation between different frames is important. When changing from one frame to another, one should be able to change the coordinates accordingly. Most of the time such a transformation can be split up in a rotation and a translation. The translation is simply done by adding the relevant vector connecting both frames, transformation due to rotations is a bit more complex. In order to correctly find the new coordinates, so-called transformation matrices and Euler angles are used. These Euler angles represent the rotations about relevant axes of the frame, while the matrices give the new coordinates. These transformations can be defined using so-called transformation matrices, the more complex the transformation the more elaborate the matrix needed.

Transformation between the two used reference frames is fairly simple in this case. The origins of the frames are always exactly the same and therefore no translation is considered. The ECF-frame rotates around its Z-axis, while the ECI is inertial and does not rotate. This means that only one rotation is performed around the Z-axis. The change from ECI- to ECF-coordinates can therefore be calculated using the transformation matrix defined as:[11]

$$\begin{bmatrix} X_{ECF} \\ Y_{ECF} \\ Z_{ECF} \end{bmatrix} = \mathbb{T}_{21} \begin{bmatrix} X_{ECI} \\ Y_{ECI} \\ Z_{ECI} \end{bmatrix}$$

With:

$$\mathbb{T}_{21} = \left| \begin{array}{ccc} \cos\phi t & -\sin\phi t & 0 \\ \sin\phi t & \cos\phi t & 0 \\ 0 & 0 & 1 \end{array} \right|$$

The angle ϕ describes the rotation between the two reference frames and can be chosen arbitrarily. As the ECI-frame is inertial as opposed to the ECF-frame, their relative rotation changes over time. Every synodic day the ECF-frame makes a full rotation with respect to the ECI-frame. A sidereal day is 84184 seconds long in which it rotates 2π radians, the rotational velocity Ω is found to be $\Omega = 7.465 \cdot 10^{-5}$ rad/s. This velocity is now used to find the angle ϕ at any moment in time, $\phi(t) = \Omega \cdot t$.

For the reversed transformation, from ECF- to ECI-coordinates, the same matrix can be used but the rotation angle changes sign. This means the negative angle is taken and the frame is rotated counterclockwise.

3.2. COORDINATES SYSTEMS

Once a suitable reference frame is established, the coordinates to describe a position in this frame are needed. The most well-known coordinate system is the rectangular or Cartesian coordinate system. In this system, the three axes X, Y and Z of a reference frame are also used to define a position. The position is described by the three values of the distance measured along the respective axis when going from the origin to the point, as can be seen in Figure 3.1. All calculations in this thesis are performed using Cartesian coordinates as they work very straightforward and can be converted between different reference frames rather easily. Cartesian coordinates are also suitable for plotting the trajectory of a spacecraft.

However, for some physical problems or definitions spherical coordinates are more suitable. The three spherical coordinates are r which is the radial distance from the origin to the point, while the two others ϕ and θ are the azimuth and the polar angle respectively, see Figure 3.1.

Figure 3.1: Cartesian and spherical coordinates visualized. [left] Definition of Kepler elements. [right]

Both Cartesian and spherical coordinates work similarly: they describe a point and its velocity at a certain point at a certain time, while changing continuously over time. A completely other kind of coordinate system are the Kepler orbital elements a, e, i, Ω , ω and τ . These six independent constants fully describe the orbit of a body in space. When time is known, the instantaneous position and velocity of the body can be calculated as well. As can be expected these orbital elements are only applicable in specific cases, being Kepler orbits or conical sections. A Kepler orbit is the trajectory an unperturbed object will follow under the influence of only gravity of the spherical main body around which it orbits. These trajectories are often treated in orbital dynamics and are therefore used in many cases. The different elements are: semi-major axis α , eccentricity e, inclination i, argument of pericenter ω , right ascension of the ascending node Ω and the time of the last pericenter passage τ .

A visual representation of their definitions is given in the right-hand side of Figure 3.1. Using these Kepler elements has a number of advantages in orbital dynamics, the most important one being the good insight of the complete orbit they provide. However, for certain orbits not all elements can be defined properly. For example, considering an orbit with an inclination of zero degrees, the right ascension of the ascending node Ω is not defined because the orbital plane does not cut through the equitorial plane. In order to avoid these problems, another set of orbital elements is constructed which avoid these singularities. These so-called equinoctial elements are p, f, g, L, h and k. These elements can be constructed using the original Kepler elements, formulas for this can be found in [23] or other literature. The same holds for the complete transformation rules between the different coordinate systems.

Comparing these systems, different characteristics and advantages are shown by these systems. Cartesian coordinates can describe the exact position and velocity of an object at a certain time very clearly. Using Kepler elements, the exact position and velocity in the reference frame are not always immediately clear. It gives however much more insight in the orbit the object follows and the position in this orbit. Because of these different properties, the state of the spacecraft is calculated in all three sets of coordinates. At each point, the state is given in Cartesian coordinates that are then converted into both spherical coordinates and Kepler elements.

22 3. Orbital Dynamics

3.3. EQUATIONS OF MOTION

The equations of motion (EoM) of a spacecraft in space are mainly governed by Newton's law of gravity: two particles attract each other with a force directly proportional to their masses and inversely proportional to the square of the distance between them. [23] This law can be written as the following mathematical formula:

$$F = G \frac{m_1 m_2}{r^2} \tag{3.1}$$

Starting from this equation and using Newton's second law, the following relation can be set up to describe the motion of a body i in an inertial reference frame, under the influence of other bodies j:

$$m_i \frac{d^2 \mathbf{r}_i}{dt^2} = \sum_{j \neq i} G \frac{m_i m_j}{r_{ij}^3} \mathbf{r}_{ij}$$
(3.2)

This relation holds for an unlimited number of bodies and can thus be used for almost all problems. However, taking into account infinite bodies is very time consuming and not needed in practical cases, therefore certain assumptions are made. These assumptions lead to the fact that Equation 3.2 can be simplified significantly.

The case where only two masses are considered is called a two-body problem, this is the case in for example the heliocentric orbit of the Earth. For this system Equation 3.2 can be simplified even more and the movement of a body around the barycentre of the system is described as:

$$\frac{d^2\mathbf{r}}{dt^2} = -\frac{G(m_1 + m_2)}{r^3}\mathbf{r} = -\frac{\mu}{r^3}\mathbf{r}$$
 (3.3)

with:
$$\mu = G(m_1 + m_2)$$

For most two-body problems the primary mass m_1 is much larger than the secondary mass m_2 , meaning $m_1 >> m_2$ holds and the smaller mass can be neglected. A consequence is that the main body is at rest at the center of mass of the system and the secondary body is orbiting it. This means that only one radius is of importance as the distance between the bodies is the same as the distance between m_2 and the origin of the system. If this is the case, Equation 3.3 describes the orbit of m_2 around the primary body m_1 . Further more the value of the standard gravitational parameter μ only depends on m_1 and the gravitational constant G. This means that μ becomes a characteristic of a celestial body, and the mass of the satellite does not play a role in the orbit it makes.

Equation 3.3 results in a perfectly unperturbed Kepler orbit as only one gravitational force is acting upon the satellite. In reality this is never the case as there will always be perturbations acting on the satellite. This does however not mean that Equation 3.3 can not be used, non-gravitational perturbations can simply be added as an extra acceleration. In the following section the effect of solar radiation pressure on the orbital dynamics is explained. Later in the chapter, other perturbations and their effects are presented and discussed.

3.4. SOLAR SAILING

In this section the effect of solar sailing on the equations of motion will be discussed and the effect of SRP will be included in the equations derived in the previous section. A spacecraft orbiting in the vicinity of a planet, for example the Earth, can be described using a two body system. For this thesis the problem described is a geostationary satellite orbiting the Earth and can be described as a two-body problem with the addition of an extra force, the solar radiation pressure. The equations of motion for a geostationary satellite carrying a solar sail are given as:

$$\frac{d^2\mathbf{r}}{dt^2} = -\frac{\mu_E}{r^3}\mathbf{r} + \frac{\mathbf{f}(r_S)}{m}$$
(3.4)

This formula described the motion in the ECI-frame, μ_E is the gravitational parameter of the Earth and \mathbf{r} the position relative to the Earth and \mathbf{r}_S is the distance of the satellite to the Sun. From this formula it can be concluded that the SRP induced force has a value that is related to the distance to the Sun, as was already seen in Equation 2.8. The distances travelled by a spacecraft orbiting the Earth are only minor related to the distance to the Sun, which is therefore taken as a constant. The value of the solar radiation pressure is thus

3.4. SOLAR SAILING 23

defined by the distance of the Earth to the Sun, in the vicinity of the Earth this value is $W_E = 1368 \text{ W/m}^2$. Starting with this pressure, the force exerted can be found by multiplying with the area. When a perfect reflecting sail is considered, the incident photons are reflected perfectly without energy loss and the situation in Figure 3.2 will be applicable resulting in two equal forces, albeit in different directions. The vectors of these two forces, due to incident f_i and reflected f_r photons, can be written down as:

$$f_i = PA(\mathbf{u_i} \cdot \mathbf{n})\mathbf{u_i} = \frac{W_E A}{c}(\mathbf{u_i} \cdot \mathbf{n})\mathbf{u_i}$$
(3.5)

$$f_r = -PA(\mathbf{u_i} \cdot \mathbf{n})\mathbf{u_r} = \frac{W_E A}{c}(\mathbf{u_i} \cdot \mathbf{n})\mathbf{u_r}$$
(3.6)

In these equations the part $A(\mathbf{u_i} \cdot \mathbf{n})$ is the projected solar sail area in the $\mathbf{u_i}$ direction, as $\mathbf{u_r}$ is defined away

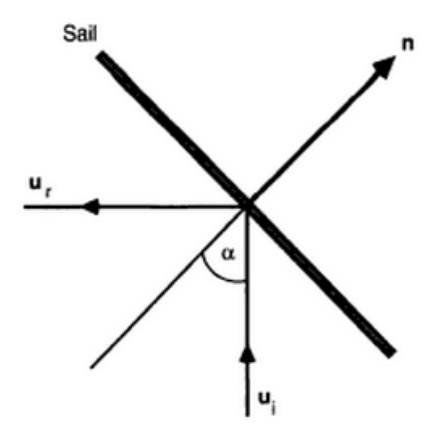


Figure 3.2: Forces acting on a perfectly reflecting solar sail.[31]

from the sail there is a minus sign in f_r . Using the vector identity $\mathbf{u_i} - \mathbf{u_r} = 2(\mathbf{u_i} \cdot \mathbf{n})\mathbf{n}$ both forces can be added up resulting in a total force, which then can be rewritten using Equation 2.7 resulting in:

$$f = f_i + f_r = \frac{2W_E}{c} \left(\frac{r_E}{r}\right)^2 (\mathbf{u_i} \cdot \mathbf{n})^2 \mathbf{n}$$
(3.7)

By introducing the sail pitch angle α as defined in Figure 3.2 the force and eventually the acceleration can be written as:

$$f = \frac{2W_E A}{c} \left(\frac{r_E}{r}\right)^2 \cos^2 \alpha \mathbf{n} \tag{3.8}$$

$$a = \frac{2W_E A}{c \cdot m} \left(\frac{r_E}{r}\right)^2 \cos^2 \alpha \mathbf{n} \tag{3.9}$$

This formulation makes calculations and visualisation more easy since only one vector is included, already determined by α . This angle depends on the orientation of the sail with respect to the Sun. As Equation 3.9 is define in an Earth-centred reference frame, the position of the frame w.r.t. the Sun, and thus the direction of the sunline, changes over time. Figure 3.3 shows the movement of the Sun in the two-body system defined using the the ECI-reference frame. With a rotational period of one year, the rotational velocity can thus be found to be:

$$\Omega_{ES} = \frac{2\pi}{Year_{sidereal}} = \frac{2\pi}{365.256363 \cdot 24 \cdot 3600} = 1.99 \cdot 10^{-7} \text{rad/s} = 0.986 \text{deg/day}$$
(3.10)

This means that the direction of the sunline is dependent on the day of the year. This implies the achievable acceleration by a solar sail also depends on the time of the year. Figure 3.3 shows the situation for a 2D-case, where the Sun rotates exactly in the XY-plane, or really Earth's rotational axis is aligned it orbital plane. Due to the tilted rotational axis of the Earth, this is not actually true and the sunline does not always lay in the equatorial plane, the XY-plane in the ECI-frame. Although the rotation should thus be defined in 3D, the rotational period, and thus velocity, stay the same as shown previously.

24 3. Orbital Dynamics

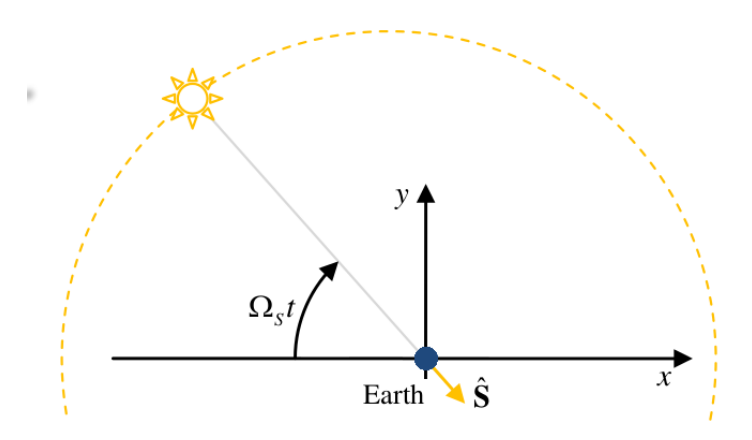


Figure 3.3: Two body system, including the direction of the sunline. [22]

For some cases it is desirable the acceleration can be easily compared with solar gravitational acceleration. In order to write the acceleration in terms of the solar gravitational attraction similar to Equation 3.4, two new parameter are introduced. The sail loading α is the mass-to-area ratio, the critical sail loading σ^* is the value where both accelerations are equal and can be found to be:[31]

$$\sigma^* = \frac{L_S}{2\pi G M_S c} = 1.53 \text{ g/m}^2 \tag{3.11}$$

The lightness number β is defined as the ratio between the acceleration due to the SRP and gravity from the Sun. This means the lightness number can be used to write the sail acceleration similar to a gravitational term.

$$\beta = \frac{a_s}{a_g} = \frac{\sigma^*}{\sigma} \tag{3.12}$$

$$a = \beta \frac{GM_S}{r^2} \cos^2 \alpha \mathbf{n} \tag{3.13}$$

The sail acceleration depends on the distance to the Sun, the lightness number and the orientation of the sail. It can now easily be implemented in the equations of motion for a two-body problem, earlier defined in Equation 3.4. The result is as follows:

$$\frac{d^2\mathbf{r}}{dt^2} = -\frac{Gm_1}{r^3}\mathbf{r} + \beta \frac{Gm_S}{r_S^2}\cos^2\alpha\mathbf{n}$$
(3.14)

As for this thesis only geostationary orbits are considered the distance to the Sun is assumed constant. This also means that the complete left part of Equation 3.13 is fixed and can be substituted by a constant, the characteristic acceleration.

$$a = a_{acc} \cos^2 \alpha \mathbf{n}$$
 (3.15)
With: $a_{acc} = \beta \frac{GM_S}{r^2}$

The characteristic acceleration a_{acc} will be the maximum acceleration at a certain distance to the Sun, achieved when the sail is directed exactly towards the Sun. In the programming of the tool, this calculation of the sail acceleration is used as it is easier to define as input. As this a_{acc} is directly coupled with the lightness number of the sail, see Table 2.2, this will give exactly the same results as long the proper acceleration is chosen.

3.5. Non-ideal Sail

The formulas describing the effects of solar radiation pressure on the orbital dynamics of a spacecraft were all based on a theoretical, perfect sail. However, due to several physical effects a solar sail will in practice never be perfect. Therefore the non-ideal deviations need to be evaluated. The two major imperfections are the reflectivity of the material and deformation of a physical sail.

3.5. Non-ideal Sail 25

3.5.1. REFLECTIVITY

In Section 3.4, the reflectivity of the sail was assumed to be perfect. Perfect reflection means two forces with both equal magnitude and angle relative to the sail normal, as seen in Figure 3.2. For a non-ideal sail its reflectance, absorption and emissivity are all taken into account, meaning the force exerted on the sail consist of three contributions, as seen in Figure 3.4:

$$\mathbf{f} = \mathbf{f_r} + \mathbf{f_a} + \mathbf{f_e} \tag{3.16}$$

The magnitude and direction of these forces can be calculated using the properties of the sail and its mate-

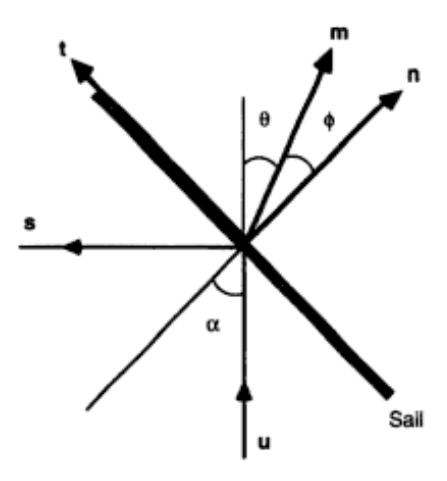


Figure 3.4: Non-perfectly reflecting solar sail.[31]

rial. The most important coefficients are the reflection, absorption and transmission coefficient, respectively named \tilde{r} , a and τ . Their meaning can be explained using Figure 3.4 as they describe the three ways photons following \mathbf{u} can proceed after hitting the sail. On a solar sail most photons will be reflected in direction \mathbf{s} , while a small part will either follow a straight line through the sail as they are transmitted and another part is absorbed by the sail and will not continue further. These coefficients can be seen as fractions of the incident photons, so they add up to one. Since the sail material is typically very reflective, the transmission coefficient τ is very small and can be neglected. Still absorption and reflection play a role and the simplified case of Figure 3.2 does not hold any more; this new situation is visualised in Figure 3.4. Due to these considerations, the resultant force is not acting perpendicular to the sail but its direction depends on the magnitude of the two forces. In Figure 3.4 the direction of the resultant force is given by the vector \mathbf{m} . The forces mentioned in Equation 3.16 can best be expressed in parts in the direction of \mathbf{n} and \mathbf{t} .

The pitch angle α is still the angle between the impending light and the sail normal, however in contrast to before the cone angle θ is not equal to α any more due to the imperfections. The difference between these angles is called angle ϕ and is a measure for the deviation of the sail. In order to find the magnitude and the angle ϕ of the resultant force the relations between the unit vectors seen in Figure 3.4 are set up:

$$\mathbf{u} = \cos \alpha \mathbf{n} + \sin \alpha \mathbf{t} \tag{3.17}$$

$$\mathbf{s} = -\cos\alpha\mathbf{n} + \sin\alpha\mathbf{t} \tag{3.18}$$

Since the transmission is neglected, all photons will be blocked by the sail, the force related to this process is the absorption component. This means that the absorption force $\mathbf{f_a}$ can be described as:

$$\mathbf{f_a} = PA\cos\alpha\mathbf{u} = PA(\cos^2\alpha\mathbf{n} + \cos\alpha\sin\alpha\mathbf{t}) \tag{3.19}$$

After this, part of the light reflected and another part is emitted. A fraction \tilde{r} will be reflected, whereas the coefficient s is the fraction of the specularly reflected light. The rest is reflected non-specularly, the direction depends on the coefficient B_f describing the deviation from the completely uniform reflection of a Lambert surface. The force due to reflecting photons thus consists of two parts, given by:

3. Orbital Dynamics

$$\mathbf{f_{rs}} = -\tilde{r}sPA\cos\alpha\mathbf{s} = \tilde{r}sPA(\cos^2\alpha\mathbf{n} - \cos\alpha\sin\alpha\mathbf{t})$$
 (3.20)

$$\mathbf{f_{ru}} = B_f \tilde{r} (1 - s) PA \cos \alpha \mathbf{n} \tag{3.21}$$

The third force f_e is due to the emission of photons and depends on the sail temperature and the emissivity properties of the sail material. Assuming a flat sail and therefore a constant temperature the force can be written as:

$$\mathbf{f_e} = \frac{\tilde{\sigma} T^4}{c} (\epsilon_f B_f - \epsilon_b B_b) \mathbf{n}$$
 (3.22)

The temperature of the sail depends on the thermal input and output of the sail; from equilibrium of these two the temperature can be found:

$$T = \left(\frac{1 - \tilde{r}cPcos\alpha}{\tilde{\sigma}(\epsilon_f + \epsilon_b)}\right)^{\frac{1}{4}}$$
(3.23)

Combining Equations 3.19 to 3.23 one can construct the total forces in the directions of both \mathbf{n} and \mathbf{t} .

$$\mathbf{f_n} = PA\left((1 + \tilde{r}s)\cos^2\alpha + B_f(1 - s)\tilde{r}\cos\alpha + (1 - \tilde{r})\frac{\epsilon_f B_f - \epsilon_b B_b}{\epsilon_f + \epsilon_b}\cos\alpha\right)\mathbf{n}$$
(3.24)

$$\mathbf{f_t} = PA(1 - \tilde{r}s)\cos\alpha\sin\alpha\mathbf{t} \tag{3.25}$$

Since both forces are directed normal to each other, the magnitude of the resulting force can be found as:

$$f = \sqrt{f_n^2 + f_t^2} (3.26)$$

The direction of the force is defined by the center-line angle ϕ , which is the angle between the force and the normal of the solar sail as shown in Figure 3.4, given by:

$$\phi = \tan^{-1} \frac{f_t}{f_n} \tag{3.27}$$

For a perfect sail the angle ϕ will be zero and the cone angle θ will be equal to the pitch angle α . This is also the case angle when the sail is perpendicular to the Sun-line, ϕ will again be zero and the deviation is only in magnitude. For all other cases of a non-ideal sail the ϕ is finite and the cone angle can be found using $\theta = \alpha - \phi$. The relation between the cone and pitch angle for an ideal and non-ideal sail is given in Figure 3.5.

It can be seen that using a non-ideal sail the cone angle is always less than the pitch angle and therefore the maximum achievable cone angle is smaller than 90° . The exact value of this maximum angle depends on the actual coefficients of the sail, but will be of similar value as shown. For this figure and calculations the properties of the considered sail are: $\tilde{r} = 0.88$, s = 0.94, $\epsilon_f = 0.05$, $\epsilon_b = 0.55$, $B_f = 0.79$ and $B_b = 0.55$.[31] With these sail properties the maximum cone angle achievable is only 55.5° and is reached with a pitch angle of 72.6° . This means increasing the pitch angle beyond 72.6° will decrease the effective cone angle. The cone angle, thus the direction of the force with respect to the Sun line, therefore can not be larger than 55.5° . When calculations using a real sail are performed, the actual coefficients of the sail should be used if known, otherwise the mentioned values can be used as a reference.

3.5.2. DEFORMATION

Apart from the non-perfect reflection of the sail material, the shape of the sail will also cause deviations from the ideal case. Due to imperfections and the physical loading of solar radiation, structural stresses will occur and cause deformations in the sail and booms. This means the sail will not be completely flat, which affects the incident area and thus the magnitude and direction of the force. The derivations and exact structural deformations are beyond the scope of this research, the numbers found by the NASA/JPL mission study for a Halley rendezvous mission are used as an reference. [31] Although these numbers are based on a solar sail size that does not seem possible, it can serve as a reference and is probably a conservative assumption for a much smaller sail. Therefore the following force model will be used to estimate the actual direction and magnitude of the force, the coefficients are given in Table 3.1. If the actual sail dimensions and properties

3.6. Perturbations 27

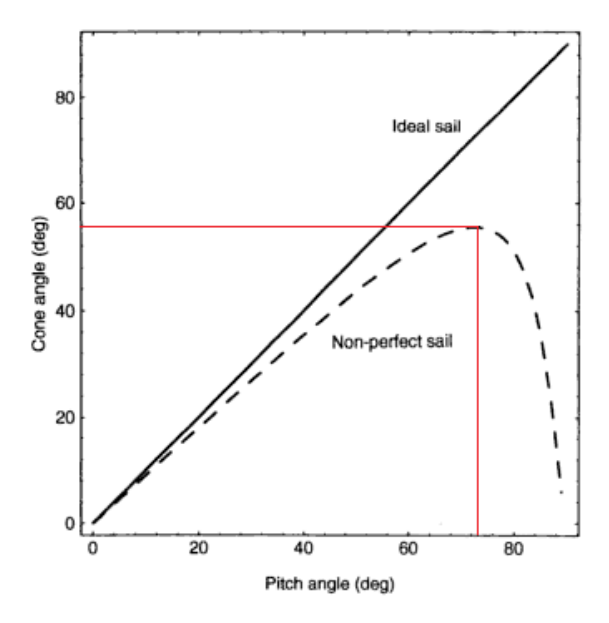


Figure 3.5: Normalized force on ideal vs non-perfect sail.[31]

are known, a new look should be taken into these coefficients. Equation 3.28 shows the relation of the force acting for a solar sail oriented normal to the Sun-line f_0 and the resulting force \mathbf{f} .

$$\mathbf{f} = f_0(C_1 + C_2\cos 2\theta + C_3\cos 4\theta)\mathbf{m} \tag{3.28}$$

Table 3.1: Force coefficients for square and heliogyro sail.

	C_1	C_2	C_3
Ideal sail	0.5	0.5	0
Square sail	0.349	0.662	-0.011
Heliogyro	0.367	0.643	-0.10

It is shown that many factors influence the performance of a sail, leading to a case deviating from the perfect sail described before. These deviation will certainly have an effect on the sail performance and the received sail accelerations will differ in both magnitude and direction. However, in this stage of the research the sail is not yet designed enough in order to make a solid reasoning for the exact deviations. Therefore for the remainder of this report, an perfect sail will be assumed. This means the equations introduced in Section 3.4 are used for the calculations. The fact that these calculations thus describe a model that is not completely valid should be kept as an consideration during further design stages.

3.6. PERTURBATIONS

The main force acting on a spacecraft is the gravitational attraction, in the case of a geostationary satellite the attraction from the Earth. This attractive force for a perfect spheroid is found using Equation 3.3. The Earth is however not a perfect sphere and this causes variations in the gravitational attraction. For spacecraft far away the Earth still seems as a point mass and these deviations do not play a role. However, for satellites in Earth orbit, these deviations should be considered as they can have significant influence. The gravity field of the Earth can best be described using spherical harmonics and so-called J-terms. J-terms are coefficients that describe the magnitude of a certain deviation of the Earth gravitational field relative to a perfect sphere. These terms can be split into three categories, zonal, sectorial and tesseral harmonics, which are shown in Figure 3.6. The gravity potential of the Earth including these spherical harmonics deviations can be described using:

$$U = -\frac{\mu}{r} \left[1 - \sum_{n=2}^{\infty} J_n \left(\frac{R_e}{r} \right)^2 P_n(\sin \delta) + \sum_{n=2}^{\infty} \sum_{m=1}^{\infty} J_n \left(\frac{R_e}{r} \right)^2 P_{n,m}(\sin \delta) \cos(m(\lambda - \lambda_{n,m})) \right]$$
(3.29)

28 3. Orbital Dynamics

$$f = -\nabla U = -\left(\frac{\partial U}{\partial x}, \frac{\partial U}{\partial y}, \frac{\partial U}{\partial z}\right) = -\left(\frac{\partial U}{\partial r}, \frac{\partial U}{\partial \delta}, \frac{\partial U}{\partial \lambda}\right) \tag{3.30}$$

These deviations are small compared to the total gravity, but for certain orbits they can play a role due to resonance. Especially for geostationary orbits these perturbations are important, as the position of the spacecraft is constant the perturbations act always in the same direction and therefore can add up to considerable amounts. For this research both the J_2 and J_{22} will be considered, their coefficients as mentioned in the previous equations are respectively $1.0826357 \cdot 10^{-3}$ and $1.8155628 \cdot 10^{-6}$. The remaining harmonics factors are small enough compared to the other perturbations and will thus be neglected. When only J_2 and J_{22} are considered, Equation 3.29 can now be written as:

$$U = -\frac{\mu}{r} \left[1 - J_2 \left(\frac{R_e}{r} \right)^2 \frac{1}{2} \left(3 \sin^2 \delta - 1 \right) + J_{22} \left(\frac{R_e}{r} \right)^2 3 \cdot \left(1 - \sin \delta^2 \right) \cos \left(2 \cdot (\lambda - \lambda_{2,2}) \right) \right]$$
(3.31)



Figure 3.6: Spherical harmonics describing the deviation from a perfect sphere, from left to right: zonal, sectorial and tesseral harmonics. [24]

3.7. FIRST-ORDER CALCULATION

In order to get a rough feeling of the amount of displacement that could be achieved using a solar sail, this section present a first-order analysis of the problem. A highly simplified 2D, static equilibrium will be assumed, no perturbations are considered, only the gravitational attraction of a perfectly spherical Earth. Using force equilibria the order of displacement achievable for continuous thrusting is derived. Both the vertical and horizontal displacement is investigated. Similar calculations were outlined in a paper by Forward in 1984[17], although only vertical displacement was considered in that paper.

The possible vertical displacement with a given sail, and thus acceleration is analysed using a simple, static force equilibrium. A satellite in the equatorial plane at a geostationary distance, r_{GEO} , from the center will be in a equilibrium position, since the gravitational attraction equals the centrifugal force. This equilibrium position holds in an Earth centred, co-rotating reference frame, from which the XZ-plane is shown. When this satellite is placed at the same position, but at a vertical displacement of z above the equatorial plane the situation changes. As the position changes, so does the direction of the gravitational force. As can be reasoned, the gravitational force now has a vertical component that needs to be compensated by the solar sail. Following some simple equations, the relation between this force and the displacement can be found. The magnitude of F_z , the vertical component of gravitational attraction, can be found using the angle θ and F_g , the total gravitational force:

$$\sin\theta = \frac{z}{r} = \frac{F_z}{F_g} = \frac{a_z}{a_g} \tag{3.32}$$

When assuming a small displacement, the change in the r can be neglected. The distance will thus stay constant, $r = r_{GEO}$. Then the acceleration needed for a given vertical displacement can be found using:

$$a_z = a_g \cdot \sin\theta = \frac{\mu}{r^2} \cdot \frac{z}{r} = \frac{\mu}{r^3} \cdot z \tag{3.33}$$

In order to express the displacement in terms of the force needed, one can rewrite this equation as follows.

$$z = a_z \frac{r^3}{\mu} = \frac{42,164,169.6^3}{3,986004.418 \cdot 10^8} \cdot a_z = 1.88 \cdot 10^8 \cdot a_z$$
 (3.34)

For this simplified example the elevation achieved is thus linearly related to the acceleration in vertical direction. This situation requires constant acceleration in the out-of-plane direction and is therefore not a

completely honest case. The direction of the sail acceleration depends on both the sail loading and the direction of the sunlight. It is therefore not possible to achieve a maximum constant acceleration solely in the Z-direction.

The total acceleration of a perfectly reflecting sail at 1 AU from the Sun is given by:

$$a_0 = \frac{2W_E}{c\sigma} = \frac{2 \cdot 1368}{3 \cdot 10^8} \cdot \frac{1}{\sigma} = 9.12 \cdot 10^{-6} \frac{1}{\sigma} m/s^2 = 9.12 \cdot 10^{-6} \frac{A}{m} m/s^2$$
(3.35)

In this equation σ is the mass-to-area ratio of the sail, or the total spacecraft, also known as the sail loading parameter. This is the total acceleration, achieved in the direction of the Sun-line if the sail is orientated perpendicular to it. The actually useful acceleration is however considerably less, as the solar radiation is direction in another direction.

$$\mathbf{a} = a_0 \cdot (\mathbf{u_i} \cdot \mathbf{n})^2 \mathbf{n} = a_0 \cdot \cos^2 \alpha \cdot \mathbf{n}$$
 (3.36)

The angle α here is called the pitch angle and is the angle between the sail and the sunline. Furthermore, this does not yet provide the vertical acceleration as \mathbf{n} is not pointing in this direction. When assuming the Sun-line along the equator and a pitch angle of 45^o the force is diminished by a considerable factor.

$$a_z = a_0 \cdot \cos^2 \alpha \cdot \sin \alpha = a_0 \cdot (0.707)^2 = a_0 \cdot 0.35$$
 (3.37)

Combining Equations 3.34, 3.35 and 3.37, the achievable displacement can be expressed in terms of the sail properties.

$$z = 1.88 \cdot 10^8 \cdot 9.12 \cdot 10^{-6} \cdot 0.35 \frac{1}{\sigma} = \frac{600}{\sigma}$$
 (3.38)

With σ defined in gm⁻² the total displacement is given in km above the equatorial plane. Using this last equation, one can easily calculate the displacement corresponding to a certain sail loading.

Using these formulas the theoretical elevation can be calculated for any given sail performance expressed in sail loading of characteristic acceleration. Section 2.4 described the performance of different types a of sails, the characteristic accelerations were presented in Table2.2. Values obtained from this table are used to calculate the corresponding achievable elevations using Equations 3.34 and 3.38, assuming both complete vertical acceleration and the case where the sail is tilted under an angle of 45°. Using the performance of the theoretical sail considered in this thesis, a constant characteristic acceleration of 1 mm/s² is assumed. When this is directed completely in the Z-direction, using Equation 3.34 the achievable elevation can be found to be 188 km. This is a quite large displacement and would be a very good result, unfortunately this is not a realistic case. When the sail acceleration is calculated using a sail rotated with 45° with respect to the sunline the displacement drops to a value of 67 km. This elevation would still be a very good result, but for this simple analysis all forces in other directions and their effects on the orbital dynamics have been ignored. What elevation is actually achievable will thus only become clear later in the report where the final results are obtained.

4

NUMERICAL METHODS

This chapter discusses the numerical methods used in this research and is split up in two parts. The first part focusses on the integration part of the simulations, the latter part describes the optimisation algorithms used. The integration method is used in order to analyse the behaviour of the spacecraft considering a single trajectory. The optimisation part compares different optimisation tools and tries to improve the resulting trajectories using several algorithms.

For a spacecraft in an unperturbed orbit, its Kepler elements remain constant and the position and velocity of the spacecraft at a certain point in time can be found using simple analytical calculations. The elements can be rewritten to another coordinate system if preferred, which will not introduce problems. However since perturbations are present this is not that easy and the state vector of a spacecraft throughout its orbit can not be found analytically. The state vector therefore needs to be integrated numerically. In order to do this in an efficient way, a proper integration method should be selected. The integrator is used to calculate how the state vector and relevant parameters change over time. Such a numerical integrator finds the acceleration of a satellite at a certain point in space and time and propagates its position after a small timestep. This process is repeated in order to find the position of the satellite after a certain amount of time. This can be done using a number of different integration methods which all have different properties and are therefore advantageous for different problems. A small selection of the possible methods will be presented in this chapter, after which the RK4 method is described in more detail, as this integrator is eventually used for the calculations.

When a proper integrator is selected, the trajectory of a spacecraft using certain initial conditions can be found. However, this is not enough as one wants to analyse the search space for the best solutions possible. This search can be accomplished in various ways, and is called the optimisation process. The second part of the chapter describes all methods that have been used for this thesis. For all these methods their working, properties and the reason why they are selected are shortly described.

4.1. INTEGRATION METHODS

The choice of the integrator used is an important choice in any optimization problem. The selected integrator mainly determines the accuracy achievable and the calculation time. For this project, first a fairly simple RK4 integrator is analysed. If the results obtainable are sufficient, this integrator will be used for further calculations. If the results are not satisfactory, other integrators will be compared to increase the accuracy. In this section a range of integration techniques is described in order to provide a short overview of the possibilities and explain the reasoning for selecting the Runge-Kutta 4 method.

4.1.1. SINGLE STEP METHODS

A single-step method assumes a linear relation between two successive points, where the slope between these points is called the increment function. The Euler method is the most simple and general single-step method, where the increment function is simply the tangent at the start point. This increment function can however be adjusted in multiple ways to become more efficient and accurate.

$$\mathbf{y_0}(t_0 + h) \approx \mathbf{y_0} + h \cdot \Phi = \eta(t_0 + h)$$
 (4.1)

32 4. Numerical Methods

The best known method making use of the set up of Equation 4.1 is the family of Runge-Kutta integrators, which are widely used in a variety of problems. The increment function Φ of a Range-Kutta method is based on multiple slope evaluations within each integration step. The first Runge-Kutta method, the RK4, was developed in the 19th century by Carl Runge and Wilhelm Kutta and forms the basis for all other RK functions. The increment function of RK4 is based on four slopes and is the result of their weighted mean.

$$\Phi_{\mathbf{RK4}} = \frac{1}{6}(k_1 + 2k_2 + 2k_3 + k_4) \tag{4.2}$$

In this equation the k-terms are coefficients describing the weights of the different slopes calculated, the values of these coefficients can be calculated or retrieved from literature. By introducing more intermediate steps and corresponding coefficients, a higher order Runge-Kuta method can be constructed, the overall setup of the method remains similar. In this way higher-order RK methods can easily be described using tables which provide the needed constants, however the derivation of correct coefficients becomes increasingly difficult for higher-order functions. Also the order of the method and the needed function evaluations are not always similar: for example two additional evaluations are needed for an order-7 method. Due to these two reasons, only limited methods of higher order are known. [13]

A possible improvement of the standard Runge-Kutta methods is the implementation of a variable stepsize. A constant stepsize is not preferable for all problems, for example when a problem consists of different phases. For these phases different stepsizes might be sufficient in order to achieve equal accuracy. In order to decide on the required stepsize, the error should be known. This can be achieved by combining two methods of neighboring order which are based on the same set of function evaluations, so-called embedded methods. For such methods the truncation error can be approximated, which can be compared to a required accuracy, and from this a maximum stepsize can be obtained. The stepsize can be adjusted accordingly, making the method more efficient. [13]

Second-order differential equations can be rewritten to a system of first-order equations, which also can have consequences on the RK method. For the case where the acceleration does only depend on position and not on velocity, the RK method can be adapted so less function evaluations are needed. These methods are called the Runge-Kutta-Nyström and can improve efficiency. [38]

EXTRAPOLATION

Methods using extrapolation are essentially extended single-step methods, which use extrapolation during these steps. Each step H is divided into n micro-steps of size h, h=H/n. This first solution is then improved by repeating the integration with a different stepsize, a process that can be performed several times. The idea behind this extrapolation is to obtain a solution and accuracy that otherwise would have been achieved with a much smaller stepsize. The most well-known extrapolation method has been developed by Burlisch and Stoer. Using such exploration methods the achievable order exceeds the order possible with Runga-Kutta greatly. This means extrapolation is a good choice for problems with very high requirements on accuracy.

4.1.2. MULTISTEP METHODS

Using Range-Kutta methods, all integration steps are performed sequentially one after another and thus previous features of the formula or integration do not influence the current step. For some problems it is however favourable to actually use previous results of the integration for the current integration step. Methods that use this principle are called multistep methods: they store the results obtained during the integration and use this information throughout the rest of the calculations. In this way more information is available and used, which improves the results and makes it advantageous for several applications. Below a simple form of a multistep method is shown.

$$y(t_{i+1}) = y(t_i) + \int_{t_i}^{t_i+h} f(t, y(t))dt$$
(4.3)

The problem with such an integral is however its dependence on itself which makes it impossible to evaluate explicitly. In order to avoid this problem, the integral is replaced by a polynomial, which interpolates the calculations made earlier to find a value for the integral.

$$\eta_{i+1} = \eta_i + h \cdot \Phi \tag{4.4}$$

Such integrals can be adjusted in several ways, but all multistep methods will use the integral of the previous step in the computation. Examples of these multistep methods are the Adams-Bashforth method and the Adams-Moulton and Predictor Corrector methods. Such methods offer advantages, especially for complex problem needing extreme precision. However, for this research the disadvantage of the complex mathematics and high calculation time are considered larger than the profits. These methods are therefore not considered in the remainder of this report.

4.2. OPTIMIZATION METHODS

Using numerical integration, the propagation of the satellite over time can be simulated. The trajectory a satellite will follow after defining the initial state and the relevant conditions can now be simulated. The goal of this thesis is however to find the trajectory that fulfils the requirements best. In order to search for the best trajectory possible, an optimisation algorithm can be used. Unfortunately there is no perfect algorithm that works best for all problems. How well an algorithm performs depends on the specific problem and the settings of the respective algorithm. For this thesis, several algorithms were used and tested during the process. The selected algorithms did not all show good performance to start with, therefore some tuning had to be done between algorithms as well as for each algorithm. An overview of the algorithms considered is given below, followed by a short description of the parameters that can be tuned. How these algorithms are implemented in the program will be discussed in Chapter 5

4.2.1. DIFFERENTIAL EVOLUTIONARY

Differential evolutionary algorithms (DE's) are a widely used optimization method. Since its development in 1994, it is seen as one of the best heuristic optimization methods and has been developed and throughout the years. The main advantages of this method are its simple use and its wide applicability. A differential evolutionary algorithm is suitable for virtually every optimization problem that searches for a global optimum and has a continuous search space. A differential evolutionary algorithm completes the following steps per generation evolution; initial population, mutation, crossover and selection. Before these start, some settings need to be defined. The number of individuals, NP, and number of generations, G, define the number of elements that will be evaluated. The size of the decision vector is set at D elements, which should all obey certain ranges defined by the specific problem. Lastly the weighting factor F and the crossover factor CR are needed during the optimization; they influence the mutation and crossover process of the algorithm.

As first calculation step, a number of NP decision vectors is randomly generated, which all have D elements. This step is only necessary for the first generation. The next step is mutation of the population, where vector differences are used to create a new mutant vector V_i for each individual. This mutation process is performed according to the following equation:

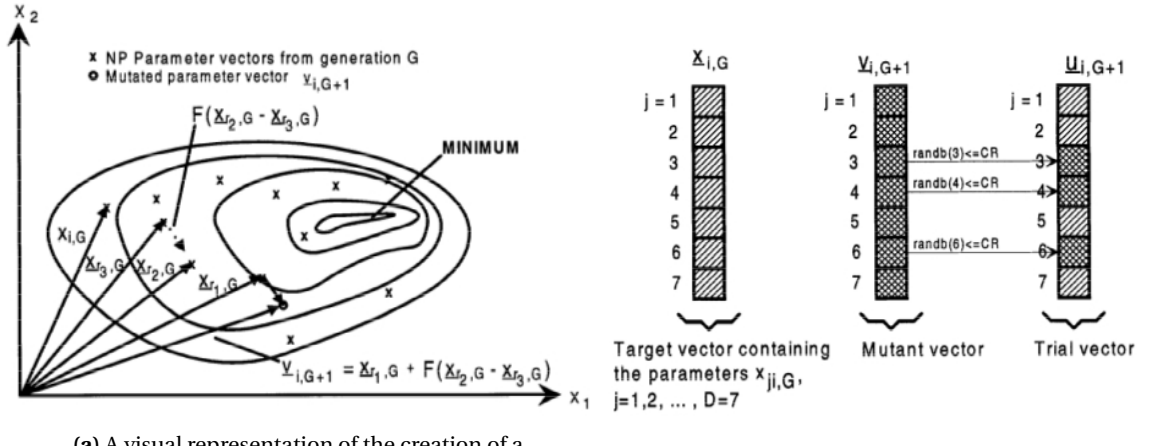
$$V_{i,G+1} = x_{r_1,G} + F \cdot (x_{r_2,G} - x_{r_3,G}) \tag{4.5}$$

The index G represents the number of the generation, so three vectors of the present population are used to create a mutant vector for the next generation. F is the weighting function mentioned earlier, it determines how strong the mutant vector deviated from its original target vector. The minimum magnitude of the weighting factor is zero (meaning no mutation takes place) the maximum value of F is 2. Figure 4.1a shows an example of this process. Crossover is the next stage, where the target vector and its mutant vector are combined to a new vector called the trial vector. For each element of \mathbf{X}_i a random value within the range $\in [0,1]$ is created. If this value is smaller than the crossover value CR crossover takes place. Crossover means that the original value of the target vector is replaced by the corresponding value of the mutant vector. The crossover factor thus defines how much crossover takes place: F = 0 means no crossover, F = 1 means the mutant vector is completely used as trial vector. As this is repeated for all elements the trial vector is created, this process is visualized in Figure 4.1b. Lastly selection takes place, where the next generation is defined. For each individual in the population, a vector is defined for the next generation. The target and the created trial vector are compared and the one with the best fitness value is selected for the next generation. After this is completed, the mutation of this newly created generation is started.

SETTINGS

As explained, several parameters influence the process of the algorithm and set the amount of mutation and crossover that is used. PaGMO offers a standard DE algorithm, which has fixed values of these parameters, set

34 4. Numerical Methods



(a) A visual representation of the creation of a two-dimensional mutant vector $\sqsubseteq_{i,G+1}$ using three existing vectors. [45]

(b) A visual representation of the crossover process. [45]

Figure 4.1: Working of the DE algorithm.

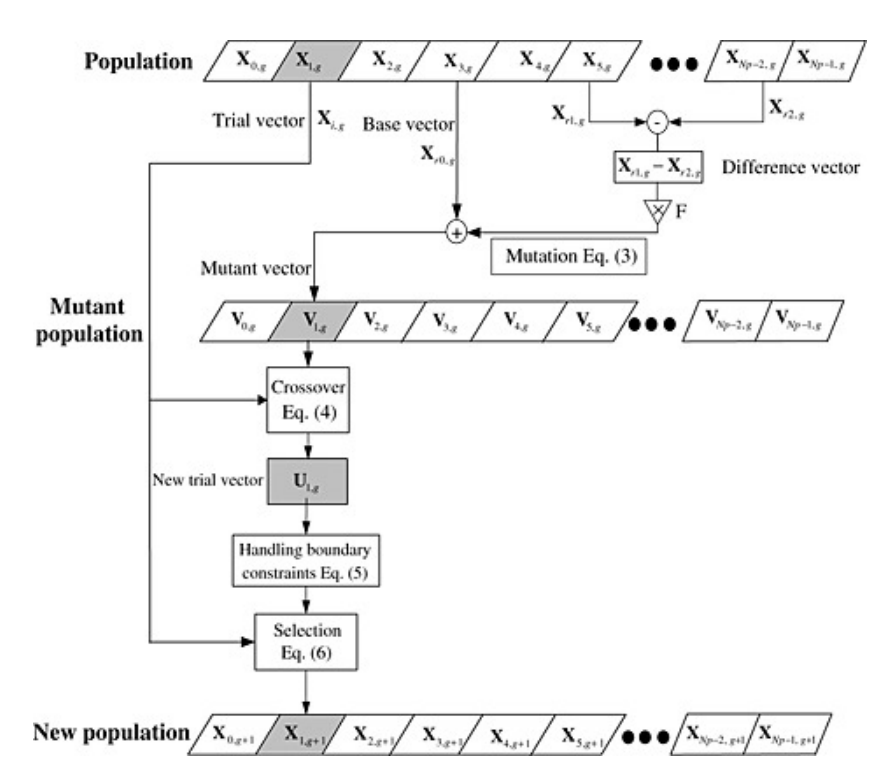


Figure 4.2: Flowchart showing the working of a DE.

at F=0.8 and CR=0.9. This setting is used a as a start and guideline to obtain the approximate possibilities and a reference for other settings. The effect of these parameters was investigated in two ways. First a number of combinations of fixed values for these parameters was tested. These changes sorted some effect, but did not improve the overall performance of the algorithm significantly and persistently.

The parameters can be defined and fixed for the complete simulation, but they can also be changed for each generation. PaGMO offers a self-adaptive DE-algorithm that changes the setting of both F and CR for each generation, this scheme is called the DE-1220 algorithm. The result and behaviour of previous generations is analysed and used to set the parameters to a value that supposedly matches with the search at that point in the optimisation, this means that the values change constantly. Using this adaptive method an improvement in the convergence was indeed obtained. During this process another method was also tested, albeit

unintentionally. A problem can be optimised using PaGMO by providing a problem definition, the algorithm to use, relevant settings and lastly the number of generations and the size of each generation. However, for programming reasons the code was set up in a way that the definition of the problem in PaGMO is defined for just one generation, this is then repeated for a certain number of generations manually. This way of programming is just as correct as the way mentioned before, results obtained using both methods were compared and proven equal. However, this was for the standard DE algorithm were all settings stay constant throughout the complete process. Using this set-up the effect of an adaptive algorithm is however nullified as the previous generations and their behaviour are not known by PaGMO. This way the values of F and CR are set random for each generation. This technique is called dither and can work well for noisy objective function and is therefore also tested.

Apart from these parameters, other variations of the algorithm can be set: settings which define the selection of the mutation and crossover vectors. These settings seem less important than the ones described before, and will therefore not be investigated further, the default settings will be used. The tuning of these parameters that define the exact working of the algorithm is explained in more detail in Chapter 6, where the tests performed and their respective results are presented and discussed.

4.2.2. MOEA/D

Unfortunately the DE's discussed before did not work as properly as expected, therefore some different algorithms were tested as well. The most interesting one of these algorithms is the so-called MOEA/D, which showed improvement in the convergence results compared to previous ones. MOEA/D stands for MultiObjective Evolutionary Algorithm based on Decomposition, and as the name already suggest is an algorithm originally written for multi-objective problems. Even though this algorithm is written for multi-objective problems it can be used for problems with only single objective as is the case for this study. In order to use the MOEA/D algorithm two objective functions need to be defined; for this research these two objective functions are simply defined to be identical. As the optimisations using the MOEA/D algorithm show a large improvement to the standard DE algorithms used, apparently the specific settings of the DE implemented in the MOEA/D are tuned just right for this particular optimisation process.

PROGRAM SET-UP

The theory and numerical methods needed to perform the propagation of the satellite and the optimisation in order to find a proper solution are discussed in previous chapters. This chapter will explain how this theory is actually used and how the simulator is programmed.

First of all the software that was used in order to create the tool will be introduced in Section 5.1, introducing the most important programs used and the reasoning behind those choices. Following this flowcharts are used to show the global structure and set-up of the program. These flowchart will of course be accompanied with an explanation about how the different programming blocks are set up and work together to propagate an orbit. Following this, Section 5.3 gives a more detailed description of the separate code blocks presented. Here the different modes that are possible are introduced together with some explanation on the calculations performed.

5.1. SOFTWARE

This section gives an overview of all software that was used during this thesis. The three most important ones, Tudat, C++ and PaGMO are described rather completely. After this other software, mostly used for the analysis of the results and producing this report is shortly mentioned.

5.1.1. TUDAT

Different coding programs are available to program code to solve numerical optimization problems such as this thesis. Many programs, languages and environments exist, all suitable to work with such problems. All these options have their advantages and disadvantages and could be compared in a similar way as done with the integral and optimization methods. However since this thesis will be performed at the Astrodynamics and Space Missions section, the programming will be done using TU Delft Astrodynamics Toolbox, Tudat. Tudat is a toolbox containing a set of C++ libraries. [37] The content of Tudat is created by students and staff as part of assignments such as a master thesis or PhD research. Since several years the code created during this research is bundled in the libraries of Tudat, thereby creating a toolbox capable of helping students during their research. Tudat is created to enable students to profit from research performed before in similar fields, by making the code used for this research available for future students. All students doing research in the department are encouraged to work with Tudat in order to create and maintain a set of libraries as complete and up to date as possible. Therefore the coding for this thesis will also be created in the Tudat environment. This is to increase the Tudat database and thus provide new building blocks for future students. Another reason is the fact that it should save time and work in programming parts that have already been done before and can be found in the Tudat library. For example, there is a range of integrators already created in Tudat that can be used with little modification, thus saving the work of creating them from scratch. Lastly it encourages to program in a logical, structured way with sufficient commenting and clarification, since it will be made available for future users.

Working within Tudat means working with code programmed in C++. Apart from this there are no large restrictions in working with this toolbox. Everything is possible as long as the developer obeys a set of rules

38 5. Program Set-Up

and guidelines which are set up by a team of Tudat managers and users. This management team consist of several staff members and is responsible for keeping the website and servers behind Tudat working properly. The team is also in charge of the logistics behind solving bugs, adding parts of code and keeping the website and guidelines up to date. These rules and guidelines exist for several reasons. First of all they are used to help new developers with starting their work in Tudat. Templates and recommendations will give the student some basis to start working in this new environment. Another goal is to ensure the quality of the code added, since code will often be used by other developers later on and it is very important that it works properly and consistently. In order to make sure all coding works properly the developer should properly validate and verify their work, for example by performing unit tests on the code. This is a requirement before the code is added to the actual Tudat library. Lastly guidelines are needed to ensure that developers program their code in a professional way, for example by providing clear commentary. This is important to improve the clarity of the programs, since working with a program written by someone else can be a difficult task if the working of a piece of software is unclear.

The most important information source for Tudat is its website; tudat.tudelft.nl. Here all information about its guidelines, possibilities and available programs is provided, all information needed should be available in the Wiki created. Apart from the website, other students and staff members of the A&S department working with Tudat can provide help and information needed to work in Tudat. In order to keep everybody informed and involved in improving Tudat further, every two weeks a meeting is planned for people currently working with Tudat where problems can be reported and discussed. [37] The course AE4-499, Space Project, consists of various assignments which all involve using Tudat and can be seen as an introductory course. It allows the students to learn working with Tudat on a fairly simple basis and will be used by the author as a first step of using Tudat.

To improve the performances of Tudat the C++ libraries Eigen, Boost, and SPICE are implemented and used as well. Eigen improves the capability of C++ for using linear algebra greatly, and is used to perform calculations using vectors and matrices. Boost supports and improves Tudat, both in performances and robustness and is needed when working with multiple functions. Lastly the SPICE toolkit, developed by NASA, can be used to retrieve ephemerides and other properties of most bodies and spacecraft in our solar system and is used mainly for verification purposes.

5.1.2. C++

All Tudat interfaces are programmed using the C++ language. C++ was created back in 1979 as a superset of the already existing language C. First it was named C with Classes and afterwards this changed to C++. The name C++ refers to ++, the variable increment operator of the language. C++ is an extension of the basic C language and should improve and evolve continuously. Since it is based on C, C++ is compatible with C and C libraries can be used with little to none modification. C++ is a strongly- and statically-typed language, which might result in writing difficulties at first. C++ is also a compiled language meaning it compiles directly to a machine's native code. These features allow huge possibilities and control and makes it one of the fastest languages. Together this has led to a broad use of C++ throughout industry and the academic world. A result is that a large number of compilers, libraries and interfaces is freely available on the internet. [3]

5.1.3. PAGMO

The part of the program that simulates a single run was written specifically for this thesis. For the optimization part, a readily available tool named PaGMO is used. PaGMO stands for Parallel Global Multiobjective Optimizer and is a toolbox developed by ESA.[1] It is an open source library and offers a wide range of algorithms to use and possibilities, while in essence maintaining very straightforward and easy in use. The PaGMO tool is freely available and can be downloaded at https://github.com/esa/pagmo, where also previous occurred issues and their solutions can be found. All information, instructions and documentation related to the use of PaGMO are provided using doxygen and can be found online.[1]

Optimising with PaGMO is quite simple, it works with any problem as long as is written in the correct form and the decision vector and the objective function are programmed correctly. As stated in the documenta-

5.2. Program Structure 39

tion, the problem should be defined in the following form[1]:

Find:
$$\mathbf{x} \in \mathbb{R}^n \times N^m$$

To minimize: $\mathbf{f}(\mathbf{x}, \mathbf{s})$

Subject to: $\mathbf{lb} \le \mathbf{x} \le \mathbf{ub}$ (5.1)

 $\mathbf{c}(\mathbf{x}) = \mathbf{0}$
 $\mathbf{c}_{\mathbf{in}}(\mathbf{x}) \le \mathbf{0}$

To clarify this set of equations it can be stated in words rather than just the mathematical notation. The decision vector \mathbf{x} will define the problem and lead to a certain value of the objective function \mathbf{f} . PaGMO will try to find the decision vector corresponding to the minimal value of the objective function. The vector \mathbf{x} should be defined as a vector in the n-dimensional real space, limited by the bounds \mathbf{lb} and \mathbf{ub} . If necessary it can also be subjected to certain constrains $\mathbf{c}(\mathbf{x})$. PaGMO can be implemented in C++, if called upon it provides the program with a set of decision vectors and receives the corresponding objective functions. These values are then analysed in order to optimise the decision vector. This set-up makes it possible that the definition of the problem, its decision- and objective function are completely free to the user and not limited by further programming or coding demands.

Apart from it being straightforward, PaGMO also offers a large number of possibilities in terms of optimisation algorithms, a large variety of algorithms is available. For this thesis a differential evolutionary algorithm seems the best method to optimise the problem at hand. Of this algorithm type PaGMO already has several options available. Later in this chapter, these different algorithms will be discussed and compared more thoroughly.

5.1.4. Other Software

All important programming and calculations are performed in C++, as both Tudat and PaGMO are written is this language. For coding, compiling and running this C++, the open source compiler QT Creator is used. C++ offers limitless opportunities in programming and enables fast computations. However, the output of these programs is solely data, there is no other visual representation possible. In order to visualize the obtained results more clearly, MATLAB is used to create the graphs. Finally the report is written in LateX using Texmaker.

5.2. Program Structure

The created tool consists of two main parts. One part calculates the trajectory a satellite makes under certain conditions. The second block is the optimisation part, the search for the most desirable orbit. In this section the set-up of both blocks will be explained and shown as a flowchart. The theory and numerical methods used are discussed in previous chapters while the first part of this chapter explained which software was used to program and simulate this. Only the structure of the program is discussed here, in the next section the working of each block is described in more detail and their relevance and effect on the program is shown.

5.2.1. SINGLE RUN

Figure 5.1 shows a flowchart of the trajectory propagation of the satellite throughout its orbit. Below some further explanation of this chart is given. Each block in the chart will be discussed, explaining its task and goal and which calculations it performs.

Problem definition This block forms the base of the run to be made, all the variables considering the behaviour, initial state and environment of the satellite are set here. These settings include the perturbations to be taken into account, the initial state of the satellite and the time of propagation. These setting can be divided into two types.

The first type consists of the variables are the numerical parameters, which define the working of the program for the coming propagation. They tell the blocks shown in Figure 5.1 what mode should be considered: *Sail* has four modes, *SRP* has three modes, *eclipse*, *side* and *perturbations* can be turned on or off, where in perturbations J2 and J22 can be turned on or off separately. The *SRP* block also needs and input of the sail loading, although this is in the program expressed in simply the maximum acceleration experienced. These variables thus define which element should be considered and which

5. Program Set-Up

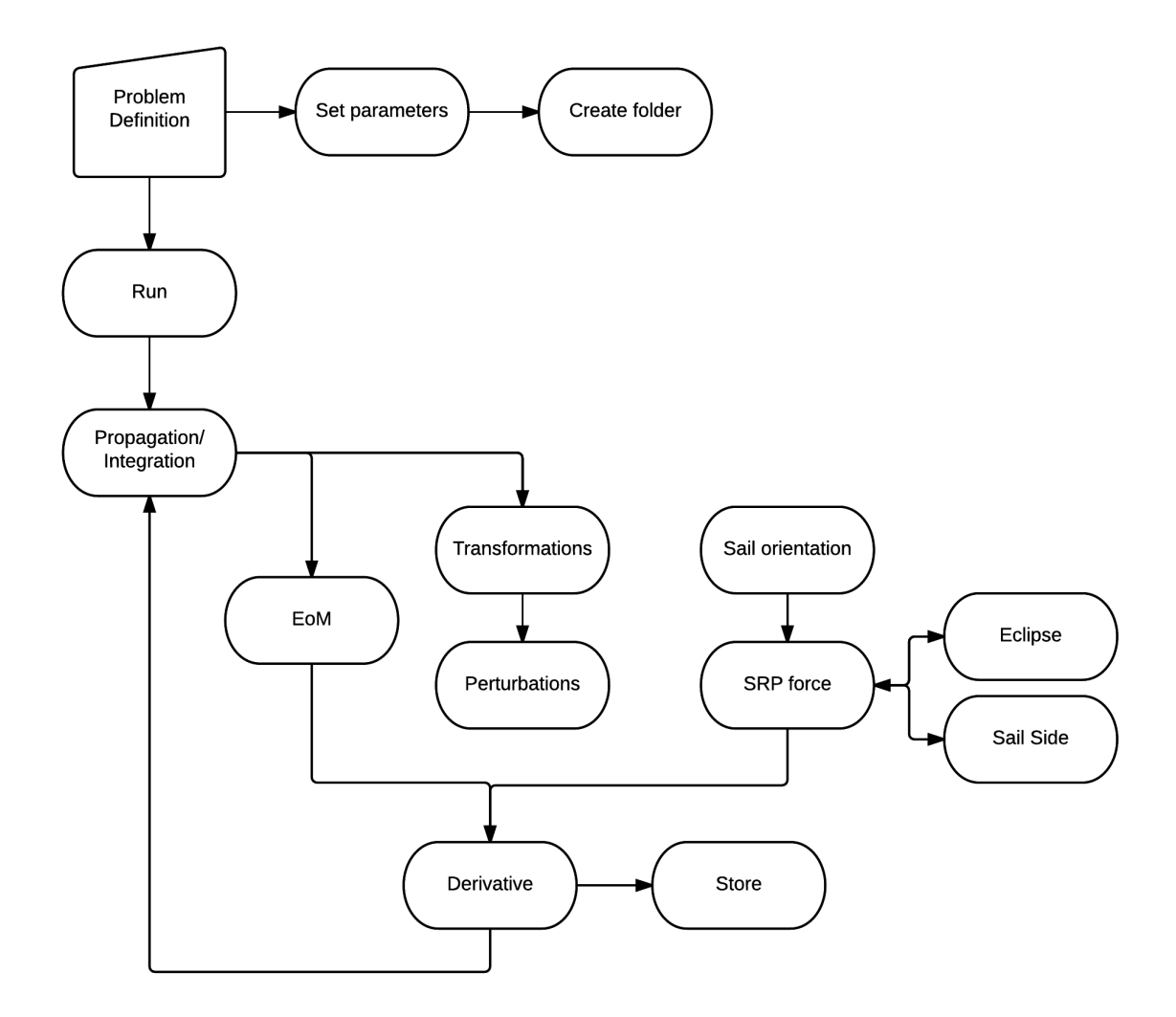


Figure 5.1: Flowchart for a single run.

equations are to be used to calculate the trajectory. Also the time step used for the integration can be seen as a setting of this kind.

The second type of variables are the ones describing the trajectory considered. The first parameter of this kind is the initial state vector, which can be set absolute or relative to a standard geostationary orbit. The desired position of the satellite is also set here. Furthermore the number of nodes and the angles corresponding with these nodes needs to be given here. Lastly the start time and the total time of the propagation are set. The start date and time is relevant since this determines the position of the Sun relative to the Earth throughout the trajectory. The start can be defined as a day of the year and the total time can be given in days, the program is able to convert both to seconds that are needed for the propagation.

Settings All these variables are defined here by the programmer. When the program is started, the first thing done is set all parameters in the relevant block, e.g. the mode of the sail is passed on to the SRP block. This is done for all blocks that need such input, which is shown in Figure 5.1 by the dashed lines connecting these blocks. Also a directory is created where all relevant data will be stored during the running of the program, and directly the settings defining the simulation to be performed are stored here as well. In this way the input for every simulation is stored separate and structured.

Run For a single run, the so-called "Run" block is activated, it resets all storage and offset parameters and then start the propagation block. This resetting of several variables is only relevant when multiple tra-

5.2. Program Structure 41

jectories are performed during a single simulation. The block also starts the integration of the satellite over the assigned time, after which the program prints the resulting objective function.

Propagation After the trajectory is fully defined, the program uses an integrator to propagate the satellite through time and thus finding the trajectory resulting from these considerations and initial state. At the start the state of the satellite is determined, and using the equations of motion, the gravitational accelerations acting on the spacecraft are calculated. Then the program calculates the sail orientation for this specific point in time, and finds the resulting sail acceleration. Lastly the perturbations are determined and they are combined with the other two accelerations. The integrator is now used to determine the next state of the satellite, after a single timestep. At this new state the process is repeated, the state is determined and using the accelerations acting on the spacecraft the next state is found. This is repeated until the final time is reached and the simulation is stopped. Also the offset from the desired position of the satellite is calculated every time step.

Integration As mentioned before, the integrator chosen is an RK4-integrator. As this code block is fully available in Tudat, there is no need to program it again and it is implemented as a whole with the rest of the code. As the RK4 is a fourth-order method, for each time-step the integrator will call the derivative block four times to get the derivatives of the state vector. Using these values the "average" derivative is calculated according to the scheme introduced in Section 4.1.1. With this final derivative the new state vector can be created. This process is repeated until the final time is reached and the propagation is complete.

Derivative The derivative function gets the current state and time as input and returns the derivative of the state vector of that point in time to the integrator. As the state vector consists of the position and the velocity of the satellite, the derivative basically is the velocity and the acceleration of the satellite in Cartesian coordinates in the ECI reference frame. The first three entries of the derivative are thus equal to the last three entries of the state vector and can easily be obtained. In order to find the acceleration of the satellite, the different forces acting on the spacecraft need to be calculated. These calculations are performed using several steps, which are performed by different blocks. The three blocks all return accelerations to this block, where they will be added to find the total acceleration. These accelerations are then put into the derivative vector which is returned to the integrator.

Position transformations The integration is performed using Cartesian coordinates in the ECI reference frame, however this alone is not always enough. For some calculations the position with respect to the Earth is needed, therefore the state vector is transformed to the ECF frame as well. Furthermore transformations to both Kepler and spherical elements can also be performed here; they might help in visualising and understanding the orbital trajectory and behaviour better. These transformations are performed using transformation matrices which are available in Tudat. The transformation between the ECI and the ECF coordinates was shown in Section 3.1, the rotation angle can be found from the time passed since the start of the propagation when the frames where defined. Both spherical and Kepler elements are calculated using a readily available Tudat method, where the spherical coordinates are expressed in the ECF frame.

Equations of motion The main acceleration experienced is created by gravitational attraction of the Earth. This main acceleration can be found using the equations of motion of a two-body problem, as given in Section 3.3. As gravity is a conservative force, the value of these accelerations solely depends on the position of the spacecraft. This position in the ECI frame is thus the input of these equations, which return the accelerations in three directions.

Perturbations As explained earlier in Section 3.6, the Earth is not perfectly spherical and the spherical harmonics of (n, m) = (2, 0) (J_2) and (n, m) = (2, 2) (J_{22}) are taken into account in this thesis. The value of these perturbations can be found using Equations 5.5 and 5.6. J_2 is a zonal function which describes the flattening of the Earth and the respective perturbation mostly depends on the distance from the Earth and the latitude of the spacecraft. The perturbation due to J_2 can be found using the position in ECF. J_{22} is a sectoral function meaning the longitude is of great influence. The longitude of the satellite is found using the spherical coordinates in the ECF frame. Combined with the position in ECF, the perturbation is calculated. As these perturbations are defined in the ECF frame, they need to be transformed to ECI coordinates.

42 5. Program Set-Up

Sail The last acceleration is the core of this program, namely the acceleration experienced from the sail force. In order to be able to find this acceleration, the orientation of the sail needs to be known at that time. As explained earlier in this chapter, the sail mode and the node settings together define the orientation of the sail at each point in time. This block therefore uses these variables together with the time to set the orientation of the sail to the correct before actually calculation the experienced acceleration.

- **SRP** In this block the acceleration on the spacecraft induced by the solar radiation pressure is calculated. Using the sail orientation and the direction of the Sunlight, the resulting force and following acceleration is calculated. The outcome of this acceleration depends on the settings specified for a certain run, in Section 5.3.4 a more detailed description of these different settings and their corresponding equations can be found.
- **Eclipse** During most of its time orbiting the Earth, a geostationary satellite 'sees' the Sun and thus a solar sail can be used. However, depending on the time of the year, the Earth is blocking the Sunlight throughout part of the orbit. This situation is called eclipse and is of great importance in this case as the solar sail can not operate during this time. The eclipse block checks if the spacecraft is in eclipse, and if so sets the solar sail force back to zero.
- Sail side A real solar sail has two different sides, of which only one side is reflective and will provide the desired acceleration. In the method used for calculating the solar sail force, this is not taken into account and no difference between both sides are considered. Therefore an extra check is needed to find out if the right side of the sail is facing the Sun. If this is not the case, the solar sail acceleration will be set to zero.
- **Offset** As the goal of this research is to find an orbit where the satellite remains at a fixed position relative to the Earth surface, we need to keep track of how well this is achieved. This is done in this block where the actual and the desired positions of the satellite are compared. The difference between these two positions, as seen from Earth, is called the offset and is calculated and saved in this block. This offset is later used in the objective function of the optimisation algorithm. For each timestep step this offset is calculated and after the complete trajectory is followed, the average offset can be determined. The exact definition of offset and the formulas used for calculating it will be presented later in Section 5.4.3, where the objective function of the program is described more thoroughly.
- Storage During each time step, the position in both the ECI and ECF frame is calculated, the same holds for the spherical and Kepler elements. Although here it should be noted that these Kepler elements are not always valid as the considered orbit is non-Keplerian one. All these coordinates are stored every 25 seconds, which was the maximum time step used, leading to 3447 points every orbit. A simple check is implemented to ensure they are not stored every evaluation of the integrator, this would make no sense as these points do not all lay on the trajectory travelled. Also for runs with smaller time steps, the information is only stored every 25 seconds. More storage seems not necessary, added to the fact that the fixed size of the storage matrices make comparison and the storing itself more easy.

5.2.2. OPTIMISATION

Previously the working of a single trajectory simulation was shown, here the set-up of the optimisation part of the program is discussed. Figure 5.2 shows the flowchart of this part, where in the block *Single Run*, the flowchart of Figure 5.1 can be inserted. Running an optimisation essentially comprises running multiple trajectories with changing the initial conditions, trying to improve the resulting orbits. The optimisation algorithms used are discussed in Section 5.1.3, but in essence they all work similarly.

- **Problem description** This block is similar to the one in the previous section, although the set parameters differ slightly. The parameters describing the working of the block and setting of the block are all similar. Only with setting up the exact problem, instead of defining the initial state and the nodes considered, now the optimisation parameters are defined. These three parameters are the chosen algorithm and its mode settings, the number of generations, and the size of each population. When these are given as input, the program can start and all relevant parameters are set.
- **Optimiser** As the optimisation is started, the first population is created. For every individual a decision vector is chosen randomly, describing the initial values and the nodes, which together define the course of the trajectory.

5.3. <u>Settings</u> 43

Propagator This part is essentially the same as for a single run, although here the parameters describing the trajectory are not stored. Only the decision vector and the offset which serves as the fitness function are saved.

Optimiser After each decision vector created for the first generation is run through the propagator, the results are returned to the optimiser. The optimiser now analyses the decision vectors and their corresponding fitness. The vector resulting in the best fitness is called the champion, its properties are also stored separately. After this a new population consisting of semi-randomly chosen decision vectors is created. These vectors are also run trough the propagator and analysed afterwards. The goal of the optimiser is to improve the fitness of the trajectories and thus create better trajectories for each new generation. This process is repeated until the total number of generations is fulfilled and a final best solution with the given optimising parameters is found.

Storage After the optimisation is finished, the most important data is stored, consisting of the decision vector and the resulting fitness of all individuals. The champions of each generation are stored separately as this makes it easier to analyse the progress of the optimisation.

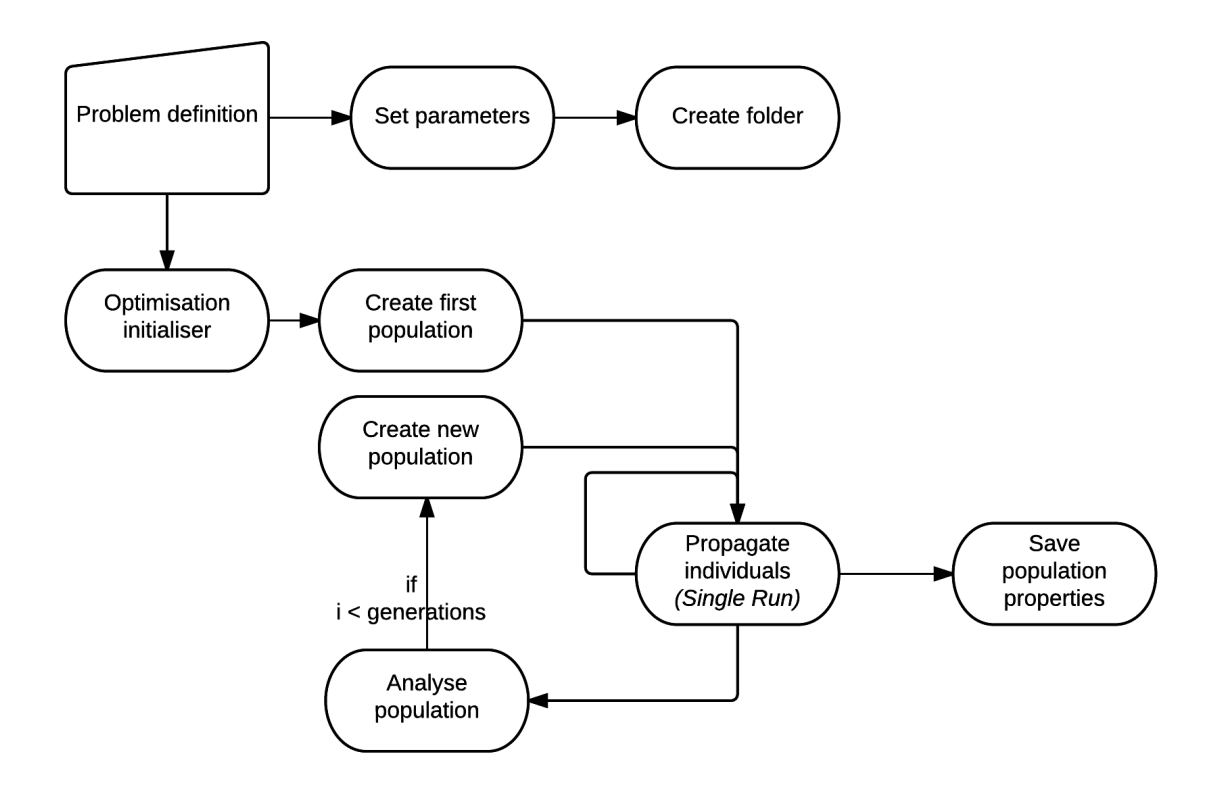


Figure 5.2: Flowchart for the optimisation process.

5.3. SETTINGS

In Section 5.2 the structure of the program was explained by means of simply mentioning the coding blocks that form the complete program. In this section these blocks are discussed a bit more detailed, explaining possible settings and showing how certain calculations are performed.

5.3.1. INITIAL STATE

An important part of the decision vector is the initial state of the satellite, where its position and velocity at t = 0 are defined. A coding block is dedicated to define the proper initial state using certain input variables. The initial state is based on a standard geostationary orbit, which is calculated using the gravitational attraction

5. Program Set-Up

of the Earth and the fact that the satellite should remain at a constant position relative to the Earth. This means the gravitational attraction of the Earth should be equal to the Coriolis acceleration, which is given by $a_{cor} = \omega^2 r$. Using this definition and the scalar form of Equation 3.3, the following equation is set up to calculate the radius of the orbits:

 $r = \sqrt[3]{\frac{\mu}{\omega^2}} \tag{5.2}$

This radius is simply multiplied with ω in order to find the orbital velocity, which is perpendicular to the radius as a circular orbit is assumed. Using these two scalar values, the X- and Y-coordinates can be calculated just as their derivatives. The Z-coordinate of a normal geostationary satellite is zero as its orbital plane lies in the equatorial plane. As displaced geostationary orbits are the subject here, the Z-coordinate can also be chosen differently. This value is simply set by the offset in Z-direction given as manual input. For the most simple case the satellite starts at the X-axis, meaning a longitude of zero. In this case the velocity is purely in the Y-direction, both Y and \dot{X} remain zero as a result. However the longitude of the satellite influences the forces acting upon it and thus its trajectory, the longitude is therefore considered as a variable. The longitude is set as a manual input and the initial position and velocity components are then calculated using:

$$\mathbf{r} = \begin{bmatrix} X \\ Y \\ Z \end{bmatrix} = \begin{bmatrix} r \cdot cos(\lambda) \\ r \cdot sin(\lambda) \\ Z_{0,offset} \end{bmatrix} \qquad \dot{\mathbf{r}} = \begin{bmatrix} \dot{X} \\ \dot{Y} \\ \dot{Z} \end{bmatrix} = \begin{bmatrix} v \cdot cos(\lambda + \frac{\pi}{2}) \\ v \cdot sin(\lambda + \frac{\pi}{2}) \\ 0 \end{bmatrix}$$
(5.3)

The \dot{Z} -component is normally set at zero, as the best result would be an orbital plane parallel to the equator. This initial state is used for single run simulations of certain settings, with certain displacement from the standard case. During the optimization phase, this state is used as a guess around which the states per individual can be chosen and optimised.

5.3.2. SUNLINE

As shown in Figure 3.2 the magnitude and direction of the sail acceleration achievable depend on the direction of the solar radiation pressure. The direction of this SRP clearly depends on the position of the Sun relative to the Earth. For this thesis the position of the Sun is calculated using a slightly simplified definition where the Earth is orbiting the Sun in a perfectly circular trajectory. The direction of the sunline is defined by two rotations; the Earth rotates around its own axis, while it also orbits the Sun. The direction of the sunline is calculated using the following equations:

$$\begin{bmatrix} X \\ Y \\ Z \end{bmatrix} = \begin{bmatrix} sin(\Omega_{ES} \cdot time) \\ cos(\Omega_{ES} \cdot time) \\ tan(23.45) \cdot cos(\Omega_{ES} \cdot time) \end{bmatrix}$$
 (5.4)

This results in a three-dimensional vector containing the different elements of the calculated sunline, in order to use this for further calculations the vector is divided by its norm in order to obtain the corresponding unit vector. This unit vector describes the direction of the sunline in the ECI frame, meaning that the rotation around its own axis is not relevant as this is an inertial frame. The direction does however depend on time, as the Earth rotation axis is tilted with respect to its orbital plane. This means that during one year the orientation of the Sun with respect to the equator changes from 0^o to 23.5^o , to 0^0 , to -23.5^o and to 0^o again. As this rotation takes one sidereal year the rotational velocity Ω_{ES} is defined by $\frac{2\pi}{siderealyear}$. For the program time is defined in seconds and so is the duration of one sidereal year. The time is defined starting from 21 December, 12:00, thus the start of winter in the northern hemisphere. On this date the sunline makes a positive angle with the equator, something that is preferable for a positively elevated orbit.

Considering the ECI-frame, the sunline makes one complete rotation per year and this change is very important for the conditions of the spacecraft and solar sail. During one day the change is 0.986^o , trajectories of three days as considered in this research thus leads to a deviation of almost 3^o . This change during one run will thus not influence the performance of the solar sail largely. It is more interesting to check the change in performance during different periods of the year. In the program the start date of the propagation can be set and the influence of the direction of the sunline can thus be investigated. The sunline block also has a setting which does not take into account the tilted rotational axis, it does only consider a change in the XY-plane. The direction of the sunlight is assumed to lay in the equatorial plane and the Z-component is therefore always zero when this setting is selected.

5.3. SETTINGS 45

5.3.3. SAIL ORIENTATION

In the program, five modes of the defining the sail orientation throughout the orbit are available. Not all are realistic or desirable, these settings were created for the sake of verification and validation of the program.

The sail orientation is defined in the program using two sail angles; the polar angle θ and the azimuth angle ϕ , as shown in Figure 5.3. The polar angle describes the rotation of the sail out of the equatorial plane, whereas the azimuth angle is the rotation around the Z-axis, thus in the plane. The angle θ is defined away from the Z-axis, while ϕ is defined from the X-axis in counterclockwise direction. Together these two angles define the normal vector of the sail \mathbf{n} , which was introduced in Section 3.4. This \mathbf{n} is defined out-of-plane of the back of the sail. This might sound strange at first, but using this definition the force experience on the solar sail points in the same direction as the vector describing the sail orientation. The definition of \mathbf{n} , θ , ϕ and their directions are shown in Figure 5.3. Combining these angels with the direction of the sunline, the pitch angle of the sail α can be determined that is needed to find the magnitude of the solar sail acceleration.

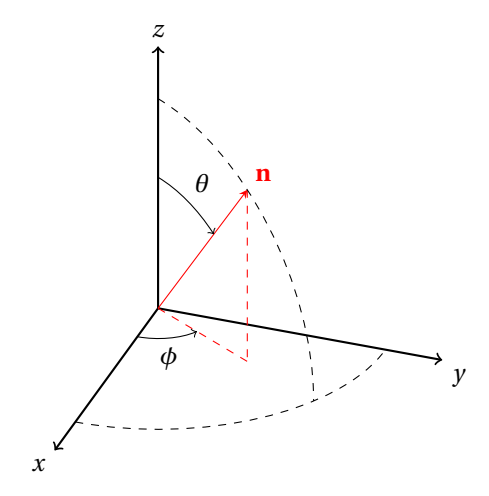


Figure 5.3: Definition of the sail orientation vector and relevant angles.

Modes

As said, the sail orientation can be defined using five different modes:

- 1 Sunline mode For the first mode, the sail is simply orientated in a manner in which it always aligns with the Sun. The program receives the vector of the sunline from the Sunline block and sets the sail orientation equal to it. This mode will result in a sail acceleration that is always maximal in magnitude and only slightly changes in direction during an orbit.
- 2 Fixed in ECI The second orientation mode means the sail is set at a fixed orientation in the ECI frame. This seems simply achievable for a spacecraft as no further attitude control is needed. This mode will result in a fixed orientation of the sail and a constant direction of the sail acceleration. The magnitude only changes slightly throughout an orbit.
- **3 Fixed in ECF** Just as in mode 2, for this setting the sail has a fixed orientation, although here it is fixed in the ECF frame. This means the sail has a fixed orientation with respect to the Earth, e.g. the sail is always facing away from the Earth. This can offer certain advantages, but also means that the obtained acceleration changes completely in magnitude and direction during an orbit.
- **4 Fixed Nodes** In the previous modes, the sail remained in a constant orientation throughout the complete orbit. However this will most likely not enable a proper solution to the research goal. In order to create more freedom in steering the sail and thus creating more possible solutions, nodes are introduced.

For this orientation mode, the trajectory is split up into several parts, which all have a certain orientation. The points where the sail is set to a new orientation are called nodes. The number of nodes N can be varied by choice of the user, the exact point where these nodes lay are determined by the number

5. Program Set-Up

of nodes. When the number of nodes, and their orientation, is defined, the program divides the total propagation time by this number and a new nodes is set after each N^{th} part of the complete trajectory. For example; when four nodes are considered, the sail starts the trajectory in the orientation defined by the first node, which it will remain on until the next node. When the spacecraft reaches one quarter of the total propagation time, the sail orientation will be set according to the second node and so on. The resulting orientation can be seen in Figure 6.6.

5 - Changing Nodes The last mode again relies on predefined nodes, however this mode is improved and made more realistic. In mode 4, the sail makes a discreet jump from one orientation to another, something which is not realistic. Therefore, now the sail is rotated slowly between the nodes, to create a smooth transition. The definition of the nodes is exactly the same as before, so at the node points the orientation angles are set. Between node points, these angles are now interpolated linearly. At the end of the propagation, the sail orientation is set equal to that at the start. The sail orientation throughout the orbit with this mode, using the same nodes settings is shown in Figure 6.7. As can be seen, at the four node points the orientation of the sail is the identical, while in between these points the sail gradually changes.

For the actual simulations the last mode is used, as this is considered the mode that best represents reality. In the next chapter the working of this programming block is verified, were also a visual representation of the last two orientation modes is presented.

5.3.4. SAIL ACCELERATION

The effect of the solar sail on the trajectory of the spacecraft is expressed in an acceleration. The direction and magnitude of this acceleration can be determined using different calculation methods, just as was the case for the sail orientation. Just as with the sail orientation, not all options lead to realistic or desirable solutions. These options are also programmed in order to check the working of the code, thus verification purposes, or simply to analyse the behaviour of the spacecraft under certain accelerations. The input for this program block is a three-parameter vector plus an integer setting which sets the mode.

- 1 Fixed in ECI The first option is the most simple solution: the direction of the acceleration due to the solar sail is defined as a vector fixed in the ECI frame. Both the magnitude and the direction are constant throughout the orbit. The input vector is taken directly as the acceleration in the ECI frame without further calculation.
- **2 Sail direction** For this mode, the direction of the sail acceleration depends on the behaviour of the sail. The direction of the acceleration is defined by the direction of the normal sail vector, while the magnitude is determined by taking the norm of the input vector, the characteristic acceleration \mathbf{a}_{acc} . This characteristic acceleration is the acceleration achieved when the sail is turned directly towards the Sun, thus the maximum acceleration for a certain distance from the Sun. This mode is far from realistic, but it can be used to investigate the effect of solar radiation pressure on an orbit.
- **3 Sail Sun** With the last mode, the acceleration is determined using both the sail and the sunlight. The calculations are performed using Equation 3.15. This means that, just as before, the sail normal vector is taken as the direction of the acceleration. However, the magnitude is not not constant but depends on the orientation of the sail with respect to the Sun. This is far more realistic, as this orientation has a major effect on the radiation received and thus the acceleration experienced. For the case when the sail is facing the Sun perfectly, the result will be equal to mode 2, however if there is an angle α introduced between the Sunline and the sail normal, the force received drops drastically.

Another mode that eventually should be implemented is the case of a realistic sail. Mode 3 calculates the magnitude of the acceleration using the using Equation 3.15 which is defined for a perfect sail. In the case of a realistic sail, the theory discussed in Section 3.5 should be used to calculate the acceleration. The magnitude would decrease by some amount while also the direction deviates from the ideal case. However, this mode is not included in this thesis for a number of reasons, the most important one being the fact that no actual sail or spacecraft is defined yet. It was reasoned that an acceleration due to a realistic sail deviates only slightly from the actual case, the order of the accelerations will stay the same. A more realistic sail acceleration should be taken into account when a sail is selected, however at this stage it is not relevant enough.

5.3. <u>Settings</u> 47

The direction of the solar sail acceleration in this research is solely determined by the attitude of the sail, since an ideal sail is considered. The direction of the Sunline relative to the sail surface determines the magnitude of the acceleration, when the sail is aimed directly towards the Sun the acceleration is maximal. This maximal acceleration is called the characteristic acceleration and its magnitude depends on both the sail properties and the solar flux. This solar flux is constant, as the distance to the Sun is taken constant. For an ideal sail only the mass-to-area ratio determines the magnitude of the acceleration for a given solar flux, for a solar sail spacecraft this ratio is called the lightness number, as explained in Section 3.4. For this thesis a simpler approach is chosen and the characteristic acceleration is simply given as an input parameter that is defined for each run. This characteristic acceleration is of course closely related to the sail lightness number and chosen keeping the corresponding lightness number in mind.

5.3.5. ECLIPSE

For certain positions of the spacecraft with respect to the Earth and the Sun, the spacecraft is behind the Earth and cannot see the Sun. This phase is called eclipse, and during this situation the sail obviously produces no force. Therefore, the program checks if the satellite is in eclipse and alters the received solar radiation accordingly. This is done by calculating the shadow function for the current constellation at each integration point. Figure 5.4 shows the relevant view for a spacecraft in eclipse. When the spacecraft is in the region 'Umbra', the eclipse is full and no light reaches the solar sail. When the spacecraft is in the penumbra region, the eclipse is partly and only a share of the radiation hits the sail. Outside both regions, the satellite is not in the shadow of the Earth and the maximum Sunlight is received.

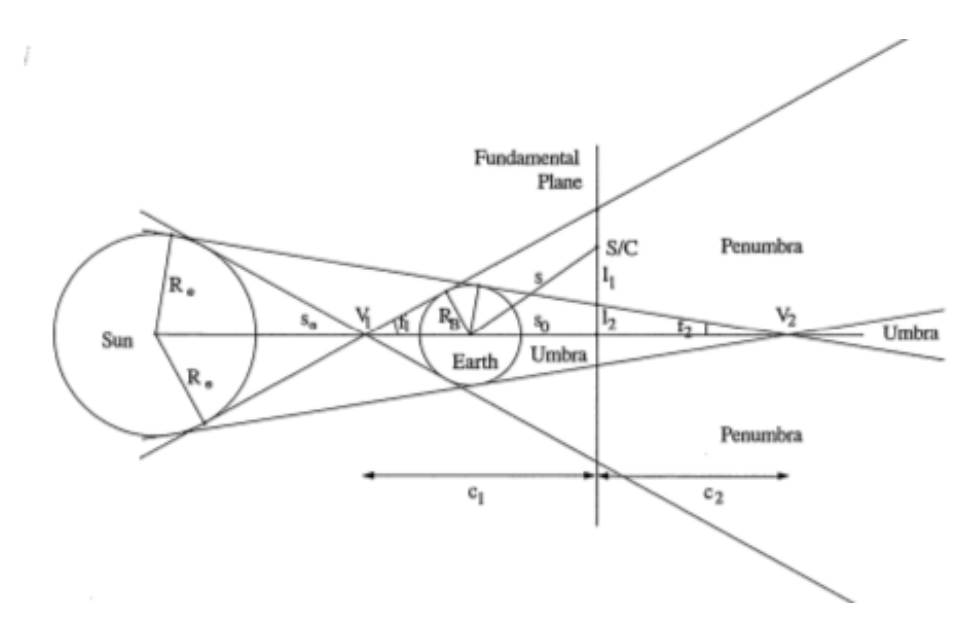


Figure 5.4: 2D-view of a spacecraft in eclipse behind the Earth.[38]

Using geometry, based on the view shown in Figure 5.4 one can calculate in which region the current position of the satellite lays, and if this is the penumbra what share of the total light falls on the sail. The shadow function now describes the part of the sunlight that is received at a certain position. A value of one means the spacecraft is in full sunlight, while a shadow value of zero represents total eclipse and thus no sunlight received at all. The exact mathematical expressions of this shadow function are quite extensive and too elaborate to put in this report. The equations are obtained from [38] and can be found there if need be. The percentage of time a spacecraft is in eclipse throughout its orbit depends largely on the altitude, a larger altitude leads to a smaller eclipse time. For a spacecraft in a geostationary orbit, the eclipse time can add up to 72 minutes.[39] This means that during this time, the spacecraft is approximately in eclipse 5% of the total time. The fact that the orbital plane is tilted with respect to the ecliptic means the eclipse conditions change throughout the year, only around spring and fall equinox the spacecraft will experience eclipse. A more thorough analysis of the eclipse of this satellite will be provided in Section 6.2 where the function block is validated.

5. Program Set-Up

5.3.6. PERTURBATIONS

Several perturbations are included in the program created, they can all be included separately from each other. As this is a first approximate study, only a limited number of perturbations that are important are included. To include the non-spherical form of the Earth, the J_2 and J_{22} effects are included, the effect of the other perturbations are reckoned too small to have a significant influence in this study. The gravity potential including the spherical harmonic terms can be calculated using Equations 3.29 and the resulting force using Equation 3.30 as was shown in Section 3.6. Equation 3.29 is however written in the potential form and given as the sum of all terms, not yet derived explicitly for the relevant terms. In the program this should therefore be rewritten to a vector form. For respectively the J_2 and J_{22} terms, this is programmed as follows:

$$\mathbf{a}_{\mathbf{J}_{2}} = \begin{bmatrix} J_{2_{X}} \\ J_{2_{Y}} \\ J_{2_{Z}} \end{bmatrix} = \begin{bmatrix} -\frac{3}{2}\mu J_{2} \frac{R_{e}^{2}}{r^{5}} \frac{1-5z^{2}}{r^{2}} \cdot r_{X} \\ -\frac{3}{2}\mu J_{2} \frac{R_{e}^{2}}{r^{5}} \frac{1-5z^{2}}{r^{2}} \cdot r_{Y} \\ -\frac{3}{2}\mu J_{2} \frac{R_{e}^{2}}{r^{5}} \frac{3-5z^{2}}{r^{5}} \cdot r_{Z} \end{bmatrix}$$

$$(5.5)$$

$$\mathbf{a_{J_{22}}} = \begin{bmatrix} J_{22_X} \\ J_{22_Y} \\ J_{22_Z} \end{bmatrix} = \begin{bmatrix} -9\mu J_{22} \frac{R_e^2}{r^4} \cos^2(\delta) \cdot \cos(2(\lambda - \lambda_{J_{22}})) \\ -6\mu J_{22} \frac{R_e^2}{r^4} \cos^2(\delta) \cdot \sin(2(\lambda - \lambda_{J_{22}})) \\ -3\mu J_{22} \frac{R_e^2}{r^4} \sin(2\delta) \cdot \cos(2(\lambda - \lambda_{J_{22}})) \end{bmatrix}$$
(5.6)

With: $J_2 = 0.00108263$, $J_{22} = 1.8155628 \cdot 10^{-6}$ and $\lambda_{J_{22}} = -14.9287^o$

Equation 5.6 uses the latitude and longitudal position of the satellite, respectively δ and λ , to find the J_{22} perturbation and is defined in the ECF-frame. Both perturbations are therefore calculated in this frame and afterwards converted to the ECI-frame coordinates. Also the coordinates of the satellite in the ECF-frame are converted to spherical coordinates using which the latitude and longitude of the satellite is determined.

Figure 5.5 shows what both terms actually mean in terms of deviations in Earth's gravitational field. The blue parts mean an increase in the gravitational field while the red parts stand for a decrease in the attraction. The J_2 term is thus the term that describes the amount of increase in the gravitational field on the equator. Although this is mainly due to the oblateness of the Earth, these equations describe the deviations in the gravity field which should not get confused with a deviation in shape. The deviations due to J_{22} are shown in the right picture, and seems quite similar although everything is shifted 90° . Lastly it should be noted that these pictures show a highly exaggerated change and are not scaled, the J_2 is in reality multiple order of magnitude larger than J_{22} .

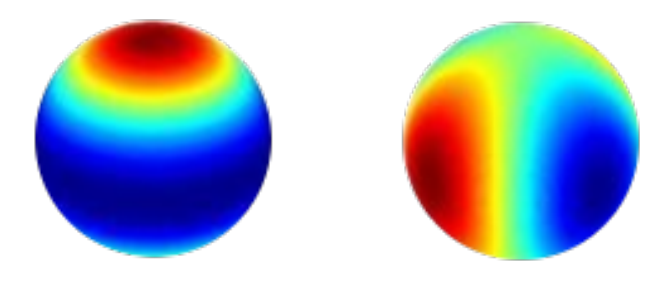


Figure 5.5: Effect of J₂ (left) and J₂₂ (right) on the gravity field of the Earth.[2]

5.4. OPTIMISATION ALGORITHMS

In this section the settings of the optimisation part of the programmed tool are discussed. As earlier explained, the scheme of the algorithms used is programmed in PaGMO and readily available, but clearly the set-up, definition and description of the problem is not. These part were programmed specifically for this thesis and will be addressed here. First the decision vector used is discussed, both its variables and its limits, which is then followed by the objective function.

5.4.1. DECISION VECTOR

The decision vector is a vector containing the parameters that vary throughout the optimization and define the exact properties of a certain trajectory. For this report, the decision vector consists of the initial state and the angles describing the sail attitude throughout the orbit. The first part of the decision vector is the initial state vector. This vector contains six elements the Cartesian coordinates of the position and the velocity of the satellite at the start of the propagation. The angles describing the sail attitude, as explained more thoroughly in Section 5.3.3 are two angles, α and ϕ . The decision vector sets these angles at certain points, the so-called node points, every node point therefore leads to two extra elements in the decision vector.

For this report the minimum number of nodes is four leading to a decision vector of 14 elements $(6+2\cdot4)$, while the maximum number of nodes considered is twenty corresponding with 26 elements $(6+2\cdot10)$. A larger number of nodes is advantageous in the sense that it leads to more freedom in steering the sail, however this advantage comes at a cost. The increased number of variables of the decision vector leads to a slower rate of convergence. This means more generations are needed to find a proper solution, leading to a longer calculation time. For the final simulations, a fix number of individuals and generations is selected. Using these numbers a comparison between the number of nodes can be made.

A similar thing can be observed concerning the ranges along which the parameters can be varied. Wider ranges lead to a greater solution space, which seems desirable as the best solution is not known beforehand. However, a larger solution space again means slower convergence and thus a longer calculation time. The considerations taken about this and the resulting chosen values for the actual simulations are discussed in the next section.

5.4.2. SEARCH SPACE

The search space defines the values the different elements of the decision vector can adopt. For the first six elements, the initial state, this search space is defined using a state, the initial guess, that is expected to be approximately the state needed. The desired perfect solution of the problem is a geostationary orbit in which the satellite follows a geostationary trajectory only with a constant displacement in the Z-direction. This goal of the optimisation process is taken as the mentioned initial guess, the ranges are set relative to this state. The magnitude of these ranges and thus of the bounds of the decision vector influence the optimisation process. Setting wide bounds creates a larger search space and thus more freedom for the optimisation, however this freedom comes at a cost. The larger search space leads to more spreading of the individuals, which will result in slower convergence. Again an assessment of has to be made, to what range does the improved freedom weigh against the growing calculation time needed. For this research the ranges of the position of the decision vector are set at 1 km while the deviation in velocity is limited at 1 m/s. These bounds and thus maximal deviations from the initial guess are based on the offset they induce when applied to a geostationary orbit.

Applying certain offsets to the initial state will result in a changed trajectory and thus a certain average offset for the trajectory. A standard initial state results in an offset of $3.4 \cdot 10^{-5}$ as was shown before. By changing the position, in all directions, with 1 meter will result in 10.6 m offset throughout the trajectory, changing the velocity with 1 mm/s² results in 158 m offset. With a requirement of 7.5 km, the deviations that relate closely to this distance are 1 km resulting in 10.6 km, and 0.1 m/s resulting in 15.8 m offset. As this velocity component seems unreasonably small, the range for the velocity is increased to 1 m/s.

The remaining elements, defining the sail orientation throughout the orbit can also be constrained. The sail can be turned in every direction, there are no physical limitations for this since it only a theoretical case and not a specific spacecraft is considered. Combined these two angles thus describe a complete sphere, however only half of this sphere has actual meaning. The only constraint used is letting the sail only point with one sail side towards the Sun. For a realistic case, this is completely valid as only one side is reflective. Also if a sail with two reflective sides would be assumed, the force could only be pointed in halve of a sphere, away from the Sun. If the sail is pointed in the other halve, the force would be in the negative direction of the normal. For any orientation a rotation of exactly 180° will induce exactly the same acceleration experienced by the sail.

Apart from the absolute angles of orientation, the difference between two consecutive node is a relevant factor. As it describes the speed at which the sail should rotate, this should be constrained so the rotations do not exceed what is practically possible. It is clear that this rotational speed is limited, however such a con-

50 5. Program Set-Up

straint is not implemented in this thesis. Even with a very conservative rate of 0.1 deg/s a full rotation would only need 3600 seconds, or one hour. This rate can only be needed when 24 nodes or more are considered (and a full rotation is needed between two consecutive nodes). As this many nodes are not used in this thesis there is no need for an extra constraint in the program.

5.4.3. OBJECTIVE FUNCTION

Now that the decision vector is defined, the input of the optimisation process is set. However the exact goal and thus output of this algorithm is needed a well. The optimisation package is programmed to minimise a freely chosen objective function. This means the goal of the optimisation, i.e. to find the most optimal displaced geostationary orbit, has to be written as a mathematical expression.

The most characteristic property of a geostationary satellite is the fact that its position relative to the Earth, or the position in the ECF-frame, has to remain constant. The change of this position after a complete orbit is however not a very good objective function, as it only looks at the state at one specific point in time. This means that the trajectory travelled in between is not considered. As this is clearly also important for communication, the difference between the desired and actual spacecraft state throughout the orbit is therefore a better measure for the fitness. The difference between these positions can be obtained by subtracting their position vector. However, the position seen from the Earth is more important than the radial distance. Therefore the spacecraft position seen from the Earth is compared to the desired one, the difference between these two is called the offset of the satellite. The difference between the actual and the desired position is thus projected on the plane described by the (normal) position vector of the satellite, resulting in the offset. This offset is calculated using the following equation:

$$\mathbf{r}_{diff} = \mathbf{r}_{ECF} - \mathbf{r}_{des}$$

$$r_{proj} = \mathbf{r}_{diff} \cdot \frac{\mathbf{r}_{des}}{r_{des}}$$

$$\mathbf{r}_{off} = \mathbf{r}_{diff} - r_{proj} \cdot \frac{\mathbf{r}_{des}}{r_{des}}$$

$$(5.7)$$

This calculation describes the offset of the satellite in a mathematical way, but this formulation is based on a physical interpretation. The first equation calculates \mathbf{r}_{diff} , the difference vector; by subtracting the vector describing the desired position from the vector of the actual position, the 3D-vector of the error between these two positions is obtained. The second step is to calculate the projection of this \mathbf{r}_{diff} in the direction of the desired position, as shown in Figure 5.6. Taking the dot product of the \mathbf{r}_{diff} and the unit vector of the desired direction gives the scalar length of this projection in the desired direction. The next step is to get the actual offset in the direction perpendicular to the view direction, this is done by subtracting the vector of the found projection from the earlier determined difference vector. After these three calculation steps one has obtained a vector describing the relevant deviation of the satellite from its desired position. In this thesis no distinction is made between an offset in for example the positive or negative Z-direction, therefore the exact direction of the offset is not relevant. This means only the length of the offset vector is important and the norm of this offset is therefore used for further calculations for this research. This leads to a single scalar that can be used as the objective function, something that is required as most DE-algorithms are designed for single objective optimisation problems.

This offset is calculated at every integration step and stored, while the cumulative projection over the complete trajectory is calculated as well. This cumulative projection is then divided by the number of integration steps in order to find the average projection. This average projection is used as the fitness of a trajectory and is thus defined as the objective function of the optimisation process. This objective function gives a proper fitness as it values the precision throughout the trajectory regarding the requirement of stable position as seen from the Earth surface.

During the work on this thesis, other objective functions using this offset were considered as well. First the cumulative offset was used as the objective function, which proved to have two disadvantages. First of all the cumulative projection is dependent on both the step-size and the duration of the trajectory; two equal trajectories will result in a different cumulative offset when the step-size changes. Furthermore, the objective function is always a large number without real physical meaning. The same disadvantage hold for an

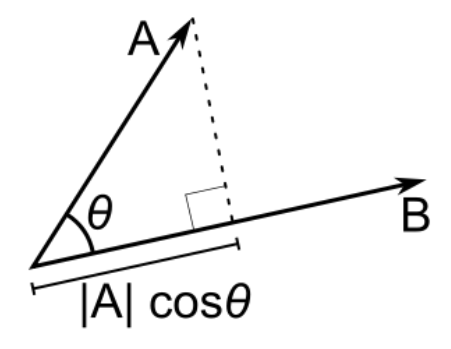


Figure 5.6: Scalar projection of B in the direction of A

objective function based on taking the third power of the offset for each time step. This variant 'punishes' a larger offset stronger and leads to a wider variation between the solution, which can be advantageous for the optimisation algorithm. However, both alternative methods did not show significant improvement when tested and were therefore discarded.

VERIFICATION AND VALIDATION

Every solid scientific research needs proper validation and verification performed in order to ensure the validity of the results. In this chapter the checks performed in order to provide a trustworthy report with reliable results are presented. This process is a combination of two things: verification and validation. Verification is the process where the correct working of the program and all its parts is examined. Validation on the other hand is the process of checking if the outcome of the simulations is a proper result. Verification can therefore be seen as an internal process where the correct working of the block is verified using a wide range of possible input. Validation on the other hand can be interpreted an external process: the result of the program is compared with results from independent sources such as previous performed research presented in literature. This way the validity of the program is checked.

Although strictly speaking validation and verification are thus different processes, they are also quite similar and are often performed simultaneously. Therefore in this chapter they are not distinguished from each other and all processes are discussed and presented together. In this chapter the processes are divided into different parts, that will be discussed separately. Firstly the parts of Tudat that are used are mentioned together with the checks done to check the correctness of these methods. Secondly a number of programming blocks defined in Section 5.2 is discussed; these blocks all concern the variable settings of the program, such as the *Eclipse* and the *Spherical Harmonics* blocks. After this the process of performing a single run is verified. Lastly the checks regarding the optimisation process are presented.

Apart from the methods and tests explicitly mentioned and shown later in this report, several small verification checks are performed during the programming of the code. This will be mentioned in the discussion about the first block *Sunline*. For the other blocks the procedure is similar, but this is not always mentioned as this explanation seems redundant.

Apart from the actual verification, this chapter also describes the tuning performed concerning the optimisation methods. These methods are tested for their correct working, along with the actual verification. However, during this process the settings of these methods were also tested. The settings of the optimisation algorithms used are tuned in order to provide the optimal performance. The considerations and tests that played a role in this process will be discussed in this chapter as well.

6.1. TUDAT

The complete tool is programmed in the Tudat environment using the C++ language. As explained in Section 5.1.1, Tudat is a toolbox developed at the Astrodynamics and Space Missions department and is used by many students there. Although Tudat is created with the greatest care and tested thoroughly, it is no professional software and therefore might be less reliable than most standard software. This means that for every command or method used, it is wise to test the correctness of these calculations. For professional software this is a good plan, for Tudat this seems even more important. This helps as a check on the validity of the method but also ensures the programmer uses the method properly. The working of most packages provided by Tudat is tested using a unit test and a sanity check. The most important packages used will be described

and validated here.

6.1.1. Transformation between reference frames

For this research two reference frames are used: the ECI and the ECF reference frames. These frames were introduced and described in Section 3.1 just as the transformation matrices needed to convert the coordinates between them. Such transformations are readily available in Tudat, as a package that is used here. During this thesis only the transformations between ECI and ECF are needed, these are fairly simple as only one rotation is considered. The origins are defined at the same point meaning that no translation is present, the only difference of the frames is the direction of the X- and Y-axis, caused by a rotation around the Z-axis. The only input that is needed for Tudat is the angle of the rotation at a certain point in time, here this angle is defined as $\Omega \cdot t$, where Ω is the rotational velocity of the Earth and t is the time in seconds. As the Earth turns 360° in a sidereal day the rotational velocity is found to be $\Omega = \frac{2\pi}{84164.1004} = 0.00007465398 \text{ s}^{-1}$. For a geostationary spacecraft this should result in a circular orbit in the ECI-frame, where X- and Y-coordinates follow sinusoids while the Z-coordinate remains zero. In the ECF-frame the initial position should be equal and stay constant over time. In Figure 6.1 and 6.2 the coordinates in both frames are plotted for one day, and thus one orbit, the thick lines represent an orbit with a longitude of $\lambda = 0^o$, while the thin lines are for a case with $\lambda = 90^{\circ}$. The thin lines are not always properly visible as the Y-direction of the second run coincides with the X-coordinates plotted before. The X- and Y-coordinate in the ECI-frame both follow a sinusoid, starting at geostationary altitude and zero respectively. The Z-coordinate stays, as expected zero. The ECF-coordinates also change throughout time although they theoretically should remain constant. Looking at the distances involved, the changes only measure $1\cdot 10^{-5}$ m. these small changes are explained as small errors in the calculations, this will be discussed later in this chapter. Looking at these results, the transformation between the two reference frame works correctly.

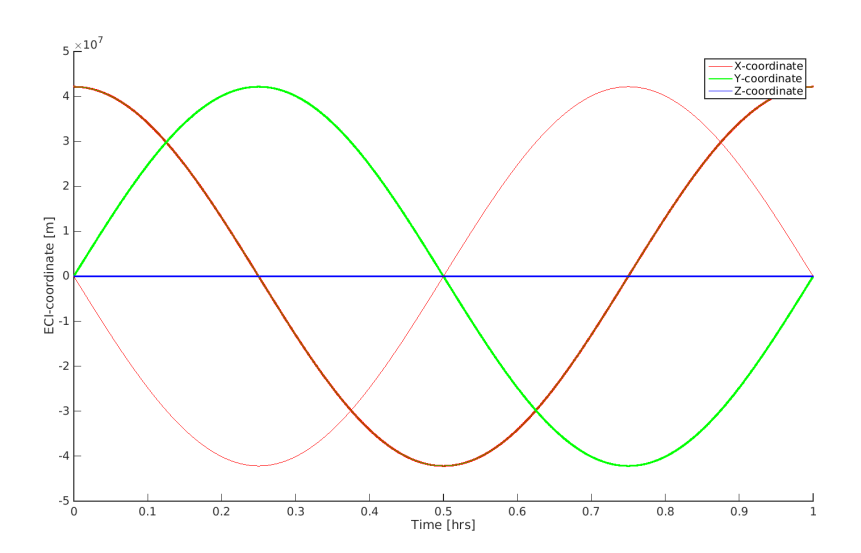


Figure 6.1: Cartesian coordinates of geostationary satellite in the ECI-frame

6.1.2. Transformation between coordinate system

Other transformations that are performed by Tudat itself are changes between the different coordinate systems. The conversion from degrees to radians and vice versa is performed using a simple ratio defined in Tudat, can be checked easily. Conversions between Cartesian and spherical coordinates are a little more complex and need a proper validation. Cartesian coordinates are straightforward and will not easily be mixed up, for spherical coordinates the angles can however be defined in multiple ways. In Tudat the angles are defined as was shown in Figure 3.1. This means the latitude angle δ is defined differently from the polar angle θ . The is defined from the equator towards the north, while the latter starts at the north pole and moves towards the south pole. This means another conversion is thus necessary if the latitude is needed.

The calculation of Kepler elements starting from Cartesian coordinates is implemented in Tudat. This is again

6.2. SETTINGS 55

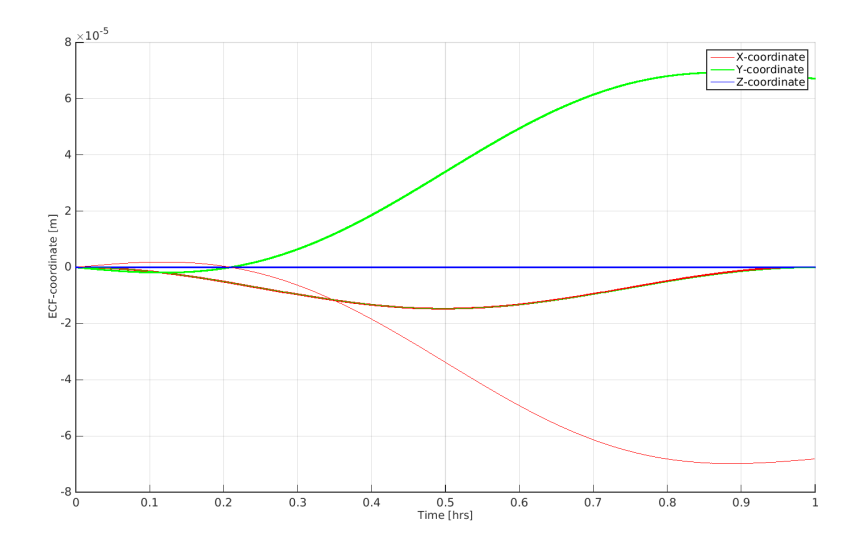


Figure 6.2: Cartesian coordinates of geostationary satellite in the ECF-frame

a conversion used a lot in astrophysics and its correctness is tested long before. However, it is important to correctly interpreted the results as the order of the elements is in contradiction to Cartesian less trivial and mistakes could easily be made here. Therefore the correct implementation of the elements is verified, while the exact values are not checked

6.1.3. TUDAT CONSTANTS

Many constants are used throughout this report; physical, celestial and mathematical constants are all needed for the calculations performed. In Tudat the most important and relevant constant are already defined and used directly without defining them as input manually. It is however important to check these constants as several things can influence the correctness of these values and thus the calculations. Therefore all constants that are used are verified using a sanity check to see if the correct definition is used. Furthermore, the constants are used throughout the complete program meaning they are implicitly when the code blocks are tested, therefore it is reasoned no further verification is needed.

6.2. SETTINGS

Apart from the code already available in Tudat, the majority of the tool consists of new code specifically created for this thesis. This code clearly also needs to be checked for proper working in order to prove validity of the results obtained using the program. In this section the most important programming blocks, as presented in Section 5.3, are tested and the results are presented and discussed.

SUNLINE

The position of the sun relative to the Earth and the spacecraft is clearly of major importance, as it directly influences the sail acceleration. The calculation of the sunline in the ECI-frame, and following the ECF-frame is validated by plotting the directions throughout the day and at different times of the year. In Figure 6.3 the tilt of the Earth's rotation axis and thus the equatorial plane with respect to the ecliptic plane is shown. Using this figure the direction the sunline is supposed to have at different dates throughout the year is verified.

Figure 6.4 shows values of the vector components of the sunline direction at December 21. The definition of the ECI-frame used is based on this day, thus the sunline points in the Y-direction. However due to the tilt of the Earth and thus the equator, the sunlight also has a vertical component. The sun shines at the equatorial plane from beneath it, meaning in a positive Z-direction. The Y-component has a magnitude of $\cos(23.5^{\circ}) = 0.92$ while the Z-component should be $\sin(23.5^{\circ}) = 0.40$., this corresponds with both values at t = 0. During one year the Earth makes one orbit around the Sun, this influences the orientation of the Sun in XY-plane. In one year the direction changes a full 365° . For an orbit of one day this means a change of just $\frac{360}{365.25} = 0.99^{\circ}$, this change is only small but can be observed in the X-component which rises

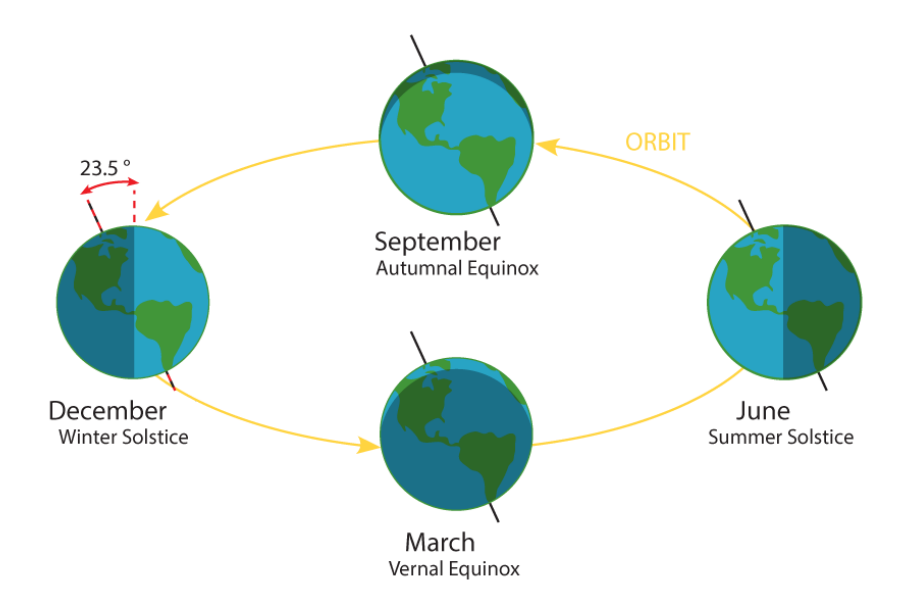


Figure 6.3: The seasons of the Earth and consequences for the sunline.

to $cos(89.01) = 0.017^{\circ}$ at the end of day one. Due to geometry, this change is even smaller in the Y- and Z-direction and these lines therefore appear to be straight even though they are not.

Figure 6.5 shows the same variables, but this this at March 21. This day is the spring, or vernal, equinox meaning the Sun shines perpendicular at the equator and the sunline has no component in the Z-direction. The situation is a quarter of a year earlier, and therefore the Earth also travelled a quarter of an orbit around the Sun. This means the direction of the sunlight in the XY-plane has shifted 90^o , as expected the light shines perfectly along the X-axis. The vector thus again has the elements that were expected, this implies the *Sunline* block works as it should.

This changing orientation of the sunline throughout the year clearly has a significant influence on the conditions and therefore the acceleration possible. This should be taken into consideration, using the same initial state and sail orientation during December and March will result in very different sail acceleration and thus trajectory.

SAIL ORIENTATION & ACCELERATION

For the calculation of the sail acceleration several parts of the code work together, both *Sail Orientation* and *Sail Acceleration* will therefore be discussed together here. For the sail orientation five different modes are available while the acceleration can be defined in three ways. The most important settings are presented and discussed here, not all combinations are presented here as this will give too much information and overlap of the results.

For the first three modes of the sail orientation are tested in combination with the second mode of the sail acceleration, the direction of the acceleration is set by the sail and has a fixed magnitude. The first mode was already verified in the last section where the sunline was plotted using these modes. The orientation fixed in the ECI- and ECF-frame were also tested and gave the desired results.

The last two modes where the sail orientation depends on the nodes defined in the decision vector are more interesting to investigate. Figure 6.6 and 6.7 are used to verify these modes, in the figures the blue arrow represent the sail normal $\bf n$ throughout the trajectory, the red arrows represent the sail acceleration and the yellow ones show the direction of the sunline. Both plots are created using a characteristic acceleration of $15\cdot10^{-5} \,\mathrm{m/s^2}$, this small acceleration is chosen so it does not lead to large deviations and the orbit stays close to the geostationary reference orbit.

For the sail orientation with fixed nodes, the orientation of the sail throughout the orbit is presented in Figure

6.2. SETTINGS 57

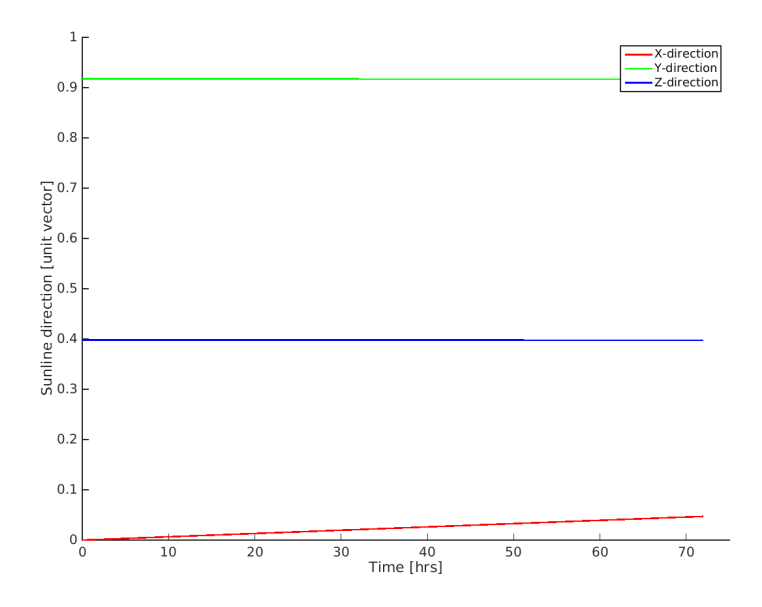


Figure 6.4: Vector describing sunline direction during three days, starting on December 21.

6.6, where the blue arrows describe the direction of the sail normal at the reflective side of the sail. For calculations the normal of the back of the sail is used, here for clarity the negative of this direction is shown, the normal of the sail in the reflective direction. In this case the sail is defined at the start by the two angles ϕ and θ , as was shown in Figure 5.3. This orientation stays fixed until the next node point is reached. Considering four nodes, the second node point is at one quarter of the orbit, there the sail instantaneously changes to the new orientation and the sail stays fixed again. In Figure 6.6 one can see that this is indeed the case, the orbit is split up in four equal parts which all show a fixed orientation. The same decision vector was used to test the last orientation mode, the results of this are shown in Figure 6.7. At the start of the trajectories, point (1;0), the sail orientation in both cases is exactly the same. This holds for the orientation at all node points, thus after each quarter of the orbit. However the sail orientation does not stay constant in between two node points, the sail turns gradually from one orientation to the next. It can be seen in Figure 6.7 that this indeed works as it was designed.

In both previous figures the blue arrows represent the direction of the sail normal, while the red one show the achieved acceleration. The blue arrows point in the direction of the reflective side of the sail and thus the acceleration will be in the negative direction. It can be seen that this is true for both figures throughout the complete trajectories. It can also be observed that the magnitude of the acceleration changes drastically depending on the orientation of the sail. The acceleration was calculated according to the third mode using Equations 3.15 and thus depends on both the sail and the sunline. Looking at Figure 6.6 one can see that the magnitude of the acceleration indeed depends on the angle α between the sail and the sunline. During the first part of the trajectory the sail is perfectly lined up with the Sun and the acceleration is maximal. The second part the sail is turned in a way that the angle between the sail and the sunline is 45^o , this means the acceleration will decrease with a factor of $\cos^2 45^o = 0.5$. Looking at the plot it seems indeed that this ratio is applied.

As it can hardly be determined exactly using these plots, Table 6.1 shows the magnitude of the sail acceleration throughout the orbit in Figure 6.6. For all node points the angles of the sail are given as well as the magnitude of the calculated acceleration just before and after the node point. As the sunline also changes throughout the day, the magnitude does not stay perfectly constant throughout one sail orientation. This is the reason the acceleration is given just before and just after the change of orientation, as the sunline changes approximately 1^o /day the theoretical value is changed using this value. For the first node point, the angles ϕ and θ are 90^o and 90^o respectively. This means that sail is aligned with the sunline and therefore $\alpha = 0^o$. As said, for the second node point angle α is 45^o and the actual acceleration should be half of the characteristic

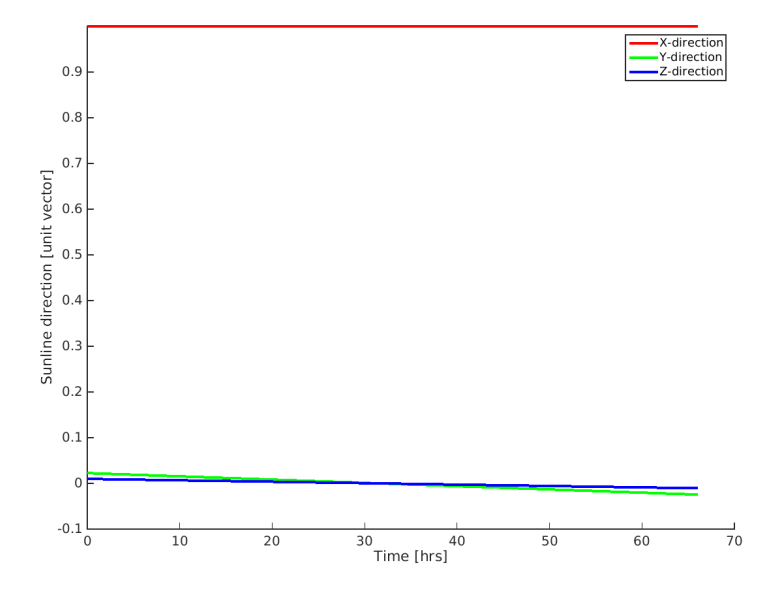


Figure 6.5: Vector describing sunline direction during three days, starting on March 21.

acceleration. However sunline has turned 0.25^o in the time passed, meaning α has also increased extra. For the third point, again $\alpha = 45^o$, however this time the angle is in the other direction and the change of the sunline causes a small decrease. It can be seen that the magnitude at all node points does correspond with the the third points, meaning both programming block work properly as they should.

Table 6.1: Acceleration achieved by sail with changing orientation, using a characteristic acceleration of $10 \, \mu \text{m/s}^2$.

Node	φ	θ	α	Magnitude	Ratio
				Acceleration	(Theory)
-	deg	deg	deg	$\mu\mathrm{m/s}^2$	-
Sunline	90	90	10	-	-
#1 start	90	90	0	10	$\cos^2 0.00 = 1$
#1 end	90	90	0	10	$\cos^2 0.25 = 1$
#2 start	135	90	45	4.957	$\cos^2 45.25 = 0.496$
#2 end	135	90	45	4.914	$\cos^2 45.5 = 0.491$
#3 start	45	90	-45	5.086	$\cos^2 -44.50 = 0.509$
#3 end	45	90	-45	5.129	$\cos^2 -44.25 = 0.513$
#4 start	0	0	90	0	$\cos^2 90 = 0$
#4 end	0	0	90	0	$\cos^2 90 = 0$

ECLIPSE

The simulator contains a function that at every integration step calculates if the spacecraft is in eclipse. The amount of sunlight received by the spacecraft is found using a shadow function, that calculates the fraction of the sunlight available. The theory of this shadow function was discussed in Section 5.3.5, here the results are validated using Figures 6.8a and 6.8b.

Figure 6.8a shows the eclipse conditions during two consecutive days starting at midnight on September 20. The plot shows the measurement points as red dots while the black line connects these points. At the start of both days, at midnight, the spacecraft is in total eclipse. After a short time, the spacecraft leaves the shadow of the Earth. First the shadow diminishes as only part of the Sun is blocked until the spacecraft is in total sunlight again, this process therefore happens as expected. The random values of these measurement points in both figures is caused by the fixed step-size of 25 s between them combined with the changing time of the eclipse periods. In Figure 6.8a he total time the spacecraft is (partly) in eclipse is found to be 4375

6.2. SETTINGS 59

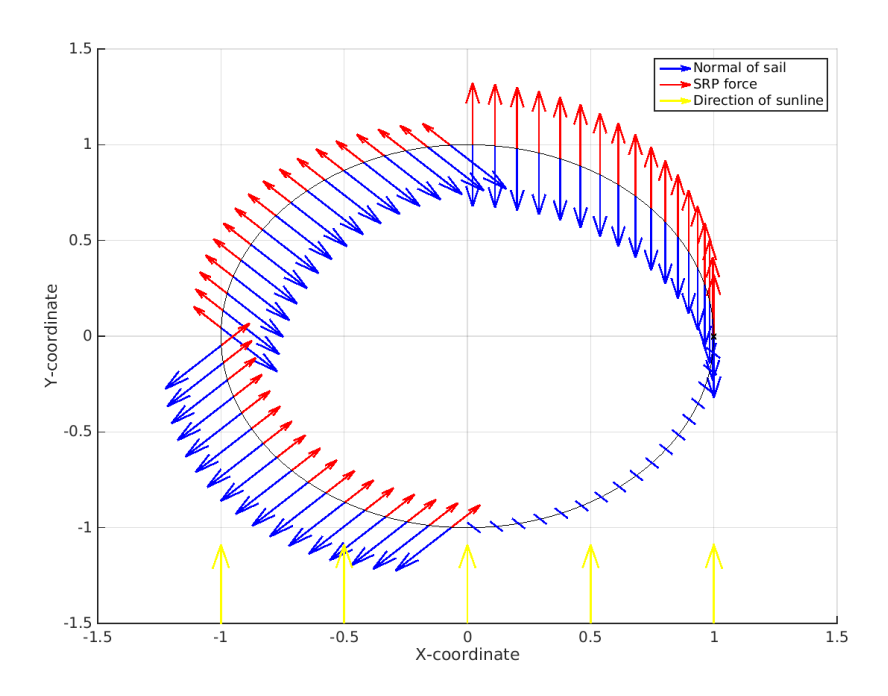


Figure 6.6: The sail orientation and the resulting acceleration using the fixed node scheme.

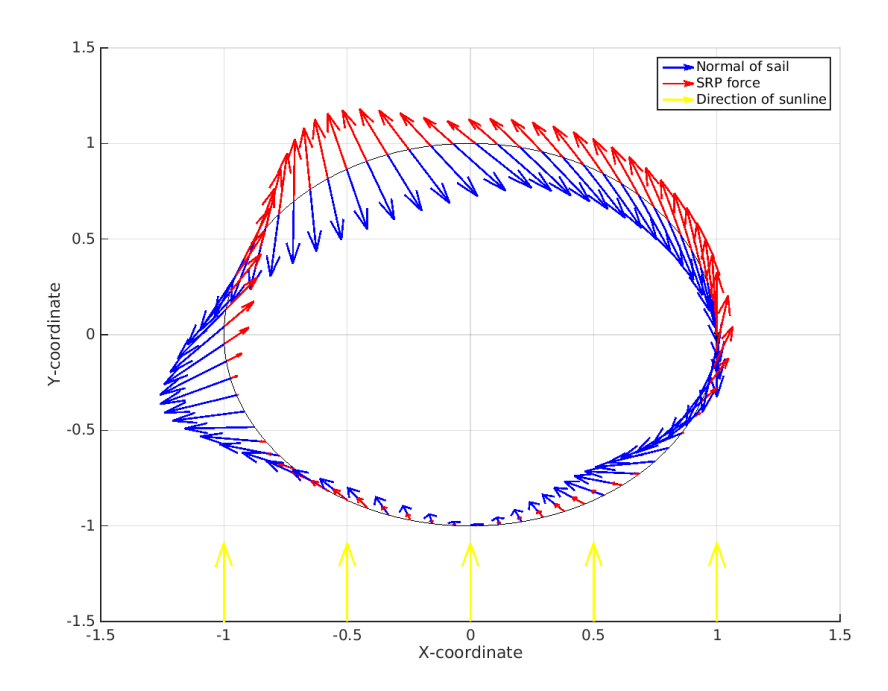
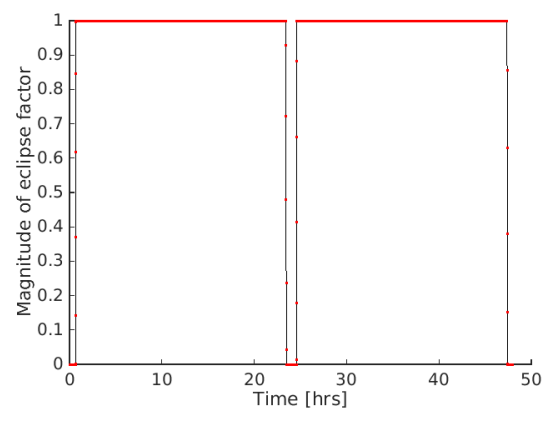


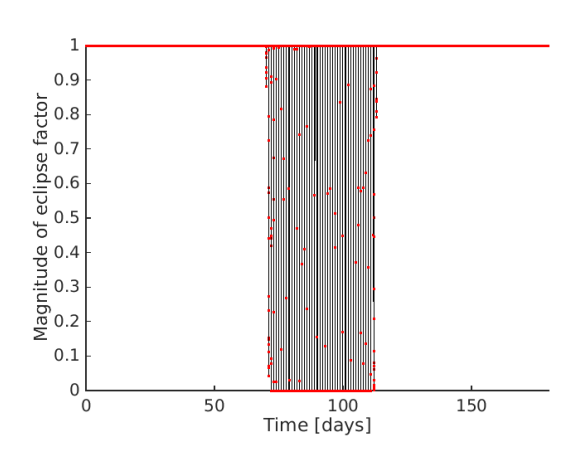
Figure 6.7: The sail orientation and the resulting acceleration using the changing node scheme.

seconds, looking at the data stored, in literature the eclipse time of a geostationary satellite is said to be 72 minutes maximally [39], or 4320 seconds. Although there is a small difference between the two, this error can be explained by the time step of 25 s between each stored measurement point and the lack of precision for the validation data. The length of the eclipse conditions is thus found to be correct.

Figure 6.8b shows the values of the shadow function during a half year, starting at June 21 until 180 days

later. From the figure it can be seen that throughout the year most of the days the satellite does not encounter eclipse conditions. This is in line with the expectations: only when the spacecraft, Sun and Earth lay in the ecliptic plane the spacecraft can be in the shadow of the Earth. The orbital plane coincides with the ecliptic two times a day, the tilted rotational axis of the Earth causes the time of these moments to change as was shown in Figure 6.3. At the summer and winter solstice, for the northern hemisphere 21 June and 21 December respectively, this takes place at 06:00 and 18:00 h. A the spring and autumn solstice, 21 March and 21 September, the times of these passes are noon and midnight. During the night, the satellite is positioned behind the Earth, only then the satellite can be in the shadow of the Earth. This means that only around the spring and autumn solstice the spacecraft is in eclipse, the rest of the years this is not the case. During the half year plotted in Figure 6.8b the spacecraft is in (partly) eclipse conditions during approximately forty consecutive days, around the autumn solstice. Looking at the results of the three figures, it can safely be stated that the eclipse shadow function works accordingly.





- (a) Value of shadow function on September 20 and 21.
- (b) Value of the shadow function over the course of an half year.

Figure 6.8: Value of shadow function. Day 0 represents June 21, day 91 represents September 21.

SPHERICAL HARMONICS

The implementation of the spherical harmonics in the model is twofold, the verification therefore as well. The two terms J_2 and J_{22} are calculation separately and their influence is therefore tested separately. Both perturbations are determined using solely the position of the spacecraft at a certain point in time and do not depend on the velocity or acceleration of the spacecraft.

The J_2 term describes the deviation of the Earth gravitational field, caused by an increased mass around the equator and therefore an increased attraction. Therefore the J_2 term depends on the distance to the Earth and the Z-coordinate, the X- and Y-coordinates do not have an influence. A geosynchronous orbit has a radius of 42,162.2 m, if a spherical Earth is considered. When J_2 is taken into account this does not exactly hold, the Coriolis force stays the same but the gravitational attraction has increased and there is no equilibrium any more.

The J_{22} term describes a deviation of the Earth sphere using sectorial spherical harmonics. As was shown in Figure 5.5, this deviation consists of bands in the latitudal direction and its magnitude thus depends on the longitude of the geostationary satellite considered. When the spacecraft moves is at a certain longitude it will be drawn to one of the red bands as showed in Figure 5.5. The effect of this attraction is a drift of the satellite in longitudinal direction, the direction depends on the longitude as is shown in Figure 6.9. The spacecraft will move towards a longitude of either 75^o or 255^o . The implementation of J_{22} in the software is tested using this figure and values obtained from literature [24]. A spacecraft in orbit at 30^o longitude is subjected to a Kepler orbit with only J_{22} considered as perturbation, the results are presented in Table 6.2. From the table it can be observed that the global values are in line with expectations. At longitudes 0^o and 30^o the longitude increases as the spacecraft drifts towards 75^o . Comparing the date found in [24] with the calculated values also proves correctness of the method. Even though the deviations are not exactly the same, the directions are

6.3. SINGLE RUN 61

all equal and the magnitudes are fairly close. Where the differences come from is not exactly known, this can be due several things, but the results are considered well enough. The case was repeated for a longitude of 0^o , the direction of the deviations stays the same, but the magnitude has decreased. This is indeed expected as the point lays further away form the stable equilibrium point at 75^o .

Table 6.2: Acceleration achieved by sail with changing orientation, using a characteristic acceleration of $10 \,\mu\text{m/s}^2$.

Longitude	Δr	$\Delta \theta$	$\Delta \phi$	Δr_{η}
deg	m	deg	deg	m
0	-66	0	$0.65 \cdot 10^{-4}$	482
30	-114	0	$0.82 \cdot 10^{-3}$	604
30 (Wakker)	-132	0	-	626

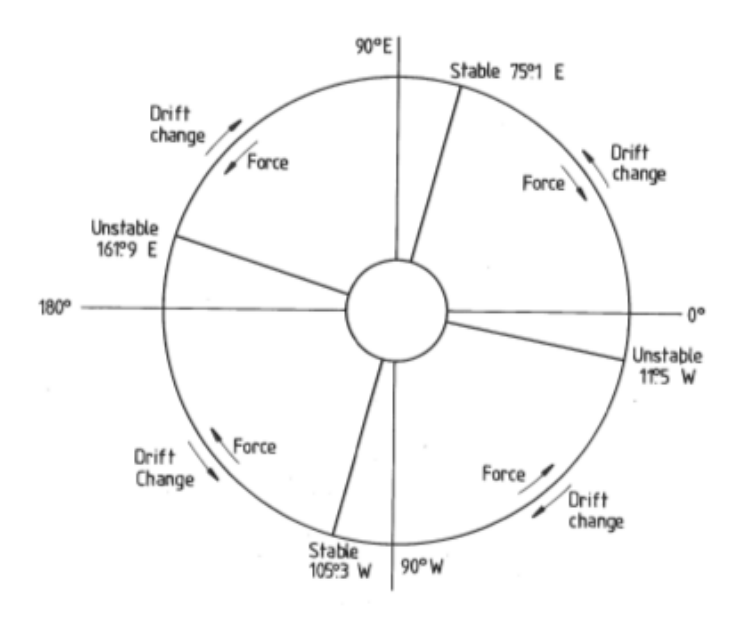


Figure 6.9: The sail orientation and the resulting acceleration using the changing node scheme.

6.3. SINGLE RUN

As all independent code blocks seem to work accordingly, it is time to see if the complete tool of all blocks combined also performs correct. This is validation is done by repeating several theoretical cases and check if the outcome corresponds to the expected results. Therefore, three simple cases where performed which will be discussed here.

6.3.1. STANDARD GEOSTATIONARY ORBIT

The most important characteristic of a geostationary orbit is the fact that its position with respect to the Earth surface is constant. Therefore a standard geostationary orbit is a perfect test-case for the working of the simulator in total and simultaneously several components. Using the *Initial State* block the initial state of a geostationary orbits is determined, which is then propagated over a complete orbit.

The result of this test is satisfying as the resulting trajectory is indeed an orbit with geostationary properties. After one sidereal day, and thus a complete orbit, the average projection of the satellite position is only $3.43563 \cdot 10^{-5}$ m. In Figure 6.1 the ECI-coordinates of a standard geostationary orbit are plotted, the thick lines represent an orbit starting at longitude $\lambda = 0^{o}$, the thin lines are regarding an orbit with $\lambda = 90^{o}$. As one can see, the X- and Y-coordinates change, but at the end of the day they are equal again to their initial values. This means that the spacecraft indeed makes a complete orbit in one day. Looking at Figure 6.2 one can see that the spacecraft indeed has an almost stable postition with respect to the Earth, the deviations are in the

order of 10^{-5} m which is basically nothing compared with the distance to the Earth of approximately $4.2 \cdot 10^7$ m.

Also when another longitude is chosen, defined in the initial state, these features exist. In both plots two trajectories are plotted, the thick lines using a longitude of $\delta = 0$ the thin lines using a longitude of $\delta = 90^{\circ}$. As one can see in Figure 6.1 the thin lines have shifted 90° back compared to the thick lines. The deviations in the ECF-frame also look similar, although a positive Y-deviations now results in a negative deviation in X-direction.

The values obtained using these simulations are also presented in Table 6.3, where among others the offset after orbit is shown. The resulting average offset of a standard geostationary orbit is approximately $3.44 \cdot 10^{-5}$, irrespective of the chosen longitude. The fact that the deviations remains very small, after ten orbits the average projection is still less than a milimeter, shows that the orbits are indeed periodic and stable and remain equal for longer periods of time.

# Orbits	δ	Average Projection
[-]	[deg]	[m]
1	90	$3.44126 \cdot 10^{-5}$
1	0	$3.43563 \cdot 10^{-5}$
3	0	$1.01909 \cdot 10^{-4}$
10	0	$3.64621 \cdot 10^{-3}$
365	0	$4.66323 \cdot 10^{-2}$

Table 6.3: Average projection of geostationary orbits.

6.3.2. DISPLACED GEOSTATIONARY ORBIT

In the previous section a normal geostationary orbits, without any displacement of perturbations was analysed and there the tool proved to work properly. This was only the most standard case and basically 2Dproblem, here it is investigated what the effect of a displacement in the Z-direction has on the orbit. When the initial state of the satellite is similar as before, only in the Z-direction an offset is introduced the trajectory of course changes. The resulting trajectory of this initial state is shown in Figure 6.10. As no perturbations act on the spacecraft the result is still a period Kepler orbit. As the initial displacement is minor, there is no considerable effect on the radius and the orbit remains almost circular with the same orbital period. The orbital plane is however tilted compared to before, after half the orbit the Z-displacement is equal as before, but the positive displacement is now negative, after the complete orbit it is positive again. After one complete orbit the average projection starting with an offset of 1880m is found to be 1879.77m. For a perfect Kepler orbit these values should be equal, the small difference can be caused by the slight change in radius and the large timestep considered for storage. The program stores its state every 25s meaning the last point is not exactly after one sidereal day. This rather large step is chosen in order to reduce the simulation time and to limit the memory space needed. During the propagation this is no problem as shown, but the downside is that the state can not be found at a more precise point in time. The resulting trajectory is exactly what was expected, meaning that the propagation of the satellite also works correctly in a 3D-problem.

6.3.3. ELEVATED GEOSTATIONARY ORBIT

The orbit propagation works fine if just the spherical Earth is considerer, now let us find out if also the addition of solar radiation pressure works correctly. The focus here lies on adding an extra force and not on the exact working of the sail, therefore an SRP value constant in the ECI-frame is assumed. In Section 3.7 a test case was proposed as a first order approximation of the possible displacements. Although this case was not realistic, it is very suitable as a validation method, and is therefore produced here. Using Equation 3.34 it was found that in order to achieve a constant offset of 1880 m an acceleration of $1 \cdot 10^{-5} m/s^2$ is required. Figure 6.11 shows the resulting trajectory, together with the case of a displacement and also added acceleration ten times smaller. As can be seen both cases result in the desired orbits, a geostationary orbit in an elevated orbital plane. The plot shows the type of orbit, but is not accurate enough to say something about the precision. With an offset of 188m the average projection after an complete orbit is 0.061m, for a displacement of 1880m the projection becomes 1.090m. From these results it can be concluded that the calculations and the simulator

6.4. INTEGRATOR 63

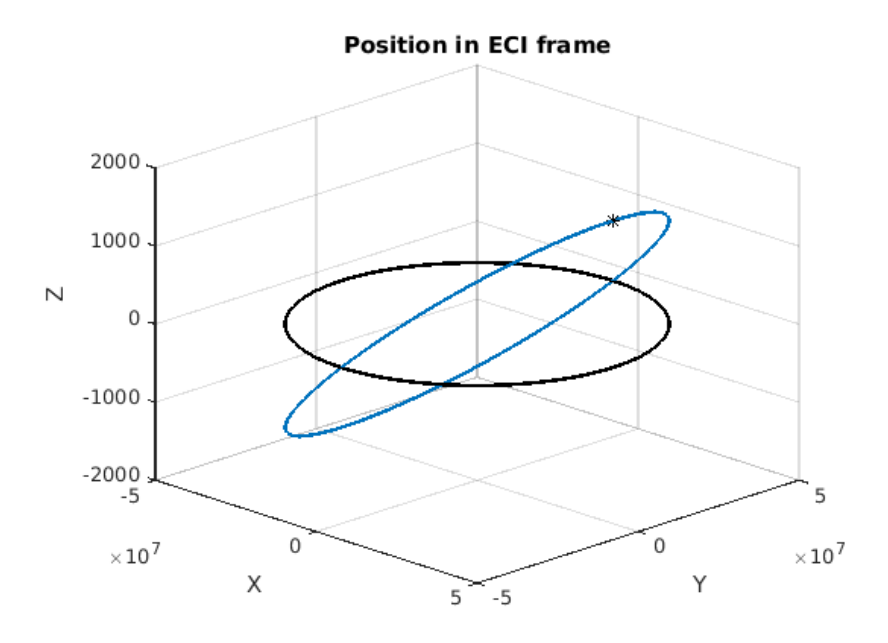


Figure 6.10: Cartesian coordinates of geostationary satellite in the ECF-frame

work properly, the small differences are assumed to have the same origin as without SRP. Another factor that can play a role is that the solution used as a displacement is rounded off slightly which introduces an error. The fact that the projection grows significantly using a larger displacement matches with the assumed origins of the errors. However, as the errors are still considered to be small, adding an extra perturbing force to the spacecraft is handled correctly by the simulation.

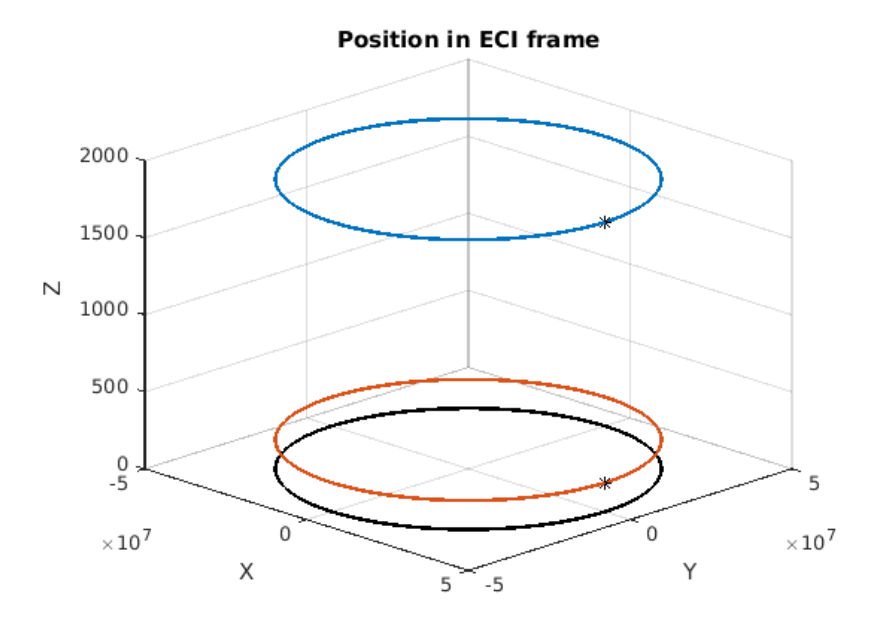


Figure 6.11: Cartesian coordinates of geostationary satellite in the ECF-frame

6.4. INTEGRATOR

In Section the selection of a integration method was presented, while discussing the importance and characteristics of this integrator. The RK4 method is used for the calculations in this thesis, a decision mostly based

on its simplicity and corresponding low calculation time. These two advantages come however at a cost, its simplicity leads to a lower accuracy compared to more complex and elaborate methods. Therefore, the accuracy of the RK4 method will be discussed here.

A great part of the relevant analysis of obtaining data is already performed in previous sections of this chapter. In Table 6.3 the average projection of a spacecraft in a geostationary orbit is shown. As the projection should be equal to zero, a perfectly geostationary orbit is considered, the projection can be seen as a calculation error. The numbers are found using an unperturbed orbit, so the whole simulations only consists of an initial state integrated using given equations of motion. The error for one complete orbit, in time this corresponds to a day, is on average $3.4 \cdot 10^{-5} m$. After 10 orbits, this error has of course grown but only up to 3,6mm, which is still considered very small. After on year of simulated orbit time, the error is still only a couple of centimetres.

Looking at the distances considered and the precision required, this accuracy of the integration is clearly good enough. The offset and projection of the resulting trajectories presented in the next chapter are in the range of kilometres. This means an integration error less than a millimetre, for a three-day simulation, is small enough to be considered negligible. This validation is only performed for a simple case without perturbations and the error will clearly grow when more perturbations are considered and more calculations are performed.

6.5. OPTIMISATION

The propagation part of the program was tested successfully, now it is time to look at the optimisation part of the simulator. The optimisation part is mostly based on the optimisation algorithm used, as these are part of the PaGMo package, they only need to be implemented correctly. This process is tested during the implementation stage itself using simple tests, which are not specifically described here. However, choosing the proper way to set up the optimisation problem and select the best algorithm is based on results from tests performed using simple cases.

6.5.1. DE-ALGORITHMS

Multiple algorithms working on the principle of a DE are available in PaGMO, a number of these algorithms are used and compared, the results are presented here. The three algorithms DE, JDE and DE $_{1220}$, all available in PaGMO were selected as three candidates. The performances of these different algorithms were assessed using a reference optimisation problem. The desired trajectory of this reference problem was defined as a geostationary trajectory without any elevation and the sunline is assumed to lay in the equatorial plane. This set up ensures that the solution is known beforehand, as no elevation is required, the same holds for the acceleration.

Figure 6.12 shows the performances of the selected algorithms for a test optimisation problem. The optimisation problem at hand has a fixed initial state, meaning the decision vector only consists of the angles defining the sail orientation. The optimisation is set to perform 200 generations, consisting of 250 individuals each, while four node points are considered. The red, blue and green line represent DE, DE_{1220} and JDE respectively, there only difference is the settings of the parameters F and CR. The green and black line are both constructed using the JDE algorithm, were the F and CR values are changed for every generation. The green one were a adaptive scheme is implemented to set F and CR, while for the black line these values were set randomly, referred to as dither. The results shown are promising as the average offset decreases quickly to a value near zero, the minimal value. Most runs are below 5 m offset after 50 generations as can be seen in Figure 6.13, which shows the same results but zoomed in. Looking closely at this figure, blue lines corresponding to the DE_{1220} algorithm seem to perform the best, while the red lines representing the standard DE-algorithm show the worst performance. For comparable tests, with for example a different number of nodes, the same results were observed, therefore the DE_{1220} algorithm was selected as the best option and used for further calculations.

Even though the performance of the optimisation algorithms seems quite good looking at Figure 6.13, this is only for a very simple problem considering only half of the decision vector. Using the same algorithm for the complete decision vector, the performance decreased rapidly. Even after testing out several settings, the

6.5. OPTIMISATION 65

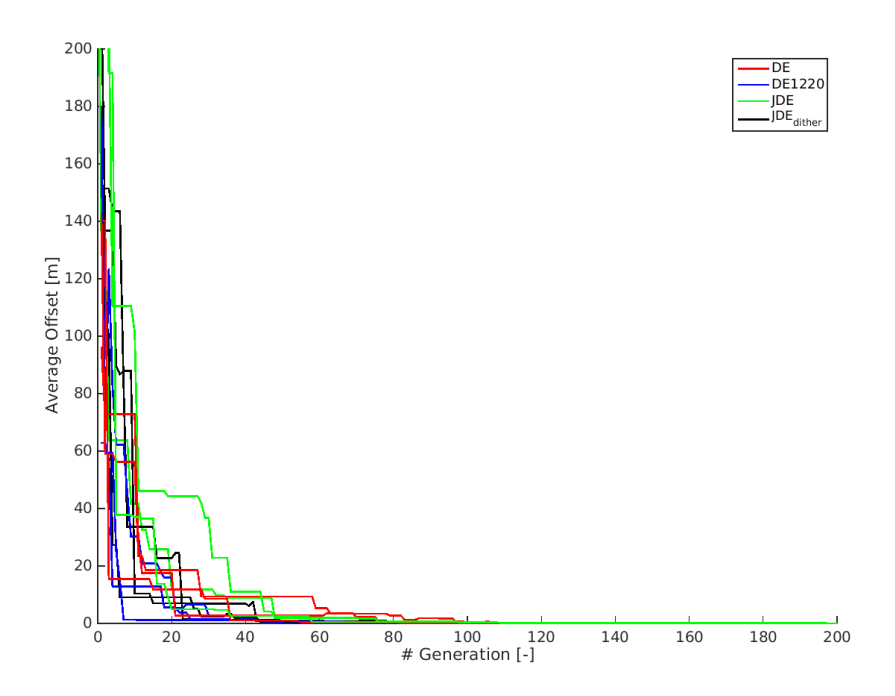
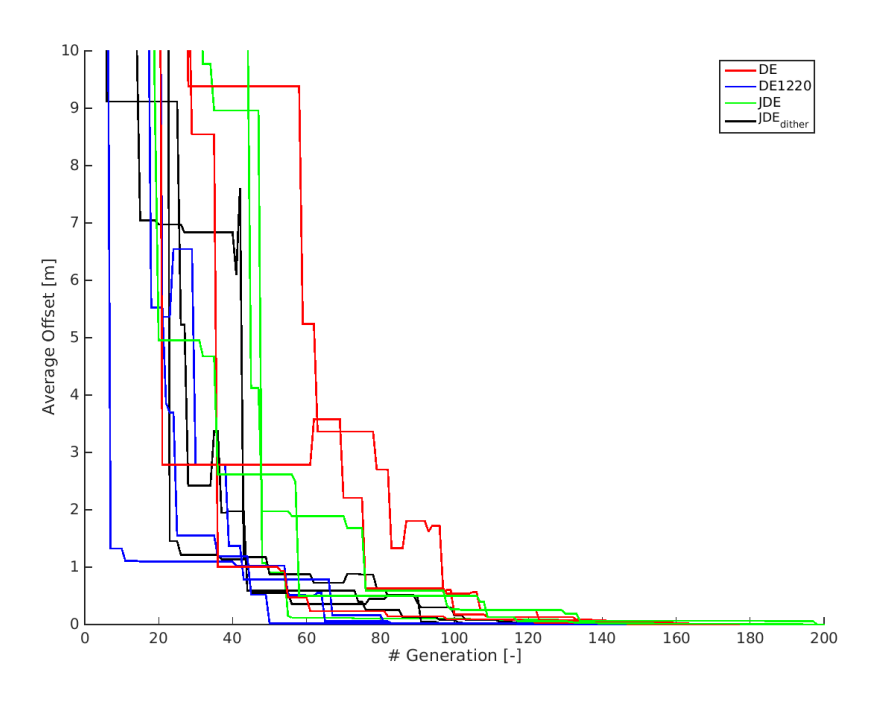


Figure 6.12: Comparison between different DE-algorithms.



 $\textbf{Figure 6.13:} \ Comparison \ between \ different \ DE-algorithms.$

results did not improve significantly enough in order to found proper, reliable and useful solutions.

MOEA/D

Tuning of the selected DE-algorithms did unfortunately not have the desired effect, it improved the performance but not too the desired level. As the MOEA/D algorithm was available in PaGMO and is based in similar principles, differential evolutionary, it was selected as a next step in the search for an appropriate al-

gorithm. A geostationary orbit with no elevation was selected as the test case, the decision vector consisted of both the initial state and four node points. For both the DE_{1220} and the MOEA/D, using a number of different settings, this optimisation was run. Figure 6.14 shows the result of these optimisations. The D=0 and S=0 as seen in the legend describe the displacement considered and the sunline mode(0 represents simplified case of sunline in equatorial plane).

From this plot it becomes clear that the MOEA/D performs much better than the DE-algorithms tested before. Apparently the settings of the DE using in the MOEA/D algorithm are tuned perfectly for this problem. For this reason, the MOEA/D was selected as the best choice for further optimisations.

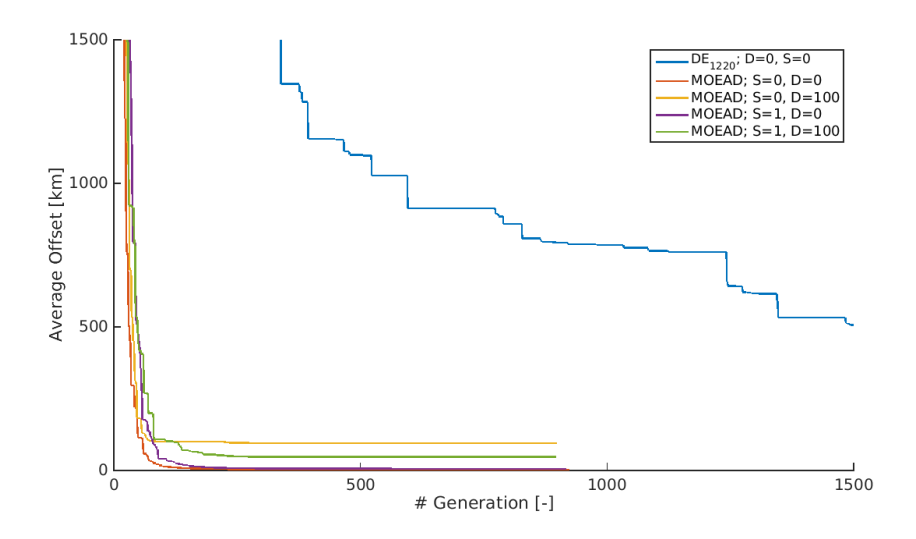


Figure 6.14: Comparison between different DE-algorithms.

6.5.2. DECISION VECTOR

As discussed before, the decision vector consists on the initial state and the angles defining the sail orientation throughout the orbit. The choice of these elements was argued in Section 5.4.1 and will not be assessed here. The part that remains and can be investigated quantitatively are the bounds of the decision vector defining the search space.

A threat in selecting the proper bounds is setting them too small, thereby eliminating the search space where the actual optimal solution is present. As the solution is not known one can only completely overcome this threat if a very large search space is selected. As this is not favourable in terms of convergence this option is not chosen here. One should therefore keep track on the solution to check it is not approaching the limits of the search space, if this is the case they are set too small and limit the optimiser. It is expected that the magnitude of the deviations from the initial guess depends heavily on the displacement desired. For an orbit displaced only one kilometre these deviations are expected to be much lower than for an displacement of 50 km. Therefore it is not useful to already verify the ranges of the decision vector and the resulting search space. The selected values of 1 km on the position and 1 m/s are therefore used for the optimisation part. However the decision vector will be analysed, if the bounds prove to be to small at any point and the values reach their limits, it should be considered to increase these bounds.

RESULTS

Now all theory, methods, program set-up and settings are discussed it is time to present the results obtained using all this knowledge and data. These results will be presented in this chapter. The whole process of programming, verifying and tuning was described before and here the final results are presented. This chapter presents the possibilities for several cases, while varying multiple parameters. The desired displacement and characteristic acceleration are the most important parameters that were varied. Furthermore, the settings of the sail and the environment also have an influence; for the latter the time of the year is an example of a parameter that has large influence.

The results are grouped according to the desired positional elevation and will thus be introduced in this way. For each case one or more plots show the best solution found for that particular set of parameters. For every trajectory this is followed by a brief analysis and at the end of the chapter a short recap of the results can be found. Every optimisation is run at least three times using different seed numbers. This provides the opportunity to say something about the convergence reached and the validity of the solutions. If all three resulting trajectories are completely different and have different fitness values as well, the optimisation has not converged properly. If this is the case, some settings have to be altered in order to improve this. Other conclusions can be drawn from comparing these different runs, as will be discussed when relevant in this chapter.

Every optimisation process is run three times, while every run consists of three consecutive orbits, the length of each simulation is thus three days. This is chosen in order to improve and assess the stability of the found solutions over a longer time. An orbit that stays fairly close to the desired position is a good result, but the actual orbit will of course be designed for multiple years. This means that the orbit should repeat itself and the final state is preferably close to the initial state. As in an optimisation typically performs around 100,000 simulations, the calculation time is an important factor: even if one orbit propagation takes a fraction of a second the optimisation process still takes several hours. When multiple revolutions are analysed, the calculation time rises accordingly. This means that it is infeasible to run an optimisation of a large number of revolutions per trajectory. However, considering only one revolution reduces the validity of the solution significantly and therefore three orbits is chosen as a compromise. As will become clear in the remainder of this chapter, this number is still low and each trajectory found clearly consists of three different revolutions, although in the best solutions these lay fairly close to each other. The calculation time of a single optimisation is approximately 8 hours, this is still acceptable but may not be increased much more.

As was explained earlier in Chapter 5 a number of settings can be chosen in order to change the conditions in which the satellite is in. As it is not needed to state every setting explicitly every time a result is presented, here the reference, standard settings are presented. Some calculations will be performed with setting that differ from the ones mentioned here, in those cases that will be made clear when presenting the results. The default process considers the most optimal time of the year, 21 December, the start of the winter in the northern hemisphere. At this date the Sun shines with an angle of 23.5^{o} relative to the equator, in upward direction. This means that the sunlight already partly is directed in the direction of the desired displacement. Furthermore, J_2 , J_{22} and the eclipse all all considered, just as the most realistic mode for the sail and determination of the sail acceleration. The sail orientation is determined by two angles defined at specific node points, while

in between these nodes the sail rotates linearly towards the direction of the next node. The acceleration direction and magnitude are naturally calculated using both the sail and sunline directions, while a perfect sail is considered. The default characteristic acceleration is set at $1~\rm mm/s^2$ and the number of nodes is standard set at $10~\rm nodes$, although this will always be mentioned along the corresponding analysis. Furthermore the settings used for the optimisation method MOEA/D are the default settings in PaGMO, with 750 generation, 150 individuals per generation and a neighbourhood size of 75. These settings were explained before and will be kept equal for all optimisations.

For each separate case discussed in this chapter, three different runs were performed and their properties are presented in a table together with all runs for that specific elevation. Per case the best solution is selected and its trajectory in the ECI-frame is plotted, just as the offset and sail acceleration throughout the orbit. The first four sections represent the four elevations considered. These sections present the trajectories found for the optimal conditions around the winter solstice of December 21. As a geostationary satellite should maintain a constant position throughout the complete year, Section 7.6 shows the results found for optimisation performed for other times during the year. Lastly in Section 7.7 a short recap of the found results is provided together with a discussion about the convergence of the optimisation process concerning the found solutions.

7.1. WINTER SOLSTICE CONDITIONS

The sail acceleration depends on the sail performance and on the pitch angle α , this angle itself depends on the orientation of the sail and the direction of the sunline. The direction of the sunline changes throughout the year, meaning the conditions for the sail acceleration change as well. For an orbit elevated in the positive Z-direction, the most favourable period of the year is during the winter solstice as the sunline is tilted towards the Z-direction. Therefore the optimisation is first run starting at December 21, the results for this start date are presented below.

7.2. 1 KM DISPLACEMENT

A one kilometre displacement above the equatorial plane is not enough for geostationary satellites to stay outside the standard belt for existing satellites. However, the results obtained could tell something about the working of the process and lessons can be learned. The optimisation for trajectories with this desired displacement of one kilometre is performed for three different magnitudes of the characteristic acceleration; 0.1, 1 and 10 mm/s². All three cases are performed three times using different seed numbers, resulting in nine trajectories. These resulting nine trajectories are presented in Table 7.1, where the properties and the average offset of the trajectories are shown together. For the best three solutions, one for each specific case the trajectory in the ECI-frame is also plotted, as well as the offset and the sail acceleration throughout the orbit. In the remainder of the chapter all results will be presented this way.

Displacement	#Nodes	Characteristic	Seed #	Average
		acceleration		offset
[km]	[-]	$[\text{mm/s}^{-2}]$	[-]	[km]
			1	0.30235
1	10	0.1	2	0.37835
			3	0.79090
			1	0.3365
1	10	1	2	22.302
			3	16.102
			1	85.016
1	10	10	2	1.053
			3	1.0061

Table 7.1: Solutions of optimisations using a 1 km vertical offset.

7.2. 1 KM DISPLACEMENT 69

7.2.1. 10 Nodes, 1 mm/s² characteristic acceleration

The best result found using an characteristic acceleration of 1 mm/s² is shown in Figure 7.1. The black line is the trajectory of a normal geostationary satellite, orbiting in the equatorial plane. The red line represents the desired trajectory, a perfectly elevated geostationary orbit at a constant elevation of 1 km above the equator. A satellite orbiting at the red line will thus have a constant position relative to the Earth 1 km above the equator, the goal of this specific optimisation. The blue line is the trajectory that is found as the best result in the optimisation process, whereas the black star indicates the initial position of the satellite. These colours are used for all the trajectory plots following in this chapter.

It can bee seen that indeed an elevated orbit is found that lies considerably closer to the desired elevated

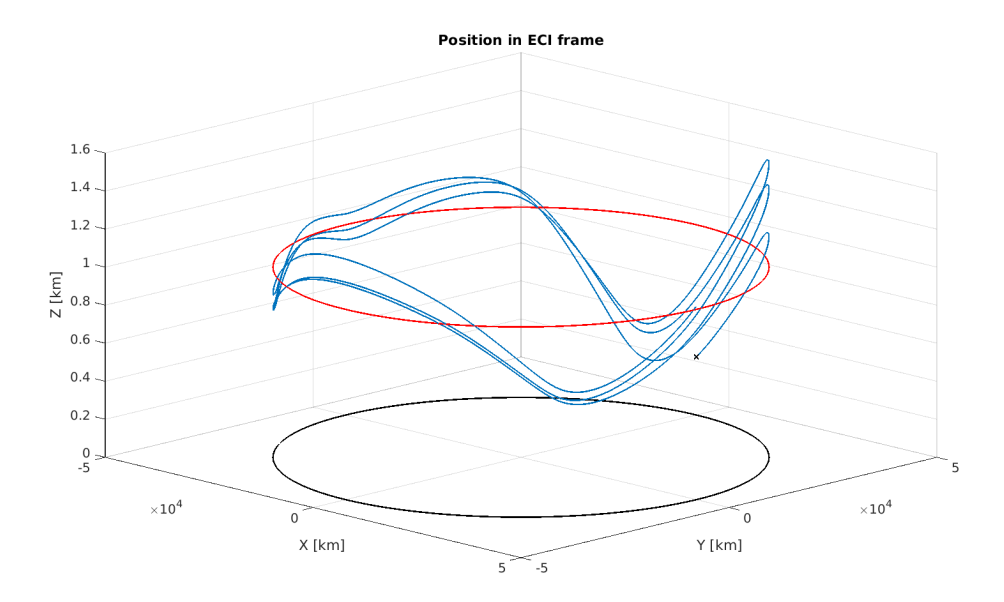


Figure 7.1: Best orbital solution considering: 1 km displacement, 10 Nodes, 1 mm/s² characteristic acceleration

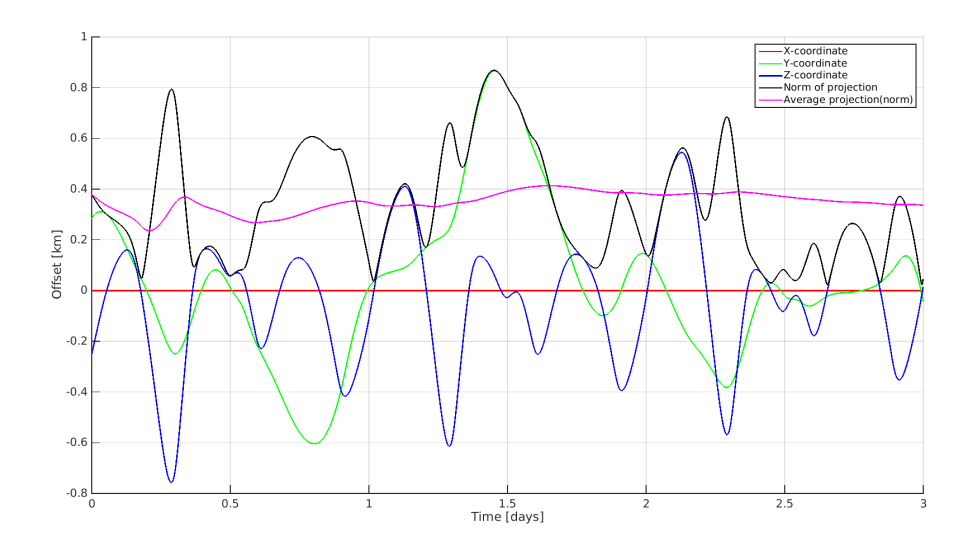


Figure 7.2: Offset throughout orbit of case 1 km displacement, 10 Nodes, 1 mm/s² characteristic acceleration.

orbit compared to a normal geostationary satellite. The average projection and thus deviation from the desired point is found to be 336.5 m for this specific trajectory. This is well within the requirements of 10 km set

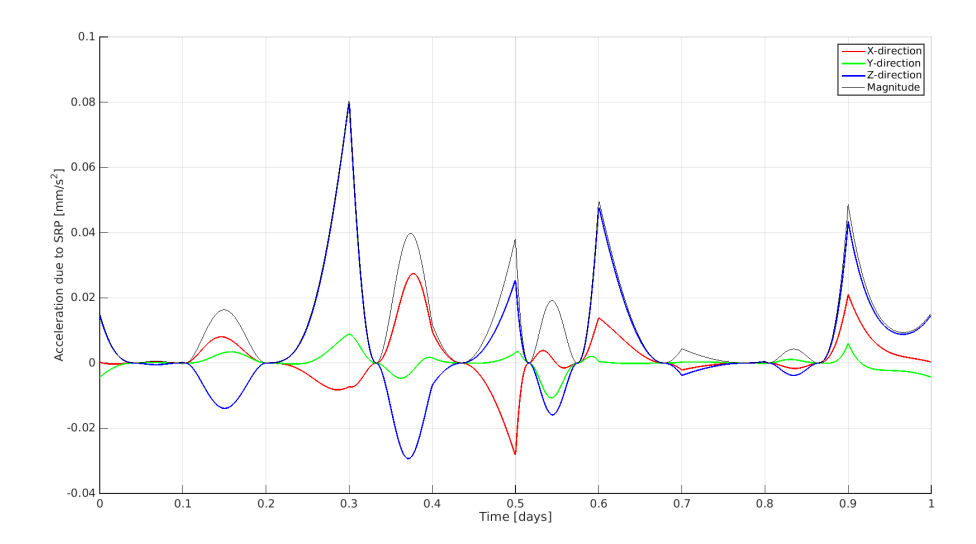


Figure 7.3: Sail acceleration throughout orbit of case 1 km displacement, 10 Nodes, 1 mm/s² characteristic acceleration.

for the allowed deviation of an elevated orbit, however looking at the scale and the actual trajectory this was expected. It is not clear yet how this results will change when the displacement is scaled up. Looking at the absolute error, the result of 336.5 m is good, however the error is roughly one third of the desired elevation which seems quite significant. It is a promising first result, the actual relevance should become clear looking at other cases.

Figures 7.2 and 7.6 show the offset and the achieved sail acceleration throughout the trajectory. Figure 7.2 shows the same trajectory as plotted before, but the position in the different directions is plotted over time for the complete orbit. The red, green and blue lines show the X-, Y- and Z-coordinates of the offset as defined in Section 5.4.3. As the displacement of 1 km is so small compared to the geostationary altitude the X-coordinates can basically be interpreted as the radial component of the offset. The offset in radial direction is only in the order of centimetres which explains that it appears to be a straight line of no offset in the plot. Looking back at the definition of the offset considered here, see Section 5.4.3, this is a logical result and is something that will be the case for all results shown in this chapter. The green line represents the Y-direction, which comes close to the offset in the velocity direction, while the blue line is the Z-component of the offset which is closely related to the actual Z-component of the position. Looking at Figure 7.2 it can be observed that the offset in Y- and Z-direction are in the same order of magnitude, although their profile throughout the trajectory is different. Figure 7.6 shows the sail acceleration throughout the orbit and proves the sail is not using its full capacity, the magnitude of the acceleration does not even reach 10% of the characteristic acceleration. This is not completely unexpected as the characteristic acceleration is quite high for the displacement considered.

It should be noted that even though the result is good, this trajectory was only found one during several runs using random seeds which all gave fairly different results in both fitness and trajectories. The results of the two other simulations performed for the same case are shown in Table 7.1 as well. The first set of runs did not result in proper solutions with average offset in the range of 15-20 km, and eventually only one of the six simulations gave such a good result. That this results was obtained is certainly nice as it proves that the optimisation works and good results are possible, but it seems troublesome that only one of six found this solution, whereas the others obtained far worse results with fitnesses several orders higher. This means that the optimisation method is far from perfect as the random choice of the individual in MOEA/D plays a major role, something that is not desirable.

7.2.2. 10 Nodes, 10 mm/s² characteristic acceleration

As the results from the previous section were not completely satisfactory, the same displacement is considered here but using a larger characteristic acceleration.

7.3. 10 KM DISPLACEMENT 71

Although the characteristic acceleration of 10 mm/s^2 is far from achievable in the near future as was discussed in Section 2.4, the results can still be interesting. If these optimisations show a large improvement, it can mean that the problem previously was that the force on the sail was not large enough. Looking at Figure 7.4 and 7.1 one can see that even though there is more acceleration and thus displacement possible, this does not improve the solution. The result is actually an increase in absolute projection and in this case the satellite moves both under and above the equatorial plane. Both of these things are clearly not preferable and therefore this result can be considered worse. Clearly the amount of acceleration was not the limiting factor before, which is good to know as this would mean this small elevation would already be infeasible, let alone larger displacements. It even seems that the characteristic acceleration is in fact too large in this situation.

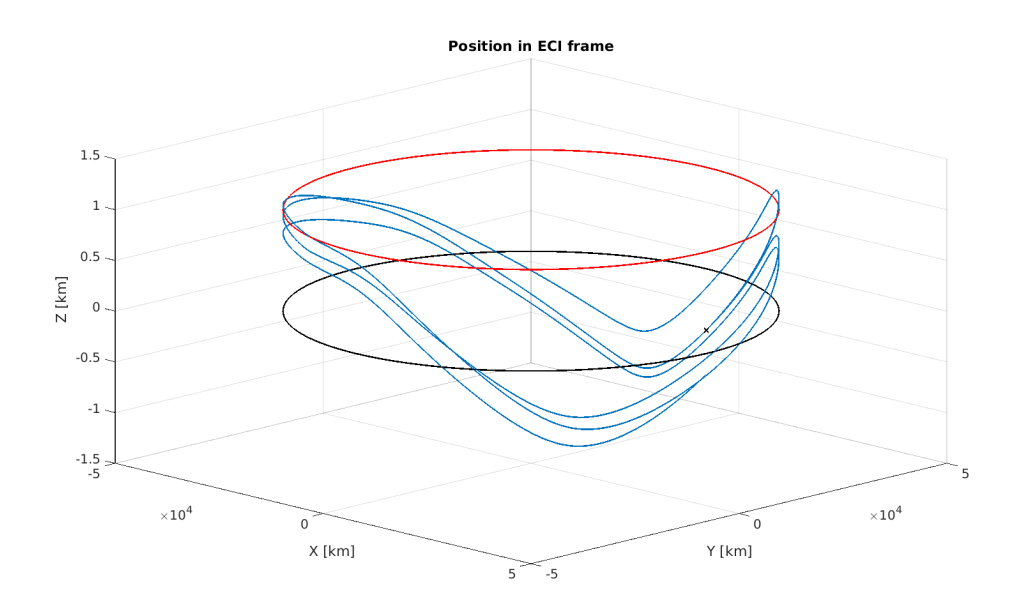


Figure 7.4: Best orbital solution considering: 1 km displacement, 10 Nodes, 10 mm/s² characteristic acceleration

7.2.3. 10 Nodes, 0.1 m/s² Characteristic acceleration

As it turned out that a larger characteristic acceleration does not automatically lead to better solutions and can even result in worse performance, here the same optimisation is performed with a smaller acceleration than before. In this case an acceleration of 0.1 mm/s^2 is used and the result is shown in Figure 7.5. It has similar characteristics as found for an acceleration of 1 mm/s^2 , with two hills and two valleys at opposite sides. The exact reason for this shape is unfortunately not known. Looking at the fitness as shown in Table 7.1 it becomes clear the result is indeed improved. Not only the best case is slightly better than the trajectory found for 0.1 mm/s^2 characteristic acceleration, all three cases show solutions in the same order of magnitude of hundreds of metres. This is a very good results, it shows that the accelerations is not a limiting factor, at least not with such a reasonable small displacement.

7.3. 10 KM DISPLACEMENT

7.3.1. 10 Nodes, 1 mm/s² characteristic acceleration

The elevation is now increased to a desired displacement of 10 km, which is a more significant value. With 3.67 km as average projection for the best obtained trajectory, the result is in absolute numbers worse than found for 1 km displacement. However this offset is again roughly one third of the desired elevation and as the displacement is ten times as high, so is the resulting error. This means that the change in position during the orbit is still within reason, but keeping the limited displacement in mind, it is considered rather large. Looking at the results for 10 km and 1 km it might be that an average projection of about one third of the desired elevation is the best achievable. This is however only seen for these two cases and therefore certainly not decisive yet, further results will show if this relation still holds.

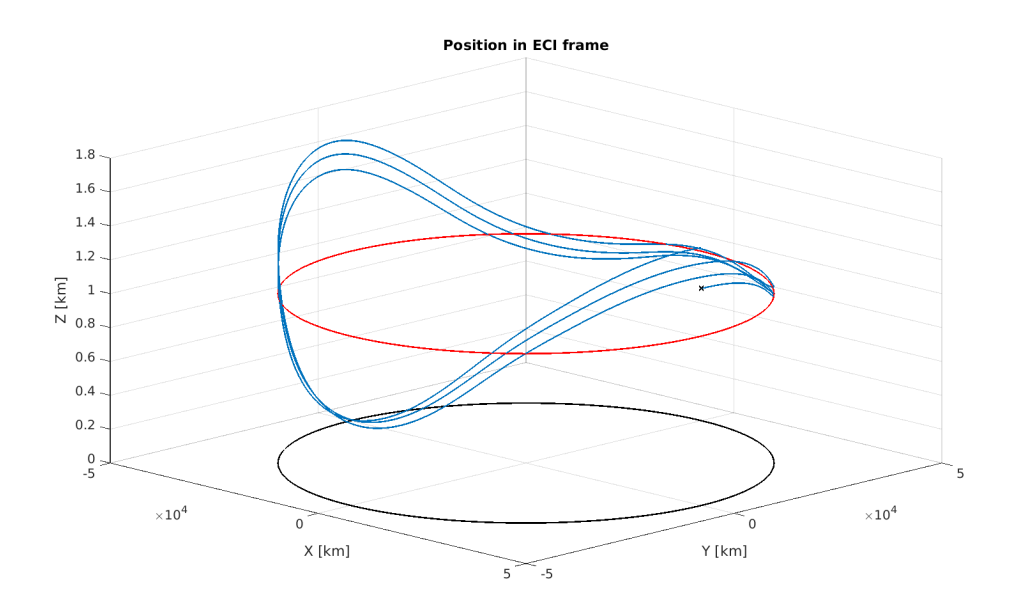


Figure 7.5: Best orbital solution considering: 1 km displacement, 10 Nodes, 0.1 mm/s² characteristic acceleration

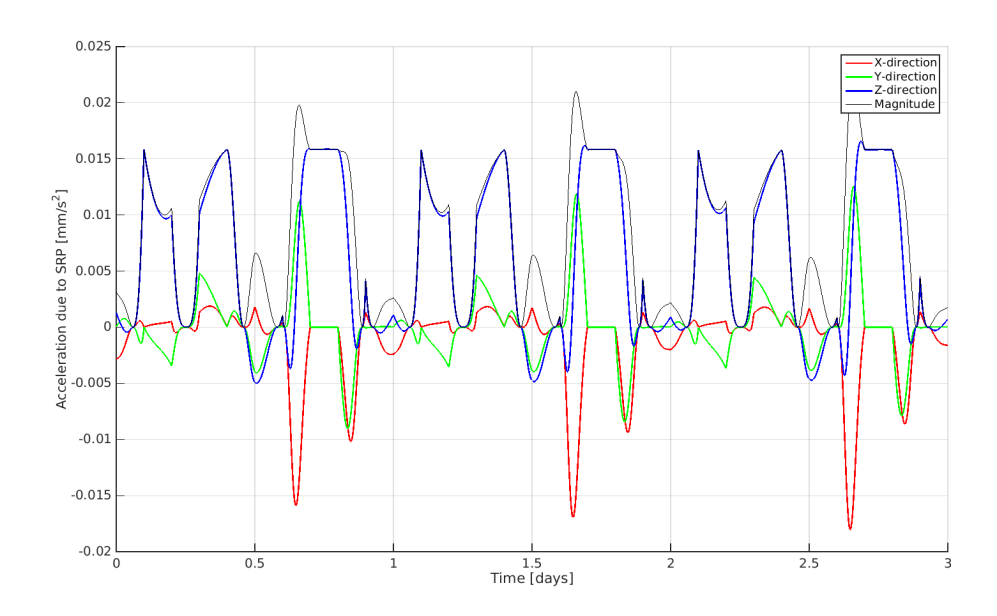


Figure 7.6: Sail acceleration throughout orbit of case 1 km displacement, 10 Nodes, 0.1 mm/s^2 characteristic acceleration.

7.3.2. 10 Nodes, 0.1 mm/s² Characteristic acceleration

As was reasoned before, the characteristic acceleration can both be too large and too small. Therefore a smaller acceleration of $0.1~\text{mm/s}^2$ is investigated with the same elevation, 10~km. This time a smaller acceleration does not lead to an improvement, but to a significant deterioration. Where the average offset was 3.67~km before, now the best trajectory has an average offset of 8.12~km. Looking at Figure 7.10~the reason for this doubled deviating can be found. Looking at the trajectory it seems safe to conclude that the characteristic acceleration is not sufficient to provide the desired elevation. Where previous solutions all lie sort of around the desired orbit, this trajectory is clearly lower that the required orbit. It seems clear that the small acceleration of $0.1~\text{mm/s}^2$ does not provide enough lift for 10~km elevation.

7.3. 10 KM DISPLACEMENT 73

Displacement	#Nodes	Characteristic acceleration	Seed #	Average offset
[km]	[-]	$[\text{mm/s}^{-2}]$	[-]	[km]
			1	8.6586
10	10	0.1	2	8.1213
			3	1.0004
			1	4.2412
10	10	1	2	8.0545
			3	3.6744
			1	2.24396
10	20	10	2	2.7563
			3	3.1229

Table 7.2: Solutions of Optimisations using a 10km vertical offset.

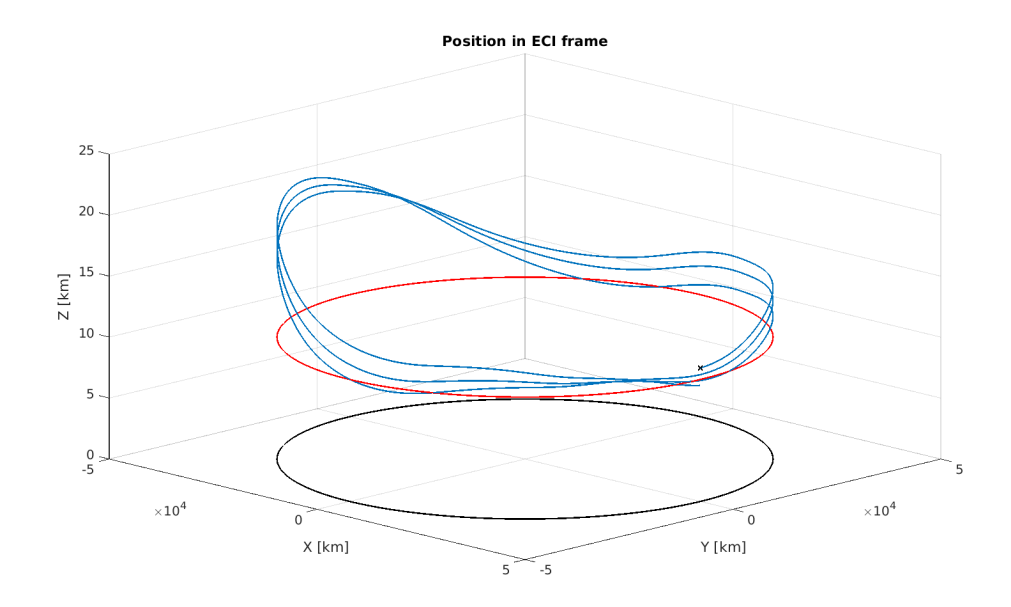


Figure 7.7: Best orbital solution considering: 10 km displacement, 10 Nodes, 1 mm/s² characteristic acceleration

When a characteristic acceleration an order larger than the standard value is tested, the result is opposite. Now the accelerations seem too large, just as before, and again not a proper solution solution in the 2-3 km is obtained. It is thus clear that the characteristic acceleration chosen is quite influential and this should be kept in mind before conclusions are based on certain optimisations considering only one value for it.

7.3.3. 20 Nodes, 1 mm/s² characteristic acceleration

For the same elevation of 10 km the number of nodes is increased to see if this improves the results. Looking at Figure 7.11 it actually looks that way, Table 7.2 shows that this is indeed the case and better solutions were found using 20 node points. It can be reasoned that this larger number of nodes leads to more freedom thus resulting in a better solution. Although this sounds very reasonable it can not be conculeded that this will be the case for all problems. During the thesis, the effect of changing the number of nodes was investigated and then in seemed a larger number than 10 did most of the time not result in better solutions. As more nodes increase the decision vector, this will influence the convergence of the optimisation process, with this case in mind it shows that for certain circumstances it gives a better solution.

Apart from the the average offset, two other improvements can be with respect to the solution for 10 nodes can be observed. Both become most clear when comparing Figures 7.8 and 7.12, showing the offset of the satellites throughout the trajectory. Firstly, the maximal offset throughout the trajectory is lower compared to

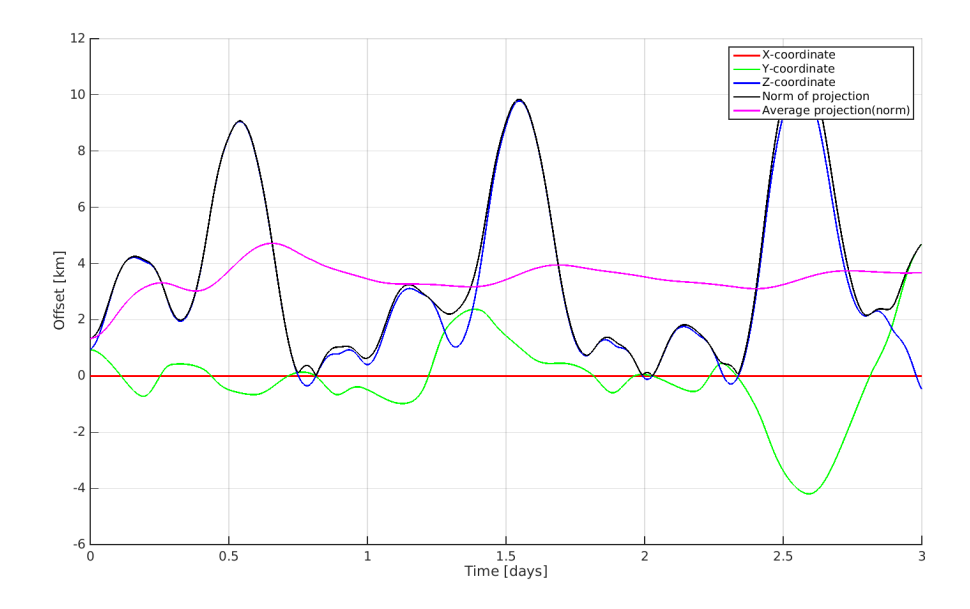


Figure 7.8: Offset throughout orbit of case 10 km displacement, 10 Nodes, 1 mm/s² characteristic acceleration.

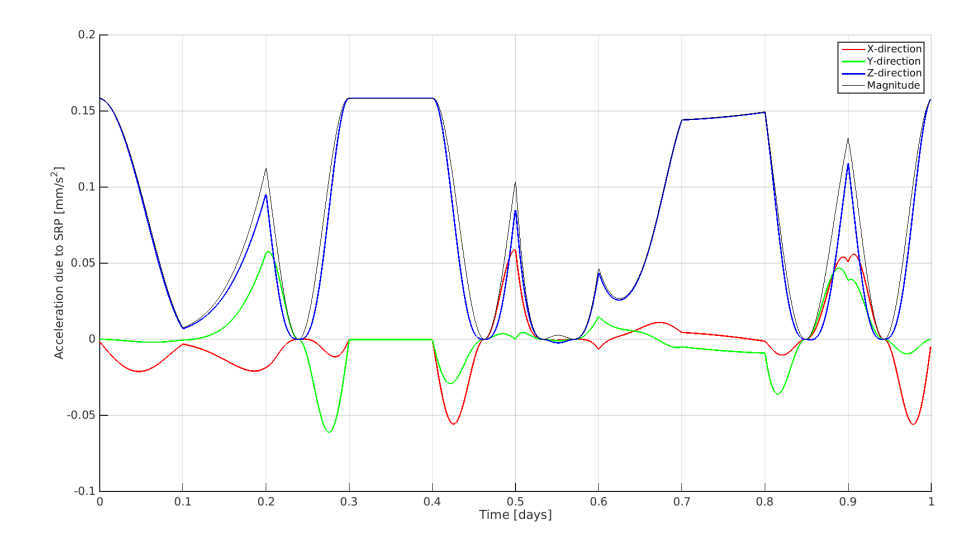


Figure 7.9: Sail acceleration throughout orbit of case 10 km displacement, 10 Nodes, 1 mm/s² characteristic acceleration.

the 10 node case. In Figure 7.7 and 7.8 it can be seen that the trajectory lies close to the desired solution for a large part of the orbit, however it has a high hill halfway the revolution. This results in a maximum offset of approximately while for the new trajectory the error does only go up to 6 km. Although this is not taken into account during the optimisation, it can be profitable. The second point is probably even more important, the three revolutions lay very close to each other. After the complete trajectory the offset is almost the same as it was at the start, meaning the orbit will repeat itself over time. Although the revolutions from the earlier solution also seem similar, looking at the offset it can be seen that the end state differs significantly with the initial state.

7.4. 25 KM DISPLACEMENT 75

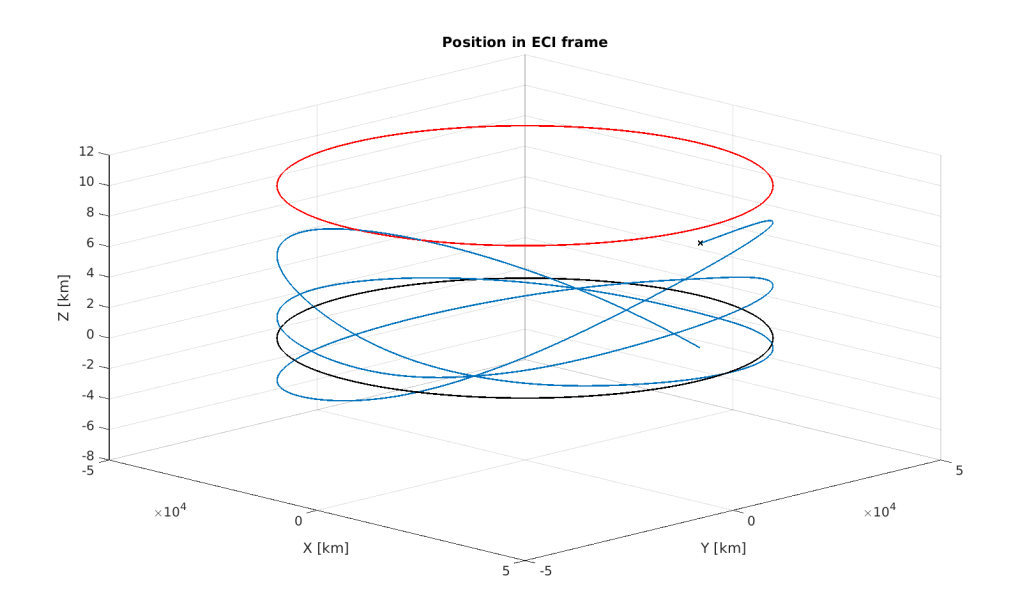


Figure 7.10: Best orbital solution considering: 10 km displacement, 10 Nodes, 0.1 mm/s² characteristic acceleration

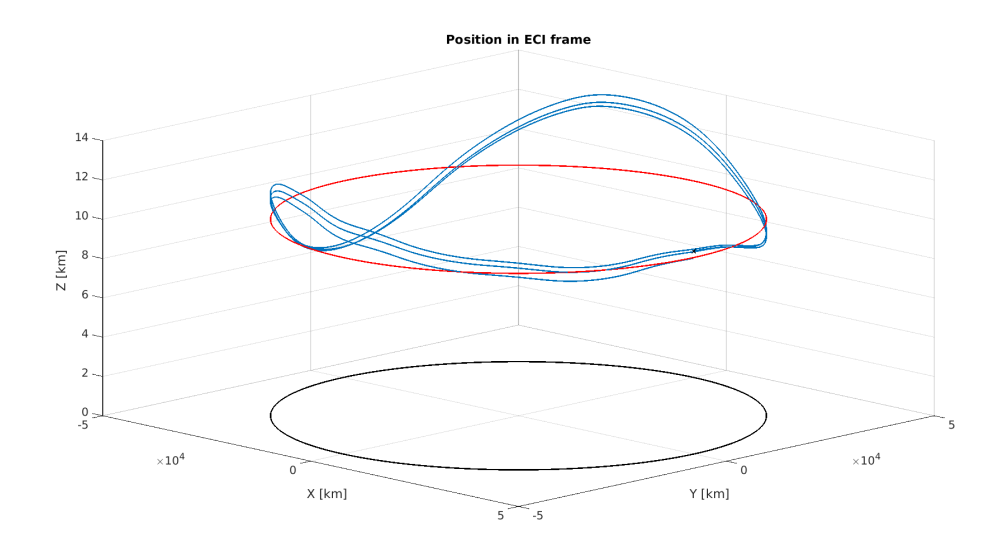


Figure 7.11: Best orbital solution considering: 10 km displacement, 20 Nodes, 1 mm/s² characteristic acceleration

Table 7.3: Solutions of Optimisations using a 25km vertical offset.

Displacement	#Nodes	Characteristic acceleration	Seed #	Average offset
[km]	[-]	$[m/s^{-2}]$	[-]	[m]
			1	4.1336
25	10	1	2	3.7934
			3	3.0344

7.4.25 KM DISPLACEMENT

 $\textbf{7.4.1.}\ 10\ \text{NODES},\ 1\ \text{MM/S}^2\ \text{CHARACTERISTIC ACCELERATION}$ A further increase of the desired displacement is the logical next step. Looking at Figure 7.14 the found trajectory looks very promising. All three orbits lie close to each other, which is preferable considering a mission

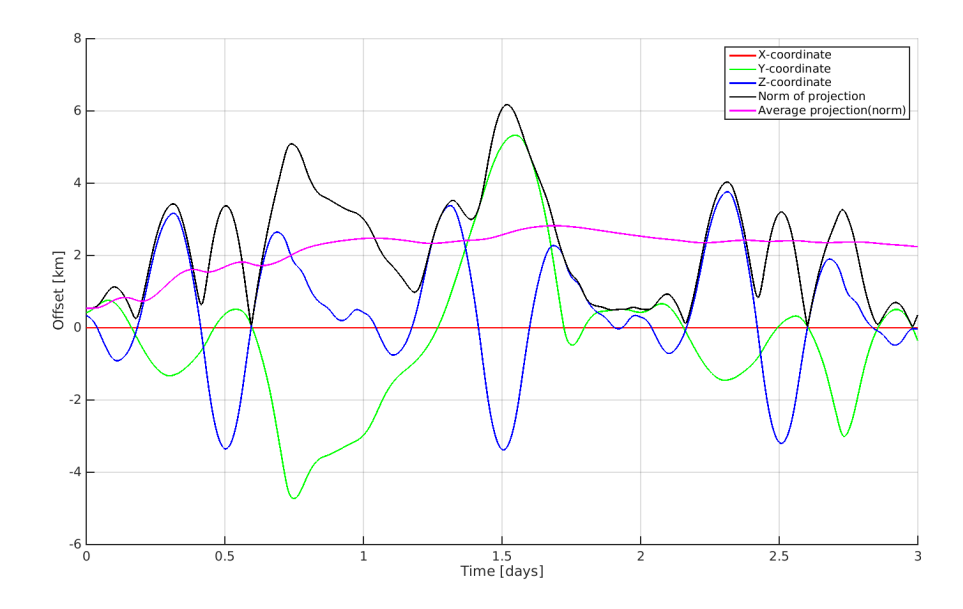


Figure 7.12: Offset throughout orbit of case 10 km displacement, 20 Nodes, 1 mm/s² characteristic acceleration.

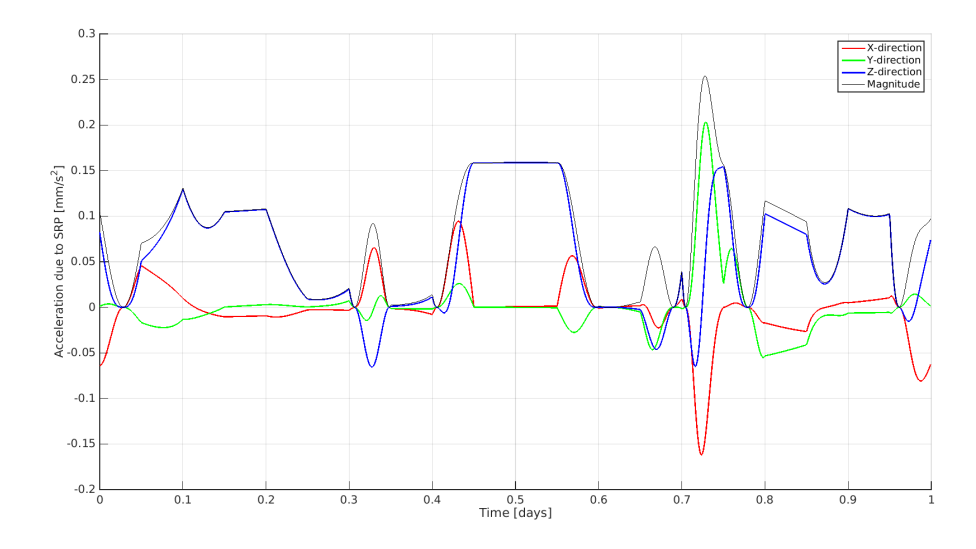


Figure 7.13: Offset throughout orbit of case 10 km displacement, 20 Nodes, 1 mm/s² characteristic acceleration.

typically lasting much longer than the three days that were simulated here. The deviation from the desired orbit is also not too large and orbit is quite stable compared to most earlier found trajectories. The average projection of the complete trajectory is found to be just 3.03 km, so of the same order as the best solutions for 10 km displacement. This is a good results, especially keeping in mind the large increase in deviation from 1 km to 10 km.

Looking at Figure 7.15 it becomes indeed clear that after three revolutions the position is approximately the same as the initial position. As said this is highly desirable as it increases the stability of the trajectory on the long run. Observing Figure 7.15 more closely a peculiar feature can be observed. As stated before he trajectory seems to repeat itself three times and this is indeed seen in the Z-component of the offset. The blue line osculates approximately 2 km below the desired displacement and makes a drop at three quarter of the revolution each time. The green line, representing the offset in Y-direction and thus the drift of the satellite seems however not to have a periodic nature. This could be a sign that even though for the observed offset

7.5.50 KM

both errors are equally important, the effect of a change in Z-direction has a far larger effect on the rest of the trajectory.

Looking at the sail acceleration achieved by the sail, one can clearly see that the increased elevation requires a larger level of thrust. The sail acceleration becomes as high as 0.3 mm/s^2 whereas before the acceleration hardly surpassed 0.15 mm/s^2 .

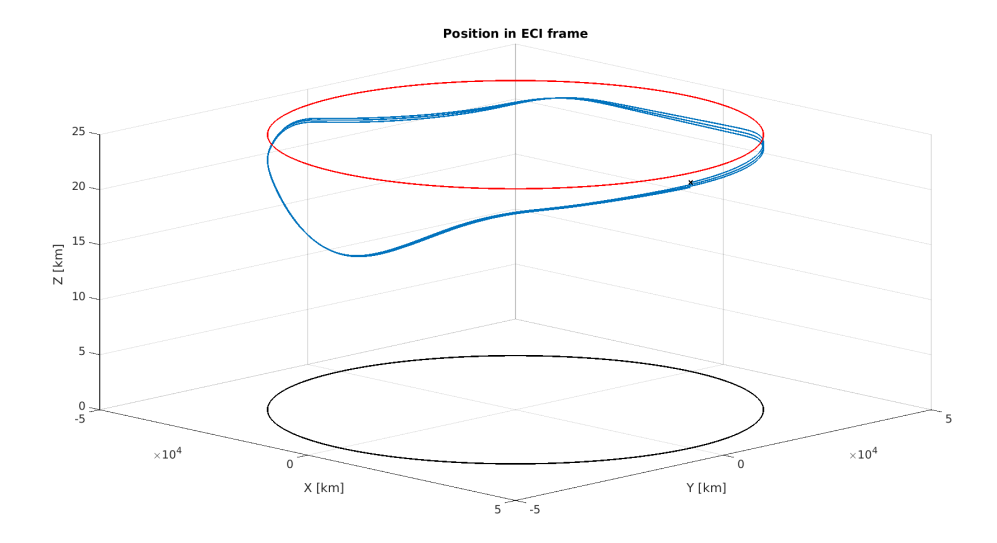


Figure 7.14: Best orbital solution considering: 25 km displacement, 10 Nodes, 1 mm/s² characteristic acceleration

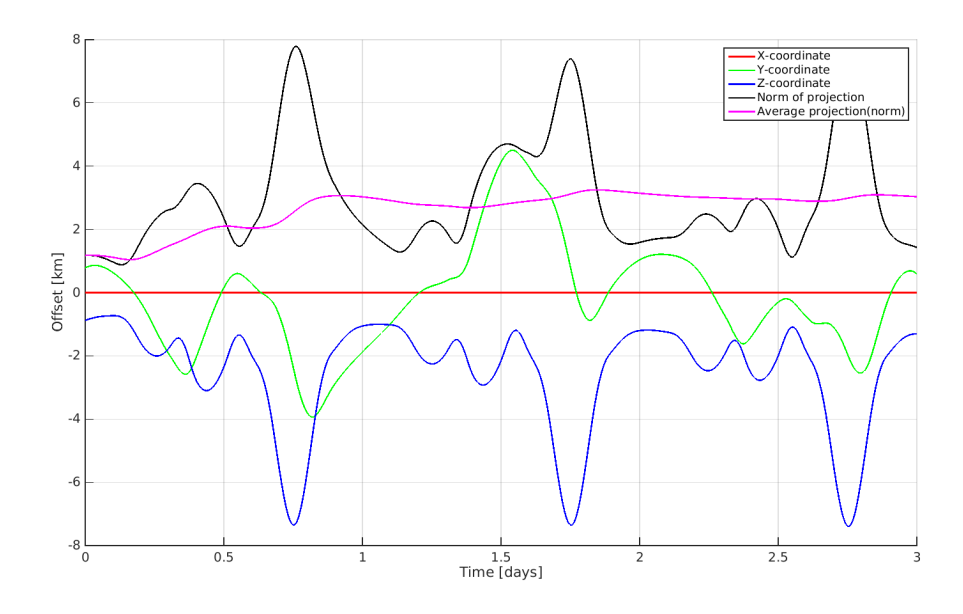


Figure 7.15: Offset throughout orbit of case 25 km displacement, 10 Nodes, 1 mm/s² characteristic acceleration.

7.5.50 KM

As the displacement of 25 km is still within the station-keeping box of standard geostationary satellites, the desired elevation is increased to a value of 50 km. The results found for this problem are presented in Table 7.4

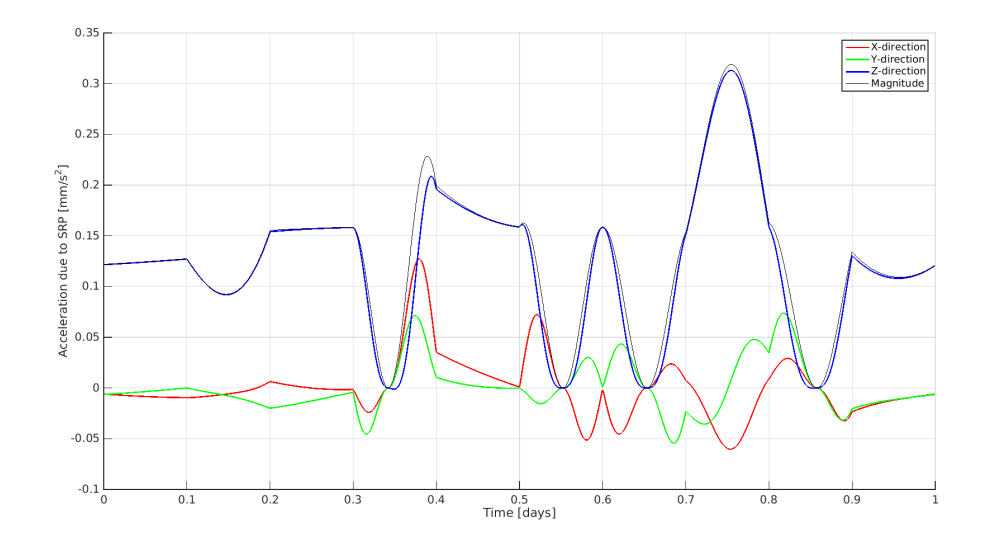


Figure 7.16: Sail acceleration throughout orbit of case 25 km displacement, 10 Nodes, $1 \text{ mm/s}^2 \text{ characteristic}$ acceleration.

Displacement	#Nodes	Characteristic	Seed #	Average
		acceleration		offset
[km]	[-]	$[\text{mm/s}^{-2}]$	[-]	[km]
			1	21.711
50	10	1	2	25.572
			3	21.190
			1	15.663
50	10	10	2	14.697
			3	13.224
			1	7.899
50	10	10	2	62.903
(larger range)			3	180.230

Table 7.4: Solutions of Optimisations using a 50 km vertical offset.

7.5.1. 10 Nodes, 1 mm/s² characteristic acceleration

The best trajectories for a displacement of 50 km using the standard performance sail all have an average offset above 20 km. The best solution is found for Seed #3 which results in an offset of 21 km. Looking at the trajectory in Figure 7.17 is seems that the acceleration was the limiting factor for this problem as the orbit falls well below the desired position throughout the complete trajectory. Looking at Figure 7.19 it can be seen that the sail induces a fairly high acceleration in the Z-direction. This acceleration pushes the spacecraft upwards as the satellite stays well above the equatorial plane, but clearly it is not enough to maintain the required altitude of 50 km.

7.5.2. 10 Nodes, 10 mm/s² characteristic acceleration

As the available thrust seemed to be the limiting factor for the previous case, the acceleration is once again increased to $10~\text{mm/s}^2$. In contrast to before, this high characteristic acceleration improves the trajectories found. The best found trajectory has an offset of 13.2 km. This means quite an improvement although the average offset experienced is still far from the desired 7.5 km. Looking at the trajectory in Figure 7.21 and the sail acceleration in 7.22 the characteristic acceleration of the sail seems high enough this time. The satellite experiences both hills above and drops below the 50 km displacement, without enough acceleration the sail cannot achieve a larger vertical displacement than at the initial state.

7.5. 50 KM 79

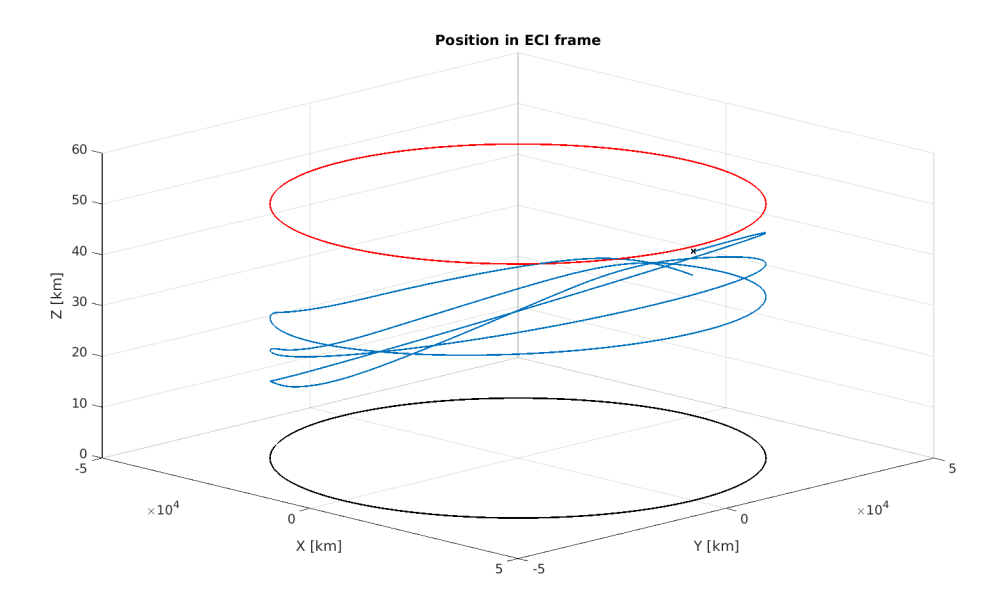


Figure 7.17: Best orbital solution considering: 50 km displacement, 10 Nodes, 1 mm/s² characteristic acceleration

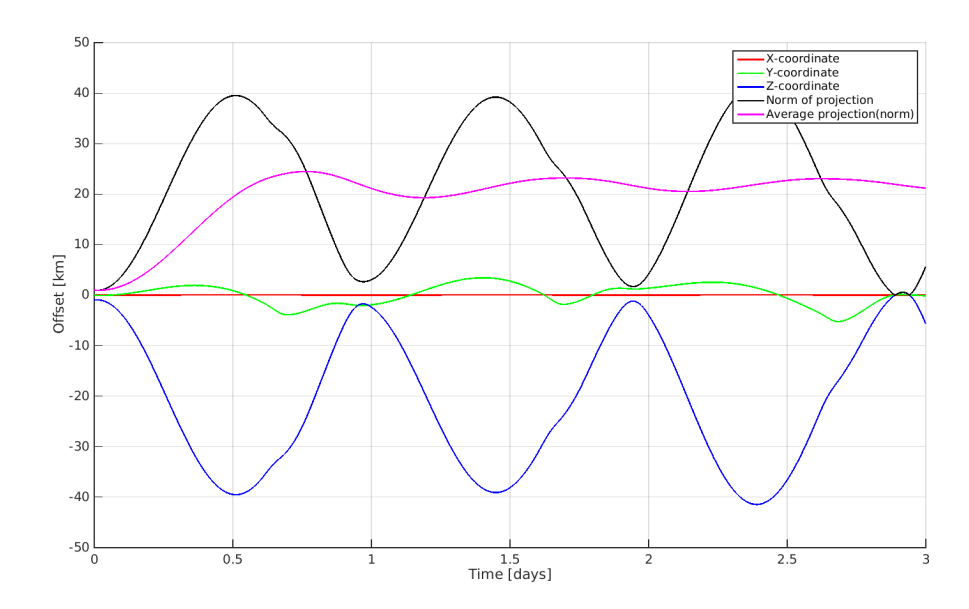


Figure 7.18: Offset throughout orbit of case 50 km displacement, 10 Nodes, 1 mm/s² characteristic acceleration.

7.5.3. 10 Nodes, 10 mm/s² characteristic acceleration, larger decision vector

Looking at both Figure 7.15 and 7.18, the offset rises to the a value of over 30 km, this is a high value, especially considering the initial state which can only deviate 1 km. Looking more closely at the decision vectors of these trajectories it becomes clear that for both cases the deviation of the initial state in the Z-direction is (almost) at the limit set at 1 km, for the second case the Y-component also reaches the limit. This behaviour suggests that the bounds are set too strict for both of these cases. Therefore the optimisation using an acceleration of 10 mm/s^2 is repeated with increased bounds on the bounds. The maximal deviation of the position in the initial state in all directions is increased to 10 km, the velocity stays fixed at 1 m/s.

The results of this optimisation can be found in both Table 7.4 and Figure 7.17. It seems that these restrictions on the decision vector were indeed a restricting factor as the average offset of the best solution has

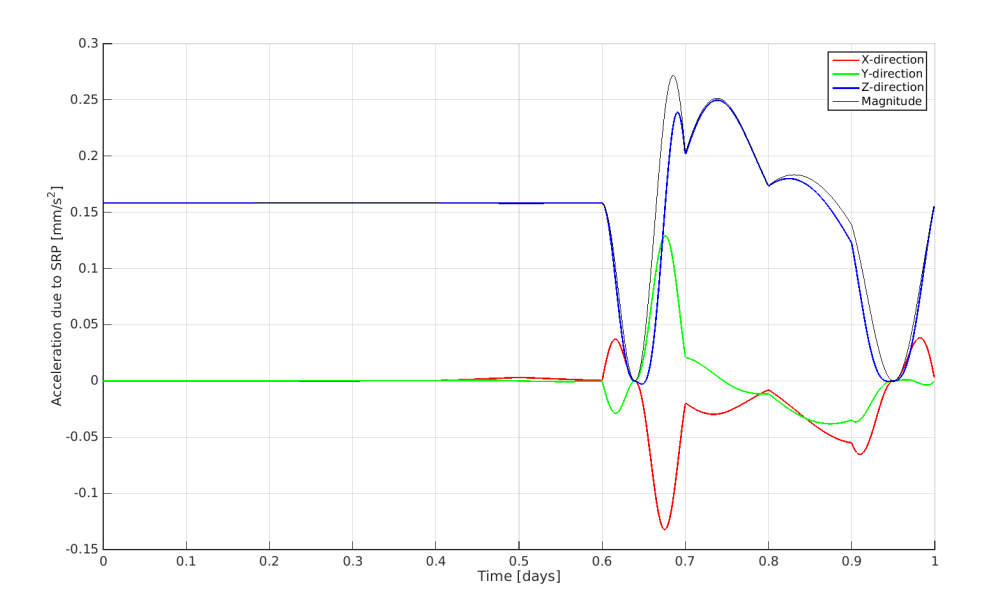


Figure 7.19: Sail acceleration throughout orbit of case 50 km displacement, 10 Nodes, $1 \text{ mm/s}^2 \text{ characteristic}$ acceleration.

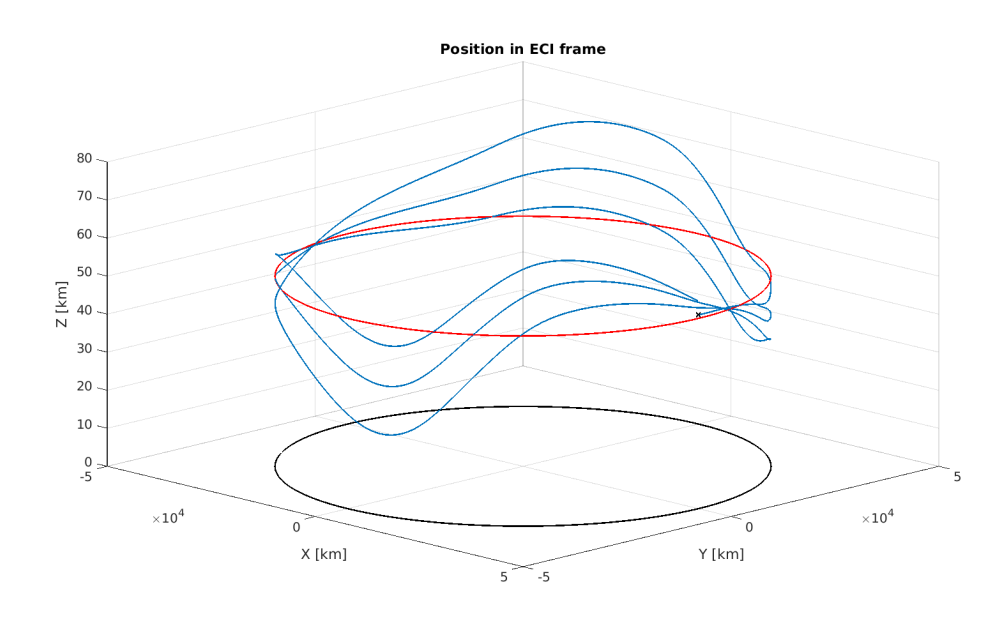


Figure 7.20: Best orbital solution considering: 50 km displacement, 10 Nodes, 10 mm/s² characteristic acceleration

dropped with 5 km. The new solution results in an average offset of 7.9 km throughout its trajectory. Looking at Figure 7.24, both the Y-and Z-component of the initial state now lay outside the previously used box. The Y-component of the new initial state again approaches the limit set with a value of 9.8 km, the Z-component now has value of -2.2 km. This means that for larger displacements it is favourable to increase the range of the decision vector in order to create a larger search space and thus more freedom for the optimisation.

Looking at the other two runs it becomes clear that the reasoning of limiting this search space in order to improve the robustness of the optimisation was also valid. The other two optimisations found trajectories with way worse performances, with offsets throughout the trajectory of 62 km and 180 km. This means that all three optimisation runs found completely different trajectories with very different performance. This is

7.6. OTHER CONDITIONS 81

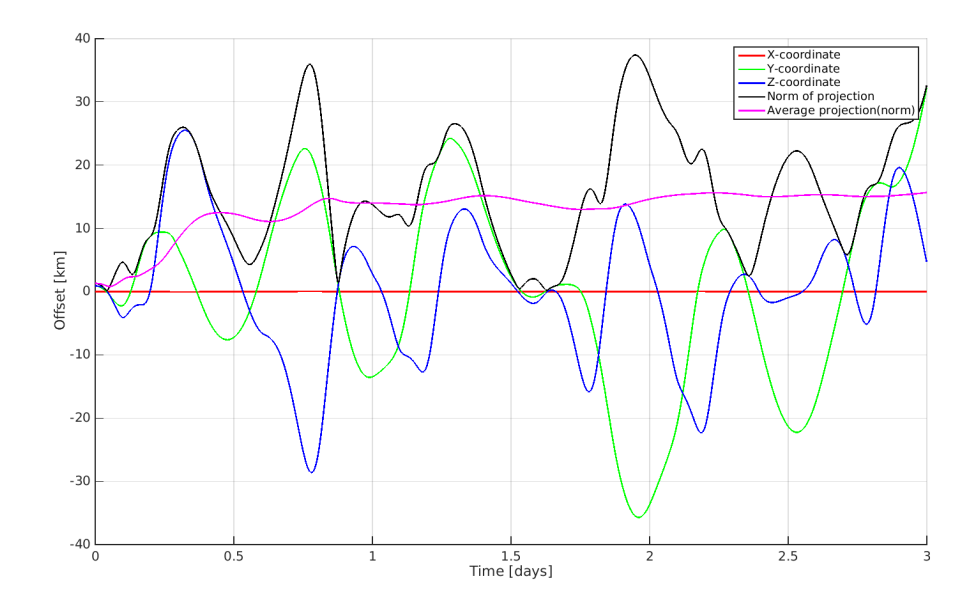


Figure 7.21: Offset throughout orbit of case 50 km displacement, 10 Nodes, 10 mm/s² characteristic acceleration.

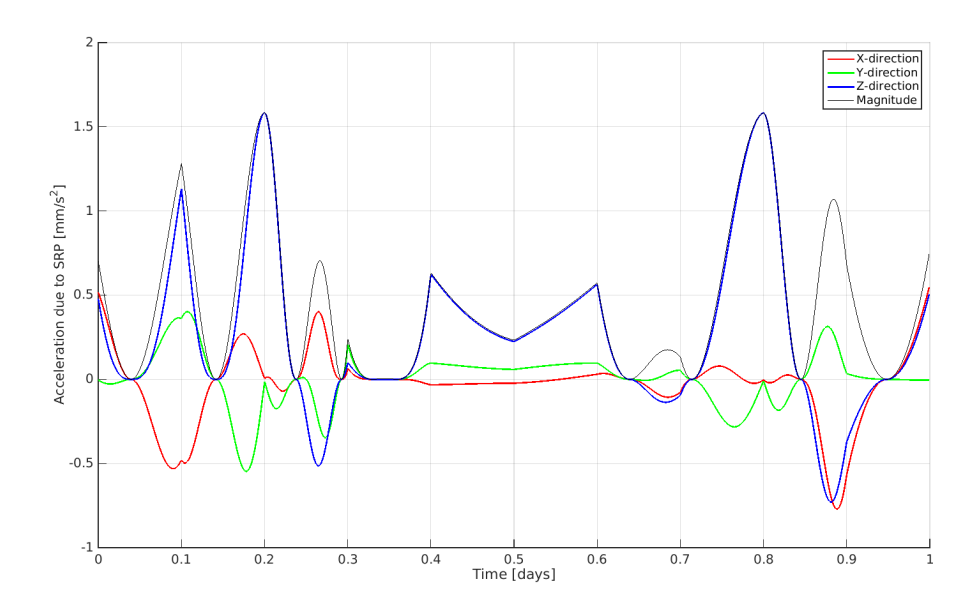


Figure 7.22: Sail acceleration throughout orbit of case 50 km displacement, 10 Nodes, 10 mm/s² characteristic acceleration.

clearly a disadvantage as sheer luck will play an important role in the optimisation. Therefore one should always a proper assessment on the set limits on the decision vector as the limits can easily become too loose or too tight, both resulting in a non-optimal process.

7.6. OTHER CONDITIONS

As the Earth's rotational axis is tilted, the sunline does rotate in the ECI-frame around all three axis. The rotation around the Z-axis results in changed orientation in the XY-plane, which does not make a difference for a solar sail satellite orbiting in a geostationary orbit. With the orbital period equal of a sidereal day, just as the rotation period, the sunline direction will make one complete rotation in the XY-plane every day. This means

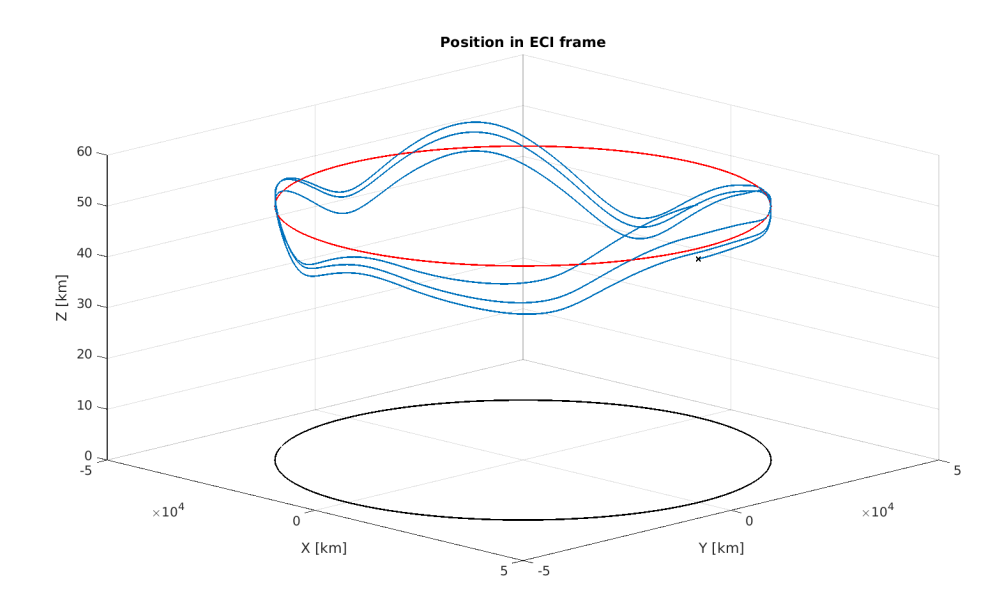


Figure 7.23: Best orbital solution considering: 50 km displacement, 10 Nodes, 10 mm/s² characteristic acceleration

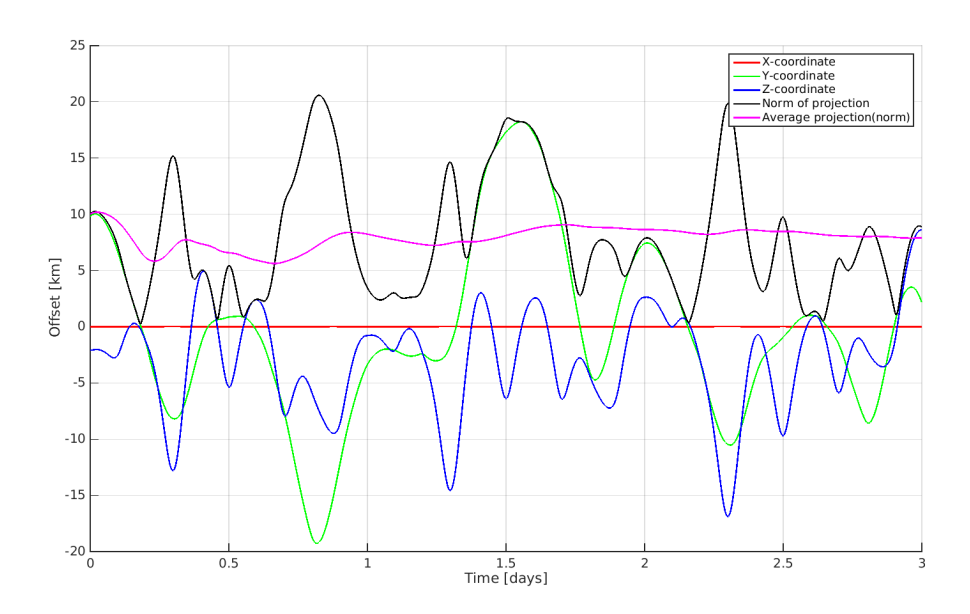


Figure 7.24: Offset throughout orbit of case 50 km displacement, 10 Nodes, 10 mm/s² characteristic acceleration.

the direction of the sunline at the start of the next orbit will be the same as it was at the start of the previous. The tilt of the sunline in Z-direction creates a complete different change in condition, here the rotational period is one year, both in the ECI- and in the ECF-frame. The result is that the Z-component of the sunline is almost constant during one orbit, it only changes 1° per day, but that its magnitude depends on the time of the year. In December the northern hemisphere is turnes away from the sun, as can be seen in Figure 6.3. This clearly has an effect on the climate, during this time of the year the temperature is significantly lower than during summer, while at the southern hemisphere this effect is reversed. Also for the type of trajectories suggested here, this change has a large influence. In December the sunline is tiled in the positive Z-direction, meaning a larger acceleration in this direction is achievable.

This will be shown by considering a sail tilted with 45° with respect to the equator and investigate the ac-

7.6. OTHER CONDITIONS 83

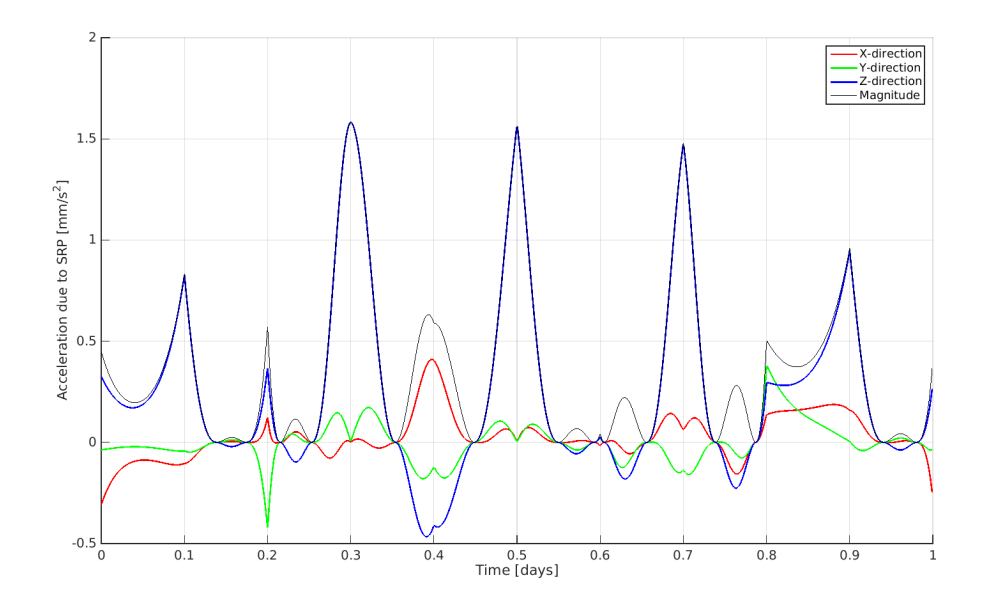


Figure 7.25: Sail acceleration throughout orbit of case 50 km displacement, 10 Nodes, 10 mm/s² characteristic acceleration.

celeration it achieves. The sail is tilted with $\theta=45^o$, which results in an α of equal size when the sunline lies in the equatorial plane. This results in an acceleration of half the characteristic acceleration, as $\cos^2 45^0 = 0.5$, as can be seen in Table 7.5. This situation is the case around March and September, during the spring and autumn equinoxes respectively. Around December 21, the winter solstice, the equatorial plane is tilted with respect to the Sun. This means the sail is directed more towards the Sun and the pitch angle decreases, since $\alpha=\theta-\beta=45-23.5=21.5^o$. The magnitude of the acceleration depends on this pitch angle and it increases to 0.866 times the characteristic acceleration. In this situation, using the same orientation at a different time of the year, the acceleration increases significantly. Lastly around June the situation is reversed, $\theta=45^o$ results in a pitch angle of $\alpha=68.5^o$ and a acceleration only 0.134 times a_{char} . The sail can of course be turned in order to achieve the same amount of acceleration as in December, but the orientation of the sail would have to be rotated by 47^o meaning direction changes completely and the acceleration will actually mostly be in the negative Z-direction. It can be concluded that the time of the year has a major influence on the possibilities

Table 7.5: Achieved sail acceleration throughout the year.

Month	θ	β	α	a
	[deg]	[deg]	[deg]	$[mm/s^2]$
Maximal	45	45	0	1
March	45	0	45	0.5
June	45	-23.5	68.5	0.134
September	45	0	45	0.5
December	45	23.5	21.5	0.866

of a solar sail and thus also on the achievable trajectories. All results presented in the previous section, were performed for trajectories under the most favourable conditions, using a starting date of December 21. As a geostationary satellite should orbit the Earth for several years it is necessary that similar trajectories can be achieved throughout the year. Therefore the case with a desired elevation of 25 km will also be carried out using a start date of both 21 March and 21 June. The results are presented in Table 7.6. The problem for March is optimised both with and without taking eclipse into account, while also the best solution during winter solstice is mentioned once again as comparison. For the best solution of each of the problem the trajectory was plotted just as with the main results. Looking at the results of these optimisations, it becomes immediately clear that the quality of the solution has indeed decreased as was expected. The average offset for the found trajectories is almost and order higher compared to the solutions during favourable conditions. It seems the

Start date	Seed#	Eclipse	Average
		considered?	offset
			km
	1	-	4.1336
December	2	-	3.7934
	3	-	3.0344
March	1	yes	20.6
March	2	yes	22.8
March	3	yes	21.7
March	1	no	24.9
March	2	no	20.5
March	3	no	20.8
June	1	-	29.8
June	2	-	24.0
June	3	-	23.9

Table 7.6: Solution of optimisation using a 25 km vertical offset.

available acceleration is not large enough to achieve the desired elevation. This can be observed looking at the offset, as this is fairly close to the elevation required, and the plots of the trajectories, the satellite does not stay close to the perfect orbit and even drops below the equator for most solutions. This is something that was observed before for cases where the characteristic acceleration was lower than needed, for example in Figure 7.10.

7.6.1. SPRING EQUINOX

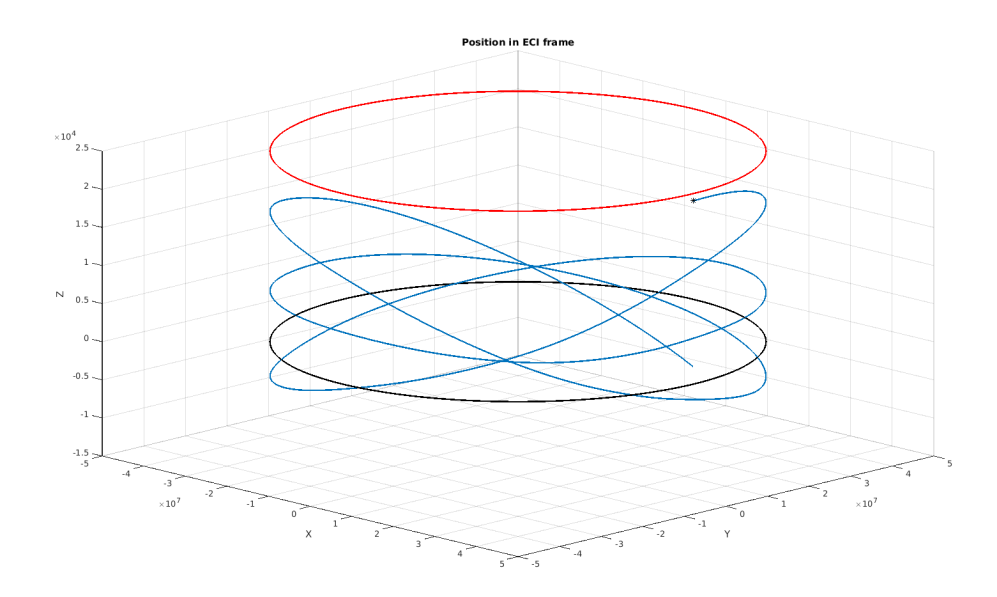
During the spring equinox, and autumn as well, the sunline lies in the equatorial plane, meaning is becomes more difficult to achieve a desired elevation. This can be observed in both Figure 7.26 and 7.27. The trajectory lies well below the desired elevation, something that was seen before with cases where the characteristic acceleration was not sufficient enough. Looking at Figure 7.27 one can see that the relations between the different directions have clearly changed. During winter solstice the Z-acceleration was always the leading component, it as clearly the largest part throughout the trajectory. In this case that has changed, the Z-component is no longer the most important. It can be observed that most of time throughout the orbit the sail acceleration is of similar magnitude in all directions. This is due to the changed sunline which is no longer tilted upwards. This decreased achievable acceleration in the Z-direction is the reason that the optimisation could not find solution closer to the desired elevation height.

Looking at Figure 7.27 another new feature can be observed, after about a quarter of the orbit the acceleration becomes suddenly zero. As the sunline lies in the equatorial plane, the spacecraft can get in the shadow of the Earth and will therefore be in eclipse. This eclipse period has a duration of approximately 72 minutes, or 5% of the orbital period. This is only a limited time and looking at Table 7.6 the effect of this eclipse period is also small, the performance of the solutions found for cases where eclipse is considered and when it is ignored can not be distinguished looking at the performance. This is partly due to the short eclipse period, but can also be related with the limited precision of the trajectories found. As the spacecraft already has trouble staying close to the desired trajectory this small deviation cause by the eclipse does not make a difference. Eclipse conditions could however become more important when a better precision is achieved and the limitation due to missed acceleration will play a role.

7.6.2. SUMMER SOLSTICE

The best trajectory found for a trajectory in June is shown in Figure 7.28, while the corresponding sail acceleration is plotted in Figure 7.29. The result is, as could be expected even worse than for the trajectory in March. The sunline is now tilted in the negative Z-direction, opposite to the wanted displacement, leading to a decrease in acceleration in upward direction and following a decrease in fitness of the solution. Looking at Figure 7.29 in is indeed clear that the Z-acceleration in the positive direction is not leading any more, during large parts of the trajectory the acceleration is even directed downwards.

7.7. DISCUSSION 85



 $\textbf{Figure 7.26:} \ \ \text{Best orbital solution considering: March, 25 km displacement, 10 Nodes, 1 mm/s}^2 \ \ \text{characteristic acceleration}$

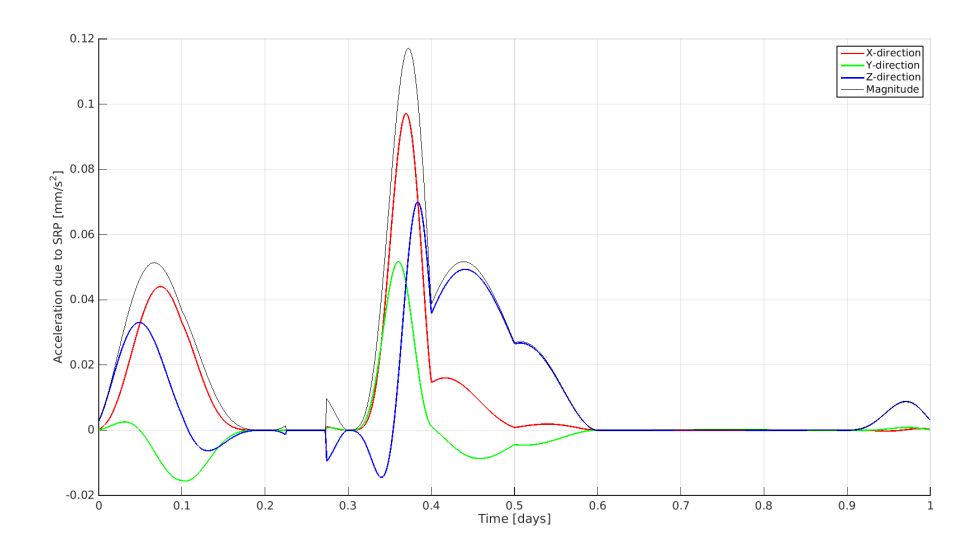


Figure 7.27: Sail acceleration throughout orbit of case: March, 25 km displacement, 10 Nodes, 1 mm/s² characteristic acceleration.

7.7. DISCUSSION

Looking at the results shown in the previous sections it becomes clear that for the first displacement considered the results are promising. For a rather small elevation of only 1 km above the equatorial plane, the sail enabled an position that was stable enough to results in an average offset of only 302 m, which is well within the required limits. However the displacement is so small in this case that it basically still in the regular geostationary belt. From this small error one can therefore not draw many conclusions, the trajectory is an improvement for the set desired orbit but it is not very useful for a real orbit.

When increasing the elevation to 10 km, the error increased by the same factor. For an desired elevation of 10 km above the equatorial plane, the average offset already rose to approximately 3.6 km. This is not a very large error, but being one third of the desired displacement, further increase of the elevation appeared

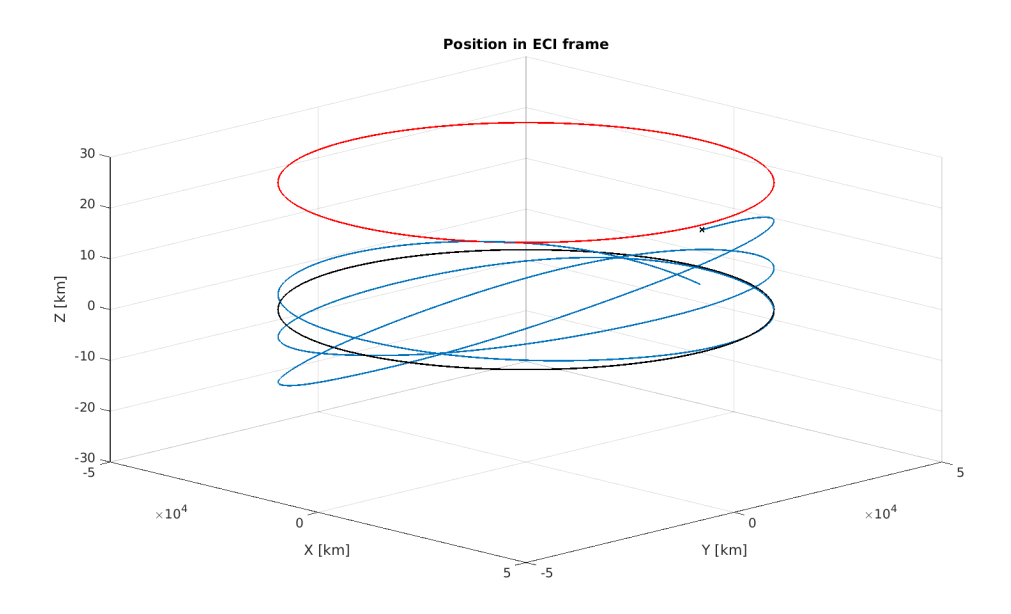


Figure 7.28: Best orbital solution considering: June, 25 km displacement, 10 Nodes, 1 mm/s² characteristic acceleration

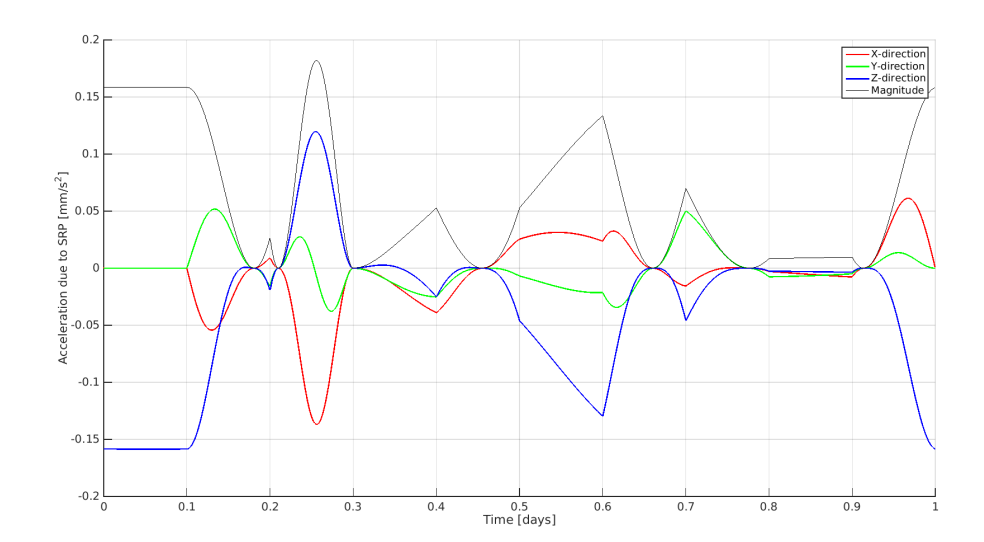


Figure 7.29: Sail acceleration throughout orbit of case: June, 25 km displacement, 10 Nodes, 1 mm/s² characteristic acceleration.

problematic. In order to try and improve this specific case, the number of nodes was raised from 10 to 20, which resulted indeed in an improvement. The average projection throughout the trajectory only adds up to 2.24 km. Increasing the elevation up to 25 km does not again lead to an increase of the offset from the desired position. This means a displacement of 25 km seems possible, resulting in an average deviation of just 3 km, a result that shows opportunities for the considered mission proposal. Increasing the displacement to 50 km, the largest elevation considered, did show that the solution for the 25 km lies close to the maximum achievable displacement considering a sail with a characteristic acceleration of 1 mm/s 2 . For an desired displacement of 50 km the average offset dropped to 21 km considering this sail, which seems to be caused by the lack of sufficient acceleration. The fact that an increased characteristic resulted in an offset of only 8 km seems to prove this point. This implies that for the selected, realistic sail performance of 1 mm/s 2 the limit on the achievable displacement lies around the before mentioned 25 km. If in the future larger, lighter, better performing sail become achievable so do trajectories with a larger displacement, proven by the 50 km dis-

7.7. DISCUSSION 87

placed orbits with an offset of 8 km.

These trajectories for geostationary orbits elevated 25 and 50 km above the equatorial plane, were found considering the most favourable conditions for the orientation of the Sun. For these conditions, valid around the winter solstice, solutions were found that fulfil the orbital requirements at a reasonable displacement of 25 km. During a year the orientation of the Sun and Earth however start to change and this has significant effects on the conditions relevant for solar sailing. During winter solstice the sunline is tilted upwards, this means that it is already pointing partly in the desired displacement direction. Throughout the year this changes and the sunline is not tilted upwards any more, in the worst case it is even tilted downwards. This changed direction of the sunline with respect to the equatorial plane causes a decrease in the vertical sail acceleration possible. Optimisation problems with these changed conditions showed a clear decrease in performance. Considering March conditions trajectories with an average offset of 20.5 km were found, compared to 3 km offset for the same problem in December. In summer time, around June the sunline is directed even more disadvantageous and the result drops to 24 km average offset. These trajectories clearly do not fulfil the set orbital requirements of an average offset of 7.5 km.

7.7.1. CONVERGENCE

Looking at the distribution of the results rather than the absolute values, a problem concerning the optimisation process becomes apparent. Performing exactly the same optimisation three times, with the only difference being changing seed numbers, thus random numbers in the optimisation algorithm, gives different solutions. Not only the exact trajectory changes considerable, also the fitness of the solutions is not constant. These large differences after several optimisation runs, mean that the optimisation process is far from perfect. It is however difficult to say how this can be improved for the problem handled in this thesis.

For any solution found for any optimisation problem the reliability of this solution can be assessed by looking at the convergence. Convergence means the algorithm found a solution that can not be improved any more and can thus be considered top be the best possible. One can look at two factors in order to investigate if this is indeed the case. The first thing is to look at the fitness of the champions, the best individuals of each generation. If the champions stay constant generation after generation, the algorithm is apparently not capable of improving the individual any further. The second requirement for convergence is that the optimisation results in similar solutions for different, separate runs. If these two demands are met the optimisation is converged.

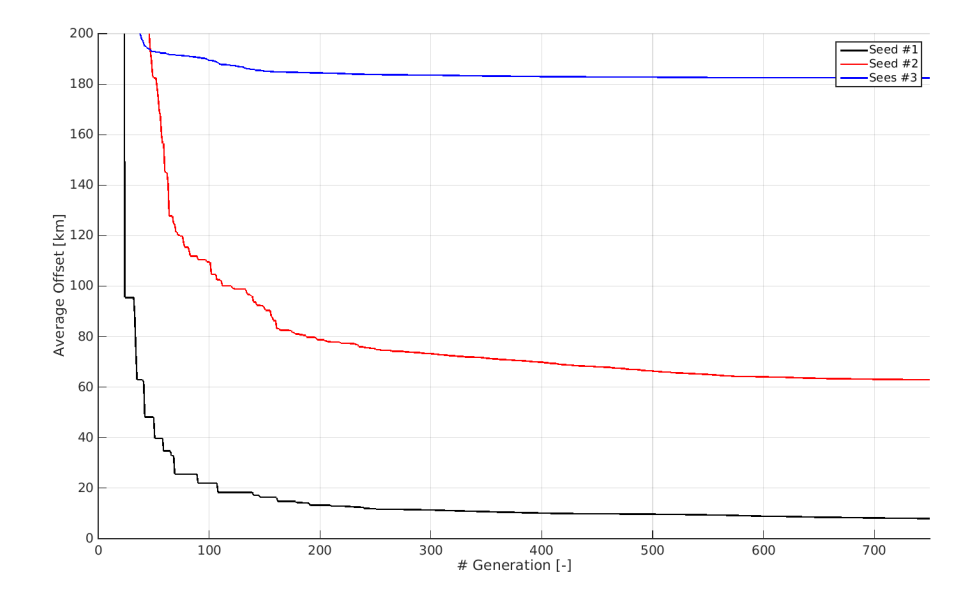


Figure 7.30: Champions throughout the optimisation for a 50 km displacement trajectory, considering wider bounds of decision vector.

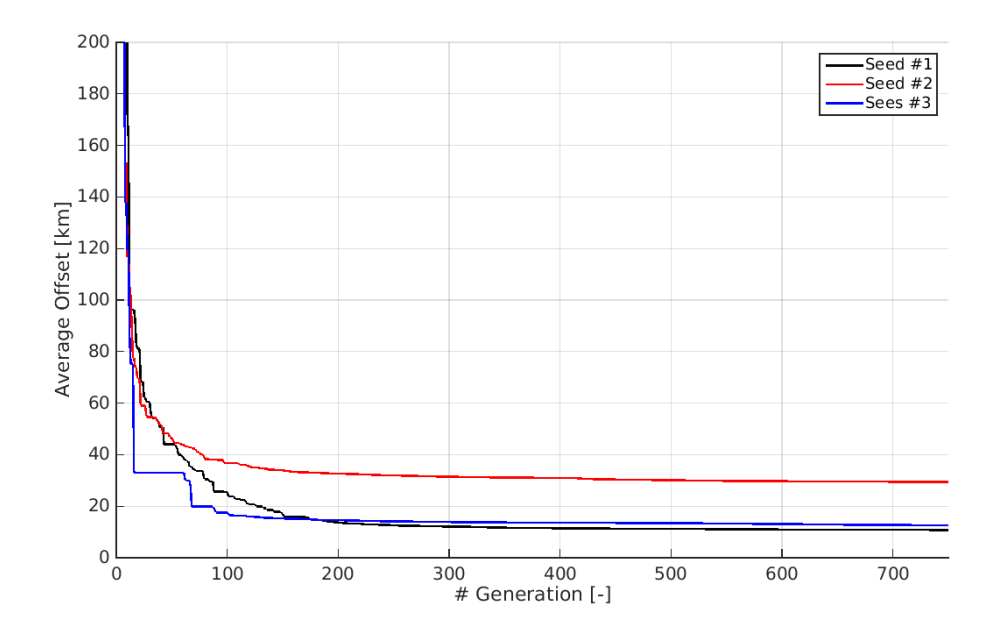


Figure 7.31: Champions throughout the optimisation for a 50 km displacement trajectory.

The results presented in this chapter were often not fully converged, this was the case for situation where the solutions differ a lot from each other. When this is the case one could try to increase the number of generations, this way the optimisation algorithm will continue to improve the result until it no longer finds a better solution. For the results presented in this chapter the problems were defined for 750 generations. Looking at the champions throughout the process almost always showed that these individual were not improving, or only marginally, for the second half of the generations. In Figure 7.30 the champions are shown of the second case described in Section 7.5.3: 50 km, 10 mm/s^2 and less strict bounds on the decision vector. Although the solutions found range from 7 km to 182 km, looking at the champions one can see that for all three cases the fitness is not improving much more for the second half of the process. It can not be expected that Seed#3 will ever come to the same solution as Seed#1, even when the number of generations is increased considerably. As was proven for this specific case, increasing the limits of the decision vector is a way to increase the search space and thus the variation of the individuals. This can lead to an improvement of the solution found, however is also comes at a cost, the chance that none of the individuals lies close to the optimal solution increases. If this is the case the optimisation will find a solution that can no longer be improved even though it is not the global optimum, so apparently the optimiser is stuck in a local optimum.

For other cases, looking at the results the optimisation seems to have converged. An example for this is the same problem as before, but now with the standard decision vector bounds. Looking at Table 7.4, the performance of the solutions for Seed#1 and Seed#3 are very similar. Looking at Figure 7.31 one can indeed see that these optimisations give very similar performance. The plot also shows that the champions do not improve significantly for the last part of the optimisation. Looking at these two factors it seems that the optimisation has indeed converged, however looking at Figure 7.32 where both trajectories are plotted one can still see clear differences. This means that both runs did not converge towards the exact same trajectory.

This behaviour can mean that the optimisation process works correctly but there is no clear optimal solution. The optimisation process is set up correctly and best trajectories found are close to the optimum. This would however mean that there are a lot of solutions that have comparable fitness, but different trajectories, leading to a number of local optima.

7.7. DISCUSSION 89

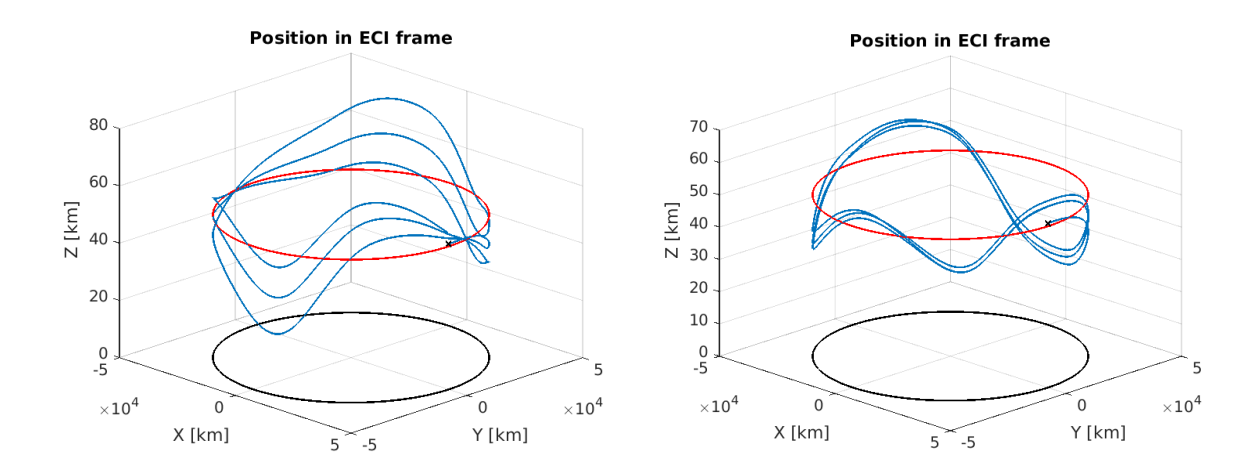


Figure 7.32: Trajectories of 50 km displacement, 10 mm/s² for Seed#1 (left) and Seed#3 (right).

8

CONCLUSIONS

This last chapter of the report will present the most important conclusions that can be drawn. The complete research discussed in this report will be reviewed shortly. The results presented in the last chapter of course play a large role in these conclusions. Furthermore a flashback to the research question and related goals is given. Lastly the report ends with some recommendations for future research.

8.1. CONCLUSIONS

In Section 1.3 The goals op this thesis where presented and the research question was defined as:

Is it possible to achieve a displaced geostationary orbit using solely solar sailing as propulsion method?

The rest of the report presented all the work performed in order to be able to answer this question. In Chapters 2 to 4 all the theory needed to perform this research was presented, also some design decisions and research choices were made here. First the orbital requirements for the displaced orbit to be designed were chosen. The average offset of the trajectory should not exceed 7.5 km. Another important choice is the selection of the optimisation method. For this process PaGMO was used, making use of several types of differential evolutionary algorithms that are available in this software. The choice for this algorithm type is difficult to judge as no real comparison is available. Several tests were performed in order to improve the working of the selected algorithms, but the optimisation remained rather slow and not did not converge as was hoped for. This means that the method is probably not the best in order to solve the problem at hand, although the best method is not known. The objective function is considered rather noisy and the search space is large, these two factors make optimisation difficult although DE's are known to handle such cases. Finally the MOEAD method was selected to perform the final optimisation processes with. Although this algorithm seemed not perfect for this problem as it is written for a multi-objective problem and actually optimises two objective functions, it was tested since the standard DE's did not perform as good as expected. This choice proved successful, convergence improved greatly compared with the standard DE's and satisfying results were obtained using it. As the MOEA/D in essence also is a DE, it seems the settings used worked well for this particular case.

Also the sail performance considered in this research is defined in the first part of the report. Based on literature and multiple mission studies a characteristic acceleration of 1 mm/s² of was selected as the most reasonable acceleration. Although it is not proven yet, it seems that such a performance is possible for mission in the coming years as long as enough focus and money is given to solar sailing missions. In Section 3.7 it was shown that this acceleration can, taking only the vertical component into account could lead to approximately 67 km vertical displacement. This is however a highly simplified case where various factors are ignored.

In the following chapter, Chapter 5, the structure of the created simulation tool was introduced and the programming choices were explained. The program set-up was introduced using flowcharts and a corresponding clarification defending the made choices. This also applies to the optimisation algorithm, both the decision vector, which basically is the input, and the objective function, defining the output, are presented. The de-

92 8. CONCLUSIONS

cision vector consist of the initial state and the sail orientation at different node points throughout the orbit. Other parameters such as the sail performance have to be varied upfront and are constant for the optimisation process. The average projection is chosen as the objective function. This projection is the scalar value of the offset of the satellite as seen from Earth, the actual difference from the desired position is thus projected on the plane normal to the line of sight towards the satellite.

After the tool was created it is of major importance to perform a proper verification and validation of the complete program and its separate parts. This verification is presented in Chapter 6, where all relevant coding blocks were tested just as the complete process of these blocks working together. During this process also the exact settings of the simulation and optimisation were discussed and a reference case was defined on which the final optimisation runs are based.

The outcome of these final optimisations is presented in Chapter 7. Here the results for different vertical displacements are shown; 1 km, 10 km, 25 km and finally 50 km. For the first three cases proper results have been obtained that meet the set requirements using 1 mm/s² as characteristic acceleration. Starting at the 1km with the characteristic acceleration of $1 \cdot 10^{-3}$ that was suggested in Section 2.4 the average projection was found to be 337m. As this is a third of the desired elevation, different values of sail performance were investigated to see if the results can be improved. Increasing the characteristic acceleration has a opposite effect, the performance was considerable decreased. However, using a smaller acceleration a better solution was found. This shows that the acceleration has, as expected, a large influence on the performance. But it also proves that a larger acceleration does not automatically lead to a better performance, the sail loading has to correspond to match approximately with the desired elevation

Increasing the vertical displacement to 10km showed a large drop in the average projection achievable. The larger perturbations needed to elevate the spacecraft apparently also decrease the smoothness of the trajectory. Using the standard sail acceleration but with an increased number of twenty nodes, the best solution for this elevation is found. The average projection of the best trajectory found for this displacement is 2244m.

When the elevation is further increased to 25km the performance again drops, however not as rapidly as seen between 1km and 10km. The best solution is found considering $1 \cdot 10^{-3} \text{m/s}^2$ accelerations and 10 nodes, the average projection of the found trajectory is only 3034km. This is a very good result, for a reasonable offset of 25km the error in the orbit and the offset from the desired fixed position is thus only 3km. This result is very promising and proves that the concept is indeed achievable; a spacecraft can be put in a displaced geostationary trajectory.

Further increase of the elevation is not possible using the characteristic acceleration of 1 mm/s^2 but has to be increased by a factor ten to realise a solution. For the standard case the solution drops to an average offset of 21 km, far from the required 7.5 km. After increasing the characteristic acceleration to 10 mm/s^2 however, the best trajectory only shows 8 km offset. This proves that indeed the acceleration was the limiting factor before.

There are however some difficulties that can not be ignored, most importantly the changing conditions throughout the year. The results presented show the possibilities during the most optimal time of the year. Around December 21, the equator is rotated away from the Sun and the sunlight therefore hits the equatorial plane form below. This means thee sunlight is already partly tilted in the needed direction. In order to assess the dependence of the solution on this conditions, the case for 25 km displacement is repeated during March and June. These changed conditions result in far less performance of the solutions found, that do not meet the set requirements. In March the best trajectory means 20 km average offset, while in June the performance decreases even further to 24 km.

Looking at the results of the optimisations using these changed conditions, it can be concluded that the earlier found trajectories can not be maintained throughout a complete year. This thus also means that the suggested concept of keeping a satellite in a displaced geostationary orbit using solely solar sailing as propulsion method seems infeasible.

8.2. RECOMMENDATIONS 93

8.2. RECOMMENDATIONS

Even though the last section answered the research question, the research is not finalised. As this thesis work and time is limited, for now the results are cherished and indeed the study is finished. However, every scientific study should have besides its explicit results a couple of recommendations. These recommendations can be of two types, either how to improve the calculations performed, e.q. by discarding assumptions made, or by suggesting new research topics that have shown necessary. The recommendations concerning this thesis work are presented in this section.

Looking at the assumptions made most are valid, especially in this phase of the research. However, if more research is performed, the assumption of a perfect sail is definitely one to look at more critical as this leads to significant deviations. Looking at a more realistic sail is thus an important recommendation, although this can only be done when a more detailed design of the sail is available.

The optimisation process did not work as good as it could have. Therefore some more research on selecting a suitable optimisation algorithm would be recommended when further research is performed on this study.

As the conclusions show that the concept of a displaced geostationary orbit using solely solar sailing is not possible, one could think of alternatives. One of the suggestions is to investigate a similar problem, but including an extra low-thrust propulsion method in order to support the solar sail where needed. This way one could still make use of solar sailing, but get around the limitation.

BIBLIOGRAPHY

- [1] European Space Agency. PAGMO: Parallel Global Multiobjtective Optimizer. http://esa.github.io/pagmo/index.html.
- [2] J. L. Ahern. Earth's Magnetic Field. http://principles.ou.edu/mag/earth.html.
- [3] S. Amaya. History of c++. http://www.cplusplus.com/info/history/.
- [4] Encyclopedia Astronautica. Communication Satellite Echo. http://www.astronautix.com/craft/echo.htm.
- [5] Shahid Baig and Colin R. McInnes. Light-Levitated Geostationary Cylindrical Orbits Are Feasible. *Journal of Guidance, Control, and Dynamics*, 33(3):782–793, May 2010.
- [6] Arthur C. Clarke. Extra-Terresrial relays, can rocket station give world-wide radio coverage? *Wireless World*.
- [7] Imke de Pater and Jack J. Lissauer. *Planetary Sciences*. Cambridge Iniversity Press, second edition edition, 2010.
- [8] Charles A. DiMarzio. *Optics for Engineers*. CRC Press, 1st edition, 2011.
- [9] Institude of Space Systems DLR. ESA and DLR Projekt: Gossamer. http://www.dlr.de/irs/en/desktopdefault.aspx/tabid-6931/11365_read-26354/.
- [10] LiveScience Elizabeth Howell. Earth's core 1,000 degrees hotter than expected. http://www.livescience.com/29054-earth-core-hotter.html, 2013.
- [11] Mulder J.A. et al. AE3202 Flight Dynamics; Lecture Notes. Delft University of Technology, 2011.
- [12] U. Geppert et al. The 3-step DLR-ESA Gosammer road to solar sailing test. *Advances in Space research*, 48, 2010.
- [13] William H. Press et al. *Numerical Recipes in C; The Art of Scientific Computing*. Cambridge University Press, second edition, 1992.
- [14] H. Fischer and A. Haerting. Why Light-Levitation Geostationary Cylindrical Orbits Are Not Feasible. *Journal of the Astronautical Sciences*, 40(3), 1992.
- [15] R.T. Foekema. Pluto solar sailing mission. Master's thesis, Faculty of Aerospace Engineering, Delft University of Technology, 2003.
- [16] R. L. Forward. Light-Levitated Geostationary Cylindrical Orbits. *Journal of the Astronautical Sciences*, 29(1), 1981.
- [17] R. L. Forward. Light-Levitated Geostationary Cylindrical Orbits Using Perforated Light Sails. *Journal of the Astronautical Sciences*, 32(2), 1984.
- [18] NASA George C. Marshall Space Flight Center. NASA facts: NanoSail-D. NASA Administration, 2010.
- [19] U. Geppert, B. Biering, F. Lura, J. Block, M. Straubel, and R. Reinhard. The 3-step DLR–ESA Gossamer road to solar sailing. *Advances in Space Research*, 48(11):1695–1701, December 2011.
- [20] S. Hardacre. PhD thesis: Control of colocated goestationary satellites. Cranfield University.
- [21] Jeannette Heiligers, Colin R. McInnes, James D. Biggs, and Matteo Ceriotti. Displaced geostationary orbits using hybrid low-thrust propulsion. *Acta Astronautica*, 71:51–67, February 2012.

96 Bibliography

[22] Hiddink Sander et al. Heligers, Jeannette. Solar Sail Lyapunov and Halo orbits in the Earth-Moon three-body problem. *Acta Astronautica*, 116:25–35, 2015.

- [23] Prof. ir. K. F. Wakker. Astrodynamics-I, Lecture Notes. Delft University of Technology, 2010.
- [24] Prof. ir. K. F. Wakker. Astrodynamics-II, Lecture Notes. Delft University of Technology, 2010, April.
- [25] The Planetary Society Jason Davis. A Kilometer Per Day: LightSail Mission Managers Refine Orbit-Raising Plan. http://www.planetary.org/blogs/jason-davis/2015/20150904-lightsail-km-per-day.html, September 2015.
- [26] JAXA. Hayabusa project science data archive. http://darts.isas.jaxa.jp/planet/project/hayabusa/index.html, 2008.
- [27] JAXA. Ikaros mission overview. http://global.jaxa.jp/countdown/f17/overview/ikaros_e.html, 2014.
- [28] JAXA/AKATSUKI. Ikaros; mission photo, movie. http://global.jaxa.jp/countdown/f17/live/missionphoto_e.html, 2010.
- [29] JAXA/JSpEC. Solar power sail demonstrator. http://www.jspec.jaxa.jp/e/activity/ikaros. html.
- [30] Les Johnson, Roy Young, Nathan Barnes, Louis Friedman, Vaios Lappas, and Colin R. McInnes. Solar Sails: Technology And Demonstration Status. *International Journal of Aeronautical and Space Sciences*, 13(4):421–427, December 2012.
- [31] Colin R. McInnes. Solar Sailing; Technology, Dynamics and Mission Applications. Springer, 1999.
- [32] Colin R. McInnes. Solar Sailing Mission Oppurtunities ans Innovative Technology Demonstration. *ESA bulletin 108*, November 2001.
- [33] NASA. Nanosail-d 'sails' home mission complete. http://www.nasa.gov/mission_pages/smallsats/11-148.html, 2011.
- [34] NASA. Nasa's first solar sail nanosail-d deploys in low-earth orbit. http://www.nasa.gov/mission_pages/smallsats/11-010.html, 2011.
- [35] NASA/L'Garde. About sunjammer; first nasa solar sail mission to deep space. http://www.sunjammermission.com/AboutSunjammer, 2014.
- [36] NASA/SDO. APOD; Watching Venus to Cross the Sun. http://apod.nasa.gov/apod/ap120605.html, June 2012.
- [37] Delft University of Technology. Tudat, website and wiki. http://tudat.tudelft.nl/projects/tudat/wiki, 2014.
- [38] Eberhard Gill Oliver Montenbruck. *Satellite Orbits; Models, Methods and Applications*. Springer, 1st edition, 2000.
- [39] Intelsat S.A. Intelsat; Eclipse Seasons. http://www.intelsat.com/tools-resources/satellite-basics/eclipse-seasons/.
- [40] C. Sickinger. Lightweight deployable booms: Design, manufacture, verification, and smart materials application. *International Astronautical Congress, IAF/IAA/IIS*, 55, 2004.
- [41] The Planetary Society. LightSail, a solar sailing spacecraft from The Planetary Society. http://sail.planetary.org/.
- [42] Mattias Soop. Handbook of geostationary orbits. Springer Science and Business Media, 1994.
- [43] Mattias Soop and W.R. Burke. *Introduction to geostationary orbits*. ESA Scientific and Technical Publications Branch, 1983.

BIBLIOGRAPHY 97

[44] Spaceflightnow Stephen Clark. Collision between rocket stages doomed falcon 1. http://www.spaceflightnow.com/falcon/003/update.html, 2008.

- [45] Rainer Storn and Kenneth Price. Differential Evolution A simple and efficient heuristic for global optimization over continuous spaces. *Journal of Global Optimization*, 11:341–359, 1997.
- [46] Steve MC Gregor The University of Texas at Dallas. U. T. Dallas-Led Research Team Produces Strong, Transparent Carbon Nanotube Sheets. http://www.utdallas.edu/news/archive/2005/carbon-nanotube-sheets.html, Augustus 2008.
- [47] C. van de Kolk. Stability of Levitated Cylindrical Orbits by Using Solar Sails. *American Astronautical Society Paper*, 1999.
- [48] Giavanni Vulpetti. *Solar Sails; A Novel Approach to Interplanetary Travel*. Springer Praxis Books, 1st edition, 2008.
- [49] John L. West. The Geostorm warning mission: Enhanced oportunities based on new technology. *AAS/AIAA Space Flight Mechanics Conference.*, 14th, 2004.
- [50] Richard Wolfson. *Essential University Physics; Volume 2.* Pearson, Addison Wesley, first edition edition, 2007.
- [51] Tsuda et al. Yulchi. Achievement of IKAROS Japanese deep space solar sail demonstration mission. *Acta Astronautica.*, 82:183–188, 2013.